

Washington University in St. Louis

Washington University Open Scholarship

McKelvey School of Engineering Theses & Dissertations

McKelvey School of Engineering

Spring 5-15-2019

A High-Throughput Screening Platform for In Vitro Elastic Fiber Production and the Mass Transport Properties of the Elastic Fiber Compromised Arterial Wall

Austin John Cocciolone
Washington University in St. Louis

Follow this and additional works at: https://openscholarship.wustl.edu/eng_etds



Part of the [Biomedical Engineering and Bioengineering Commons](#)

Recommended Citation

Cocciolone, Austin John, "A High-Throughput Screening Platform for In Vitro Elastic Fiber Production and the Mass Transport Properties of the Elastic Fiber Compromised Arterial Wall" (2019). *McKelvey School of Engineering Theses & Dissertations*. 443.

https://openscholarship.wustl.edu/eng_etds/443

This Dissertation is brought to you for free and open access by the McKelvey School of Engineering at Washington University Open Scholarship. It has been accepted for inclusion in McKelvey School of Engineering Theses & Dissertations by an authorized administrator of Washington University Open Scholarship. For more information, please contact digital@wumail.wustl.edu.

WASHINGTON UNIVERSITY IN ST. LOUIS

School of Engineering and Applied Science
Department of Biomedical Engineering

Dissertation Examination Committee:

Jessica Wagenseil, Chair

Kathy Flores

Robert Mecham

Lori Setton

Jin-Yu Shao

A High-Throughput Screening Platform for *In Vitro* Elastic Fiber Production and the Mass
Transport Properties of the Elastic Fiber Compromised Arterial Wall

by

Austin Cocciolone

A dissertation presented to
The Graduate School
of Washington University in
partial fulfillment of the
requirements for the degree
of Doctor of Philosophy

May 2019
Saint Louis, Missouri

© 2019, Austin Coccione

Table of Contents

List of Figures	vi
Acknowledgements.....	vii
Abstract.....	viii
Chapter 1: Introduction	1
1.1 Motivation and Research Aims.....	1
1.2 Summary of Chapters	2
Chapter 2: Elastin, Arterial Mechanics, and Cardiovascular Disease	4
2.1 Elastin	4
2.1.1 Elastin characterization.....	4
2.1.2 Regulation of tropoelastin expression.....	5
2.1.3 Coacervation and crosslinking.....	6
2.1.4 Elastic fiber assembly	7
2.1.5 Elastolytic enzymes	7
2.2 Arterial Mechanics.....	8
2.2.1 Arterial wall structure	8
2.2.2 The windkessel effect	10
2.2.3 Arterial stiffness and passive mechanical behavior	11
2.2.4 Energy storage and return	15
2.3 Elastin as a Signaling Molecule.....	15
2.3.1 Tropoelastin	15

2.3.2 Elastin-derived peptides.....	16
2.3.3. Elastin receptor complex.....	17
2.3.4 TGF- β sequestration.....	18
2.4 Cardiovascular Disease.....	19
2.4.1 Genetic elastinopathies	19
2.4.2 Mouse models of genetic elastinopathies	21
2.4.3 Effects of graded elastin amounts in mice	22
2.4.4 Acquired cardiovascular diseases	26
2.5 Tissue Engineering.....	34
2.6 Summary and Future Directions	35
2.7 Acknowledgements.....	36
2.8 References.....	37
Chapter 3: <i>In Vitro</i> Screening for Enhanced Elastic Fiber Crosslinking by Drugs and Small Molecules.....	49
3.1 Introduction.....	49
3.2 Methods.....	56
3.2.1 Cell culture.....	56
3.2.2 Cell pellet hydrolysis	58
3.2.3 Competitive ELISA for desmosine quantitation.....	58
3.2.4 Ninhydrin assay for total protein quantitation	60
3.2.5 Small molecule library NCI Diversity Set V	60
3.2.6 Small molecule library primary screening.....	61
3.2.7 Small molecule library hit selection and primary screen verification	61
3.2.8 Small molecule library secondary screening and replication	62

3.3 Results.....	62
3.3.1 Time course <i>in vitro</i> elastic fiber synthesis.....	62
3.3.2 β APN as an inhibition control.....	63
3.3.3 DMSO cytotoxicity.....	63
3.3.4 Suitability of insulin and TGF- β 1 as positive controls.....	65
3.3.5 Suitability of antihypertensive drugs as positive controls.....	66
3.3.6 Primary screening.....	67
3.3.7 Secondary screening.....	70
3.4 Discussion.....	71
3.5 Summary.....	73
3.6 Limitations.....	75
3.7 Acknowledgments.....	75
3.8 References.....	76
Chapter 4: Mass Transport in Arteries with Compromised Elastic Fibers.....	78
4.1 Introduction.....	78
4.2 Methods.....	80
4.2.1 Transport theory.....	80
4.2.2 Animal tissue preparation.....	83
4.2.3 Experimental setup.....	83
4.2.4 Elastase treatment.....	84
4.2.5 Hydraulic conductance.....	85
4.2.6 Solute flux.....	86
4.2.7 Solute uptake.....	87
4.2.8 Elastin histology by VVG of carotid cross sections.....	87

4.2.9 Two-photon microscopy of elastin auto fluorescence in <i>en face</i> carotids	88
4.2.10 Statistical analysis	88
4.3 Results.....	89
4.3.1 Elastin histology shows compromised elastic fibers	89
4.3.2 Elastin auto fluorescence reveals changes in elastic fiber density.....	90
4.3.3 Hydraulic conductance is influenced by elastic fiber integrity.....	90
4.3.4 Total solute flux reveals size exclusion properties	92
4.3.5 Solute uptake is variably affected by elastic fiber disruption treatment.....	94
4.3.6 Change to effective pore radius is not adequate to describe results	96
4.4 Discussion.....	97
4.5 Conclusions.....	103
4.6 Limitations	104
4.7 Acknowledgments.....	106
4.8 References.....	107
Chapter 5: Conclusions	112

List of Figures

2.1 Domain structure of the human elastin gene.....	5
2.2 Structure of the elastin network in arterial elastic laminae.....	9
2.3 Organization of the elastic laminae in large and small arteries	10
2.4 Effects of elastin amounts on arterial mechanical behavior	14
2.5 Effects of elastin amounts on arterial wall structure and composition	23
2.6 Effects of elastin amounts on arterial morphology	24
2.7 Effects of elastin amounts on medial calcification caused by MGP-deficiency.....	32
3.1 Non-linear regression of the desmosine ELISA standard curve	60
3.2 Results from the elastic fiber screening platform development.....	64
3.3 Changes to desmosine-to-total protein ratio with growth factor treatment	65
3.4 Changes to desmosine-to-total protein ration with antihypertensive drug treatment	67
3.5 Scatterplot of the NCI Diversity Set V library primary screen results	68
3.6 Hit selection and verification of the primary screen	69
3.7 Elastin-to-total protein ratios from a secondary screen of positive hits.....	70
4.1 Quasi-elastic light scattering data for FITC-dextran particle radius.....	81
4.2 Structural effects of elastase treatment and salt inhibition of elastase on carotids	85
4.3 Histological cross sections of <i>Fbln5</i> ^{+/+} , <i>Fbln5</i> ^{-/-} , and elastase-treated carotids	89
4.4 Elastin auto fluorescence of <i>Fbln5</i> ^{+/+} , <i>Fbln5</i> ^{-/-} , and elastase-treated carotid <i>en face</i> sections	91
4.5 Effects of compromised elastic fibers on volumetric fluid flux	92
4.6 Effects of compromised elastic fibers on net solute flux	93
4.7 Effects of compromised elastic fibers on solute uptake.....	95
4.8 Reflection coefficient and effective pore radius in tissues with compromised elastic fibers ..	97

Acknowledgments

I would like to express sincere gratitude, first and foremost, to my PhD advisor Prof. Jessica Wagenseil. Her investment into my professional development has enabled my growth as a scientist and engineer. The completion of this dissertation is afforded by her guidance, patience, and immense knowledge.

My thanks is extended to the rest of the Wagenseil lab members during the tenure of my PhD. I especially want to acknowledge Dr. Gabriela Espinosa, Jie Hawes, Elizabeth Johnson, Dr. Jungsil Kim, and Dr. Marius Staiculescu for their encouragement and insightful discussion in my research.

I would also like to thank the rest of my thesis committee: Prof. Kathy Flores, Prof. Robert Mecham, Prof. Lori Setton, and Prof. Jin-Yu Shao for their multifaceted support in providing feedback, direction, and insight.

Lastly, I would like to acknowledge the funding sources that supported this research: NIH grants R01 HL115560, R01 HL105314, and T32 EB018266.

Austin Cocciolone

Washington University in St. Louis

May 2019

ABSTRACT OF THE DISSERTATION

A High-Throughput Screening Platform for *In Vitro* Elastic Fiber Production and the Mass Transport Properties of the Elastic Fiber Compromised Arterial Wall

by

Austin Cocciolone

Doctor of Philosophy in Biomedical Engineering

Washington University in Saint Louis, May 2019

Research Advisor: Professor Jessica Wagenseil

Elastin comprises nearly 50% of the wall in large elastic arteries and has a broad variety of physiological roles. As a structural extracellular matrix protein, elastin is responsible for the reversible elasticity in large arteries that dampens pulsatile flow and ultimately reduces the workload on the heart. Structural compromise to the elastic fiber network is apparent in the elastin genetic disorders, supravalvular aortic stenosis and autosomal dominant cutis laxa-1, and acquired elastin disorders including hypertension, atherosclerosis, artery calcification, aneurysms, diabetes, and obesity. All of these disorders lead to an increased incidence of cardiovascular related death and the compromised elastic fiber network plays an important role in the degeneration of cardiovascular function. Elastin also serves as an important biological signal in both the development of the arterial vasculature and the progression of several of the previously mentioned cardiovascular disorders. Elastin's physiological role is often overlooked in strategies being developed to treat these cardiovascular disorders. The work of this thesis has focused on two areas in particular that elastic fibers have been underrepresented; the generation of elastic fibers *in vitro* and the importance elastic fiber network on determining the mass transport properties of the arterial wall.

Tissue engineered arteries lack a proper elastic fiber network, in part because elastin content is difficult to quantify and because inducing elastic fiber formation *in vitro* is challenging. We developed a platform for measuring elastic fiber production *in vitro*. We used a competitive ELISA for desmosine, an amino acid unique to elastic fibers, to detect elastic fiber production. We made adjustments to the cell culture conditions of rat lung fibroblast cells to improve their output of elastic fibers. We used this platform to perform a high-throughput screen on a small molecule library to search for molecules that could induce elastic fiber production. We also used our platform to screen the effect of minodixil and diazoxide on elastic fiber production as these antihypertensive drugs have been shown by other researchers to induce elastin gene expression but their effect on mature elastic fiber production was undetermined.

Drug delivery in pharmaceutical strategies for treating aneurysm formation, arterial stiffness, and atherosclerosis is a rapidly developing area. However, current models of mass transport in the arterial wall make numerous assumptions that either diminish the contribution of the elastic fiber network or ignore it completely and there is a lack of empirical investigation on the transport properties of the arterial wall. We hypothesized that the elastic fiber network serves to limit transport across the wall. We developed *ex vivo* methods for measuring transmural advective transport of solute and fluid in mouse carotid arteries at physiological pressure and axial stretch. We investigated the effect of disrupting the elastic fiber network on arterial wall transport using a genetic knockout of Fibulin-5 (*Fbln5*^{-/-}) or treatment with elastase. Fibulin-5 is an important director of elastic fiber assembly. Arteries from *Fbln5*^{-/-} mice have a loose, non-continuous elastic fiber network. The changes in transport properties of elastic fiber compromised arteries

we observed have important implications for the kinetics of biomolecules and pharmaceuticals in arterial tissue following elastic fiber degradation due to aging or vascular disease.

Chapter 1

Introduction

1.1 Motivation and Research Aims

Elastin is the main component of elastic fibers, an extracellular matrix (ECM) protein that enables elastic extension and relaxation in large arteries. Elastin insufficiency or disorganization and improper assembly, fragmentation, or biochemical modifications of elastic fibers change the passive mechanical behavior of the large arteries and ultimately disrupt cardiovascular dynamics in multiple ways. Both genetic and acquired cardiovascular diseases are associated with elastin and elastic fiber defects and have an increased incidence of cardiovascular related death.

Mutations in the elastin gene may cause either supravalvular aortic stenosis (SVAS) or autosomal dominant cutis laxa-1 (ADCL1). Acquired cardiovascular diseases including arterial stiffness and hypertension, diabetes, obesity, aneurysms, atherosclerosis, and arterial calcification are associated with elastic fiber degradation or biochemical modification. This degradation initiates a destructive arterial remodeling cascade that is difficult to stop and may be impossible to reverse.

Elastin gene expression and elastic fiber assembly occur primarily during development and are essentially turned off afterwards. Although elastin's resiliency provides it with a long half-life of 70 years, the lack of elastic fiber matrix turnover makes it susceptible to fragmentation and degradation accumulation. Preserving the elastic fiber matrix or promoting *de novo* elastic fiber production through pharmaceutical intervention and tissue-engineered arteries are potential

strategies for intervening on elastinopathy progression. Crucial to the development of these interventions is an improved understanding of elastic fiber assembly and degradation.

Through the investigations presented in this dissertation, we aimed to advance the knowledge of elastic fiber assembly and degradation. We have developed a platform for screening molecules for activity in promoting elastic fiber production. We used this platform to investigate factors that have demonstrated elastin gene upregulation by other researchers and also performed a high-throughput screen on a library of small molecules. Additionally we have investigated the effects of elastic fiber degradation on the transport of molecules across the arterial wall by performing a series of mass transport studies on elastic fiber compromised tissues.

1.2 Summary of Chapters

Chapter 2 of this dissertation broadly reviews the physiological role of elastin and the animal models which have largely enabled the current state of knowledge on elastin. We summarize the multi-step process of elastic fiber assembly and the challenges and recent advances in generating functional elastic fibers *in vitro*. We discuss the unique mechanical properties of large elastin containing arteries that are dependent upon elastic fiber integrity and amount. We review the genetic disorders supravalvular aortic stenosis (SVAS) and autosomal dominant cutis laxa-1 (ADCL1), which are caused by mutations in the elastin gene. Additionally we review hypertension and arterial stiffness, diabetes, obesity, atherosclerosis, calcification, and aneurysms and dissections which are acquired diseases associated with elastic fiber defects.

In chapter 3 we present our work towards the development of a screening platform capable of identifying compounds from a molecular library that induce increased elastic fiber production *in vitro*. We chose a competitive ELISA for the determination of elastic fiber content and we report our cell culture conditions which demonstrate elastic fiber producing capability. We used our screening platform to look for potential candidate factors to serve as positive controls for elastic fiber production. We then performed a high-throughput screen on a library of nearly 1600 small molecules and state the results of the primary and secondary screen.

In chapter 4 we investigate the mass transport properties of mouse carotid arteries with compromised elastic fibers. This research was enabled by two different animal models; the Fibulin-5 genetic knockout (*Fbln5*^{-/-}) which have an improperly assembled elastic fiber matrix in the arterial wall and an elastase treatment we developed to degrade the arterial elastic fiber matrix. We developed experiments for the measures of hydraulic conductance, advective solute transport, and tissue uptake of solute for these elastic fiber compromised tissues and their comparison to intact tissues.

Chapter 5 is a summary of the major conclusions of this dissertation and their significance in furthering current knowledge and offer potential future directions that may build upon these discoveries.

Chapter 2

Elastin, Arterial Mechanics, and Cardiovascular Disease¹

2.1 Elastin

2.1.1 Elastin characterization

Elastin is an elastic protein polymer that is highly resilient due to extensive post-translational crosslinking of the monomeric precursor, tropoelastin. Reviews focusing on tropoelastin and/or elastin have been written by Vrhovski and Weiss (1) and Kozel et al. (2). Due to the numerous crosslinks at lysine residues and having a composition of nearly 75% hydrophobic residues, elastin is extremely hydrophobic (1). The precursor, tropoelastin, is a 70 kDa protein transcribed from a single elastin gene in the mammalian genome (3-5). The human elastin gene is 45 kb, located on chromosome 7, and contains 34 exons of which each exon encodes either a hydrophobic or crosslinking domain in an alternating pattern (6-9) (Figure 2.1). Elastin is only present in vertebrate animals and there is extensive homology amongst human, chick, bovine, and rat species at the nucleic and amino acid levels (1). During an organism's lifespan, elastin gene expression and protein synthesis occur within a narrow timeframe initiating late in embryonic development and terminating in adolescence with essentially no *de novo* elastin production throughout adult life of the animal (10-17). The narrow timeframe of elastin expression and synthesis is unusual for an ECM component, as generally ECM production is dynamic throughout the organism's lifespan. Because of elastin's resilience and a half-life of

¹ Reprinted with additional changes from Cocciolone AJ, Hawes JZ, Staiculescu MC, Johnson EO, Murshed M, Wagenseil JE. *Elastin, arterial mechanics, and cardiovascular disease*. Am J Physiol Heart Circ Physiol. 2018 Aug 1;315(2):H189-H205 with permission from the American Physiological Society © 2018.

nearly 70 years, the limited time period of expression and synthesis is sufficient for the protein to last a lifetime in most species (18, 19).

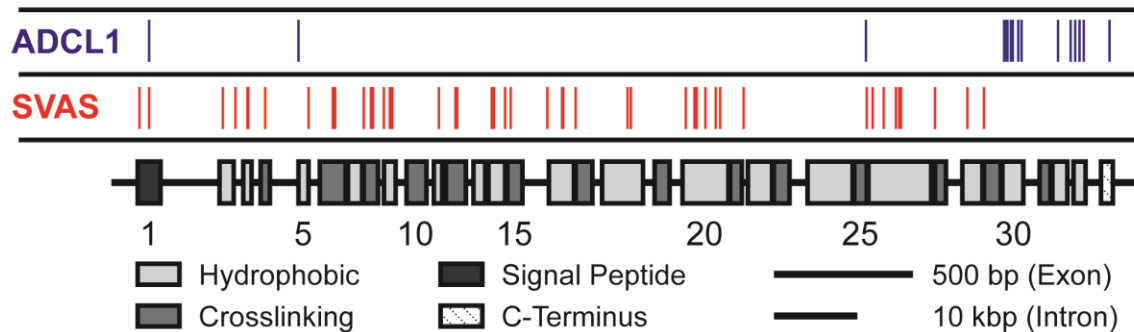


Figure 2.1 - Domain structure of the human elastin gene. Alternating hydrophobic and crosslinking domains are generally transcribed by individual exons. The locations of 64 unique polymorphisms (Human Gene Mutation Database, www.hgmd.cf.ac.uk) associated with either SVAS (red, 49 mutations not including large deletions) or ADCL1 (blue, 15 mutations) are indicated.

2.1.2 Regulation of tropoelastin expression

Immunohistochemistry studies in developing chicken lung (20) and aorta (21) show that tropoelastin expression correlates with smooth muscle differentiation markers and suggest that transcription of elastin is developmentally regulated. Tropoelastin mRNA levels are decreased in adult compared to neonatal rat lungs, but tropoelastin pre-mRNA levels are similar, suggesting that post-transcriptional regulation turns off tropoelastin expression in adulthood (22). An element in the open reading frame specifically binds a cytosolic protein that destabilizes tropoelastin mRNA. Binding affinity increases in adult compared to neonatal lung fibroblast cells, mediating rapid tropoelastin mRNA decay, and decreasing overall mRNA levels. Binding affinity is decreased by TGF- β 1 (23), which stimulates tropoelastin expression in human fetal lung fibroblasts by stabilizing its mRNA (24). Active Smads and *de novo* tropoelastin expression are required for TGF- β 1 mediated tropoelastin mRNA stabilization in cell culture (25). TGF- β 1 immunoreactivity is present at the sites of arterial elastin expression as detected by *in situ* hybridization, supporting a role for TGF- β 1 regulation of tropoelastin expression *in vivo* (26).

TGF- β 1 may additionally regulate tropoelastin expression through interactions with the promoter region in a tissue-specific manner (27). IGF-1, vitamin D, and IL-1 β also modulate tropoelastin expression, at either the promoter level or through increased mRNA stability (1). Cytokine regulation of tropoelastin expression has been reviewed by Sproul and Argraves (28).

2.1.3 Coacervation and crosslinking

In the arterial wall, tropoelastin is primarily produced from vascular smooth muscle cells (VSMCs) in the media (21, 29), although it can also be produced by endothelial cells (ECs) in the intima (30, 31) and fibroblasts in the adventitia (32, 33). After secretion to the extracellular space, tropoelastin simultaneously undergoes coacervation and crosslinking. Crosslinking is facilitated by enzymes from the lysyl oxidase family, in particular lysyl oxidase (LOX) and lysyl oxidase like-1 (LOXL-1). The role of LOX in elastic fiber assembly has been reviewed by Lucero and Kagan (34). Coacervation is a reversible and thermodynamically driven self-assembly of tropoelastin into globular aggregates that occurs spontaneously at physiological temperatures and is a consequence of the numerous hydrophobic regions in tropoelastin (35-40). LOX activity appears to depend on coacervation, as LOX demonstrates higher affinity for insoluble, coacervated tropoelastin and is less effective at crosslinking tropoelastin at temperatures below the threshold for spontaneous coacervation (41, 42). While accepted that coacervation is a critical step to crosslinking, it is unclear whether this is due to induced conformational changes in tropoelastin or to tropoelastin sequestering (1, 42, 43).

Through the activity of LOX, an oxidative deamination reaction converts many lysine residues into allysine (44). It is suspected that the presence of an aromatic residue adjacent to and on the C-terminal end of lysine sterically inhibits LOX activity, preserving several lysine residues for

downstream reactions in the crosslinking process (45). Following side chain oxidation, a sequence of spontaneous condensation reactions occurs between the newly formed allysine residues and unreacted lysine residues to form covalent crosslinks called desmosine and isodesmosine between tropoelastin units. Desmosine and isodesmosine are unique to elastin and serve as a basis for quantification of elastin amounts in tissues (46).

2.1.4 Elastic fiber assembly

Elastin forms the core of elastic fibers and is the most abundant component of the mature structure. The other major component is a scaffold of microfibrils, which are composed mostly of fibrillin-1 and -2 (47, 48). Elastic fiber assembly involves nearly 30 different proteins that are tightly coordinated spatially and temporally (43). The function of only a handful of these associated proteins is understood and elucidation of the function of others is an active area of investigation. Reviews focusing on elastic fiber assembly have been written by Kielty et al. (43), Wagenseil and Mecham (49), and Yanagisawa and Davis (50). Spontaneous tropoelastin coacervation and the crosslinking catalyzed by LOX at the cell surface initiates the assembly process. There is evidence that some of the associated assembly proteins, namely fibulin-4 and/or -5 (FBLN4, -5), serve to modulate the size and conformation of the developing elastin aggregates (51). These elastin aggregates are then shuttled to the microfibrils that are anchored to the cell surface through integrins. Finally, further crosslinking occurs, again through LOX, to develop the mature elastic fiber which provides elasticity to the large, elastic arteries.

2.1.5 Elastolytic enzymes

Proteases capable of degrading elastin or elastic fibers are known as elastases. In total, 12 elastases have been identified, however they are non-specific to elastin. Neutrophil elastase (Ela-

2), cathepsin G (CatG) and proteinase-3 (Pr-3) are serine-class proteases that may have a stronger affinity for tropoelastin than crosslinked elastin. They have been found in atherosclerotic plaques, are secreted from neutrophils, and likely contribute to atherosclerosis progression (52). Ela-2 and CatG are also secreted from VSMCs in the pulmonary artery (53). Four matrix metalloproteinases (MMP-2, -7, -9, and -12) have elastolytic activity. All four MMPs are secreted by macrophages, linking elastic fiber degradation and inflammation. MMP-2 and -9 are also produced by VSMCs and are able to activate latent TGF- β (54). There are three levels of post-translational regulation of MMP activity. MMPs are initially secreted as inactive pro-MMPs that require proteolytic cleavage of the propeptide; activity is also turned on by the deactivation of a cysteine switch; and MMPs are regulated by specialized inhibitors called tissue inhibitors of matrix metalloproteinases (TIMPs) (55). Another four elastases, also secreted by macrophages, belong to the cysteine class: cathepsin L, S, K, and V (CatL, -S, -K, and -V). CatL, -S, and -K are also expressed by VSMCs (52). Pepsin A is the final known elastase, but as a digestive enzyme released in the stomach it is unlikely to play a role in vascular remodeling.

2.2 Arterial Mechanics

2.2.1 Arterial wall structure

The structure of the arterial wall is divided into three layers: intima, media, and adventitia. The intima is a single layer of ECs directly adjacent to the arterial lumen that sits on a basement membrane constructed of type IV collagen, laminin, and proteoglycans (56). The middle and largest layer, the media, is further sublayered into lamellar units defined by fenestrated sheets of elastic fibers (Figure 2.2), or elastic laminae. These laminae are separated by a region composed of VSMCs, thin elastic fibers, collagen (mostly types I and III), and proteoglycans (57-60). An internal elastic lamina separates the media from the intima. Elastic fibers and collagen

interconnect the elastic laminae forming a continuous network with three-dimensional helical structure in which the fibers are oriented in a near circumferential direction (58). The number of lamellar units decreases along the arterial tree with larger elastic arteries, such as the descending thoracic aorta, having approximately 60 units in humans (61) and muscular arteries closer to the periphery having fewer than three units. The number of lamellar units scales with physiologic pressure and arterial size across mammalian species, providing a constant wall tension/lamellar unit (62). Cross-sections of a large and small artery from a mouse, demonstrating the number and organization of elastic laminae in the wall, are shown in Figure 2.3. An external elastic lamina exists between the media and the outermost layer, the adventitia, in large arteries but is absent in the smallest muscular arteries. The adventitia contains fibroblasts, fibrocytes, and a collagen-rich matrix. Large arteries in large animals contain a vasa vasorum in the adventitia to supply blood to the outer wall cells that are too far from the arterial lumen for diffusion of oxygen and nutrients across the wall.

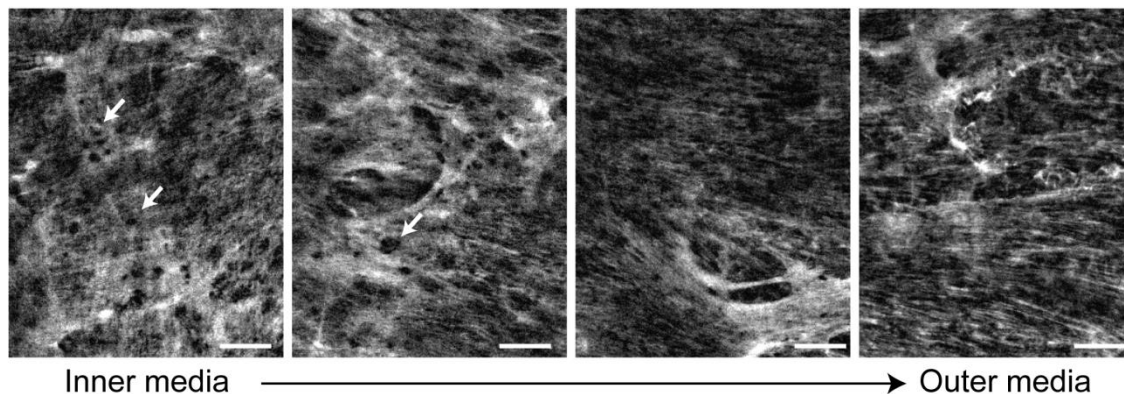
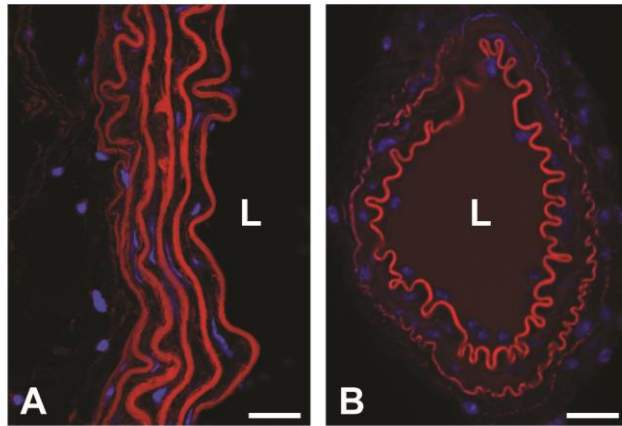


Figure 2.2 - Structure of the elastin network in arterial elastic laminae. *En face* images of elastin in a WT mouse ascending aorta obtained using nonlinear fluorescence microscopy (63). Dense, fenestrated (arrows) elastin network is observed in elastic laminae near the inner media (left). The network appears more fibrous toward the outer media (right). Circumferential direction is horizontal; axial direction is vertical. Scale bars = 20 μm .

Figure 2.3 - Organization of the elastic laminae in large and small arteries. Cross-sections of a mouse descending aorta (A) and mesenteric artery (B) stained for elastin (red) and cell nuclei (blue) (64). The descending aorta has multiple layers of elastic laminae. The mesenteric artery has an internal elastic lamina at the luminal surface and a thin external elastic lamina at the adventitial surface. The lumen is marked with an “L”. Scale bars = 20 μm .



2.2.2 The windkessel effect

Elastin is only present in vertebrate animals with a closed circulatory system and pulsatile pressure and flow (65). The amount of elastin is highest in the large, elastic arteries closest to the heart and decreases as one moves distally in the cardiovascular system (66). Elastic fibers provide reversible elasticity to the large, elastic arteries. This allows the aorta to deform elastically under an applied hemodynamic load, with no permanent deformation and no energy dissipation when the load is removed. Stephen Hales in 1733 recognized the importance of arterial elasticity in cardiovascular function and Otto Frank in 1895 formalized Hales' ideas into a mathematical model of the Windkessel effect (67). A Windkessel is an air chamber that was used in fire engines during the 18th century to convert pulsatile pumping into a constant flow of water. In the cardiovascular system, the Windkessel effect dampens the pulsatile flow from the left ventricle (LV), so that the distal vasculature receives almost constant perfusion. Blood ejected from the LV during systole distends the aortic wall and during diastole the aorta reversibly returns to its original configuration. The strain energy stored during systolic deformation is returned as work to further pump blood downstream during diastole. If the Windkessel effect is compromised, for example by increased arterial stiffness in aged or diseased arteries, the microvasculature of downstream organs, especially in the brain and kidney, can be

damaged (68). Furthermore, the Windkessel effect reduces cardiac afterload and perfuses the coronary arteries during diastole, hence cardiac function can deteriorate when the Windkessel effect is compromised (69).

The Windkessel effect can be compromised through genetic or acquired elastinopathies that alter elasticity of the arterial wall. Elasticity can be altered by increasing wall stiffness or increasing energy dissipation so that less stored strain energy is available to do work on circulating blood. Increased wall stiffness also increases the pulse wave velocity (PWV) of traveling pressure waves in the cardiovascular system. Reflected waves from arterial branch points normally augment diastolic pressure, but increased PWV causes the reflected waves to return earlier in the cardiac cycle and augment systolic blood pressure, leading to systolic hypertension, decreased diastolic perfusion, and increased pulse pressure which can further damage downstream organs (70).

2.2.3 Arterial stiffness and passive mechanical behavior

Arterial stiffness is a structural mechanical property that depends on the material properties and geometry of the arterial wall. Common measurements of stiffness include Peterson's modulus, distensibility, and PWV (71) and almost always refer to deformation and loading in the circumferential direction. We will call these measurements "structural stiffness" values.

Peterson's modulus and distensibility can be measured *in vivo* or *in vitro*, while PWV is usually measured *in vivo*. PWV can be determined simply and reproducibly in the clinic by recording the time it takes for a blood pressure pulse wave to travel a specified distance in the arterial tree (usually from the carotid to the femoral artery) (72). PWV is a measure of structural stiffness because the value is related to the Young's modulus of the arterial wall (a material property), the

wall thickness, arterial diameter, and the density of blood according to the Moens-Korteweg equation (71). The derivation of the Moens-Korteweg equation assumes that the aorta is a perfect cylinder with no tapering or branches, made up of a linear elastic, isotropic material that experiences small deformations during the cardiac cycle, none of which are precisely true. While PWV is a useful measure of structural arterial stiffness, the assumptions accompanying its use must be kept in mind.

Arterial wall material properties are nonlinear and vary with the direction of deformation and loading (i.e. circumferential vs. axial), hence they cannot be quantified by a single measurement, such as the Young's modulus in the Moens-Korteweg equation. However, estimates of arterial material properties can be obtained by linearizing the mechanical behavior within a given deformation or loading range in a specified direction to provide an incremental Young's modulus for comparison across samples (71). Material stiffness values can also be obtained by fitting constitutive models to detailed *in vitro* mechanical testing data and calculating derivatives of the conjugate stress and strain measurements (73). Fitting constitutive models allows comparison of material behavior and stored strain energy for any loading condition in any direction, but requires multiple experimental protocols for each sample and is dependent on the suitability of the chosen constitutive equation.

The passive mechanical behavior of large, elastic arteries is determined mostly by the amount and organization of elastic fibers and collagen fibers in the wall. VSMCs contribute to arterial mechanics through active contraction or relaxation and by producing the surrounding ECM proteins, but they do not contribute substantially to the passive mechanical behavior (74).

Although there is only one elastin protein, there are multiple collagen proteins. The most abundant arterial collagens are types I and III, with lesser amounts of IV, V, and VI. The amounts and transmural organization of collagen types depend on location in the cardiovascular tree (60). Elastic arteries show nonlinear behavior with maximum distensibility near physiologic pressures and reduced distensibility at high pressures (75), presumably to protect the cells and protein components from irreversible damage due to excessive deformation. Selective digestion of elastic fibers or collagen fibers with proteases indicates that the resistance to stretch in elastic arteries at low pressures is due to elastic fibers, while the resistance to stretch at high pressures is due to collagen fibers (76-79). Experiments on the aorta from mice lacking elastin (*Eln*^{-/-}) demonstrate a reduction in the circumferential material stiffness at low pressure, consistent with the observed role of elastic fibers in protease experiments (80). However, experiments on arteries from elastin haploinsufficient mice (*Eln*^{+/-}) with 50-60% of normal elastin levels show similar circumferential stress-stretch behavior to wild-type (WT) mice (Figure 2.4), which has been attributed to remodeling of the cardiovascular system during development and maturation (81, 82).

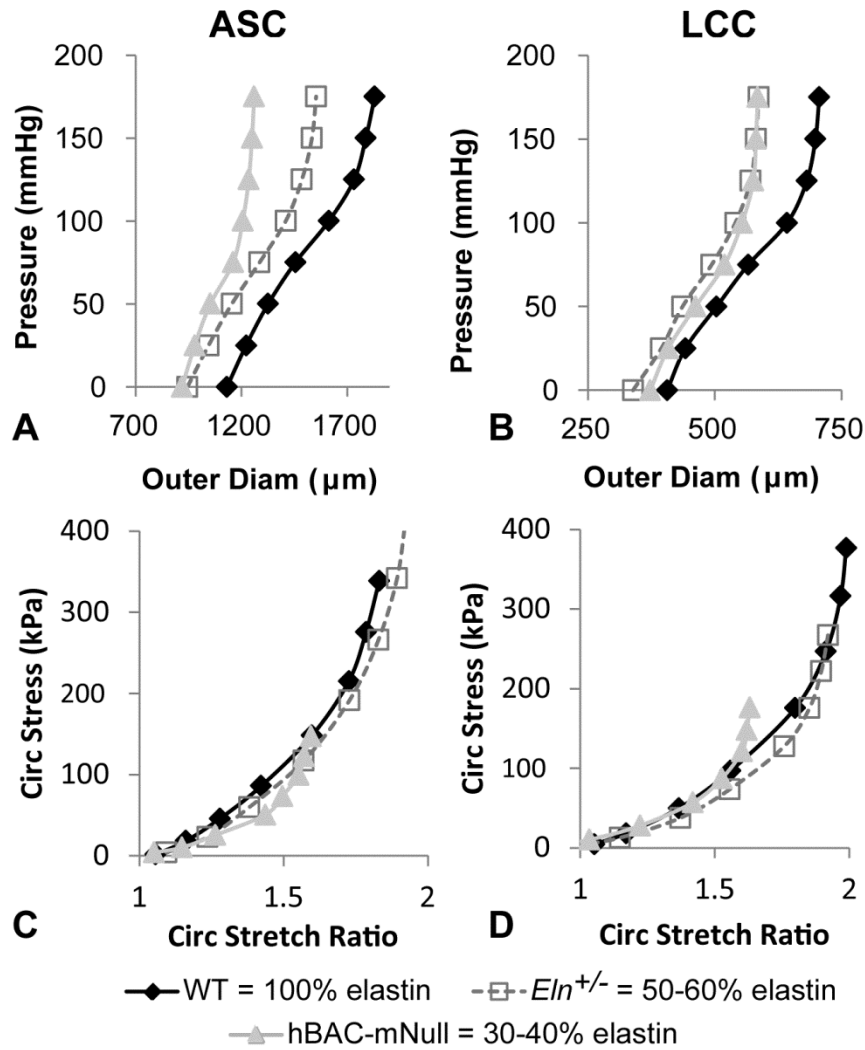


Figure 2.4 - Effects of elastin amounts on arterial mechanical behavior. Representative pressure-outer diameter (A, B) and circumferential Cauchy stress-stretch ratio (C, D) curves (81) for the ascending aorta (ASC) (A, C) and left common carotid (LCC) (B, D) from WT (100% elastin), $Eln^{+/-}$ (50-60% elastin), and hBAC-mNull (30-40% elastin) mice. Decreased elastin amounts shift the pressure-diameter behavior for both artery locations, but the difference between $Eln^{+/-}$ and hBAC-mNull pressure-diameter behavior for the LCC is negligible. For both artery locations, the stress-stretch behavior is similar between WT and $Eln^{+/-}$ mice, but becomes more nonlinear at lower stretch ratios for hBAC-mNull mice. The data highlight the importance of examining structural (pressure-diameter) and material (stress-stretch) mechanical behavior, as well as differences between artery locations in the structural response to reduced elastin amounts. The results suggest that mouse arteries can remodel to maintain WT material behavior when elastin amounts are 50-60% of normal, but cannot fully remodel and adapt the material behavior when elastin amounts are 30-40% of normal.

Remodeling of the arterial wall in response to genetic or acquired elastinopathies is important for determining the physiologic mechanical behavior. Production and reorganization of collagens (83) or other ECM components, such as proteoglycans (84), are often observed in response to defects in or degradation of the elastic fibers. Additional collagen deposition or a shift in the ratio of different types of collagens in the wall may increase stiffness of the wall, affect the Windkessel function, and the strain energy storage capacity (85). Additional proteoglycans may pool in the wall and provide a catalyst for arterial dissections (86).

2.2.4 Energy storage and return

Because elastin is a highly resilient protein, it allows the wall of the large arteries to deform with little energy loss on loading and unloading. Energy loss is small, but finite at 15-20%, and this value appears to be consistent across various species (87). Energy loss is attributed to viscous losses from VSMCs (88) or proteoglycans (89). The relative contributions of different components to the viscoelastic behavior of arteries have been determined using protease digestion in a similar manner to the elastic contributions for different pressure ranges. Recent experiments on newborn mouse aortae lacking elastin (*Eln*^{-/-}), lysyl oxidase (*Lox*^{-/-}), or fibulin-4 (*Fbln4*^{-/-}) show that properly assembled and crosslinked elastic fibers are necessary for low energy loss (80). Many investigations do not include energy loss in mechanical studies on large elastic arteries, but this may be an important consideration in diseases with highly fragmented elastic fibers.

2.3 Elastin as a Signaling Molecule

2.3.1 Tropoelastin

While we have focused so far on the mechanical effects of structural changes in elastic fibers, elastin and its degradation products have chemical signaling effects as well. For example, soluble

tropoelastin can regulate cell phenotype. Adding tropoelastin to the culture media of VSMCs from *Eln*^{-/-} mice inhibits proliferation (90) and increases stiffness as measured by atomic force microscopy (AFM) (91). Karnik et al. showed that a specific domain within tropoelastin, VGVAPG, induces actin polymerization in VSMCs through a G protein coupled pathway (92). The VGVAPG peptide is a potent chemoattractant for VSMCs (92), fibroblasts, and monocytes (93). Sites have been identified at the C-terminus and central region of tropoelastin that mediate binding to $\alpha_v\beta_3$ and $\alpha_v\beta_5$ integrins, which are involved in numerous signaling pathways (94, 95). Non-integrin mediated interaction between tropoelastin and the cell membrane has also been identified through the binding of fractionated tropoelastin to heparin sulfated proteoglycans (96). Tropoelastin expression is detectable in adult human aorta at decreasing levels with aging (97), implying that reduced tropoelastin, as well as degradation and modification of existing elastic fibers may modulate age-related changes in the arterial wall.

2.3.2 Elastin-derived peptides

Elastic fibers can be degraded and fragmented by mechanical fatigue, calcification, glycation, lipid peroxidation, and protease digestion (98). The resulting elastin-derived peptides (EDPs) are bioactive and retain the VGVAPG peptide sequence found in tropoelastin, rendering similar signaling capability. EDP levels in the blood are increased in humans with obliterative arteriosclerosis of the legs, type IIb hyperlipidemia, hypertension, diabetes, and ischemic heart disease (99). Whether the increased levels of EDPs are a cause or consequence of the disease is unknown. Recent studies in mice suggest that while elastic fiber fragmentation may be secondary to the genetic or acquired disease, circulating EDPs contribute to further disease progression. Chronic doses of EDPs, as well as VGVAPG peptides, increase the size of atherosclerotic plaques at the aortic root in two different atherosclerosis susceptible mouse models (100). EDPs

are capable of binding the lactose-insensitive receptor found on the surface of macrophages, implicating a role for EDPs in macrophage migration in inflammation and atherosclerosis progression (101). A single dose of EDPs, as well as VGVAPG peptides, causes hyperglycemia in mice (93). Rat aortic VSMCs incubated with EDPs show increased expression of typical bone proteins, which may contribute to arterial calcification (102). An antibody to VGVAPG blocks EDP signaling to inflammatory cells and protects against elastase induced emphysema in mice (103). The VGVAPG antibody also reduces aortic elastic fiber fragmentation, macrophage infiltration, and TGF- β 1 activity in a mouse model of aortic aneurysm due to reduced fibrillin-1 levels (104). Finally, VGVAPG sequence-carrying EDPs have been shown to interact with the galectin-3 receptor, which is involved in melanoma chemotaxis and expression of MMP-2 and -3 (105). A review summarizing the effects of elastin degradation and EDPs in cardiovascular aging and disease has been written by Duca et al. (98).

2.3.3 Elastin receptor complex

Many of the chemical signaling effects of tropoelastin and/or EDPs are thought to be mediated by the elastin receptor complex (ERC) (52). The ERC is composed of two membrane-bound subunits, protective protein/cathepsin A (PPCA) and neuraminidase-1 (Neu-1), plus the elastin binding protein (EBP). EBP (also known as S-Gal) is a splice variant of lysosomal β -galactosidase that retains the ability to bind galactosugars, but has lost enzymatic activity. In addition, the splice variant has a 32-peptide sequence capable of binding tropoelastin (106). In elastogenesis, EBP is thought to be responsible for shuttling tropoelastin to the cell surface and antagonistic interaction between EBP and galactose or lactose may release tropoelastin to the extracellular space (107). Neu-1 appears to control signal transduction by ERC through the

catalytic conversion of ganglioside to lactosylceramide (108). Downstream signaling of the ERC diverges depending on cell type but reconvenes at the activation of ERK1/2 (98).

2.3.4 TGF- β sequestration

TGF- β is secreted from cells in the form of a large latent complex (LLC) that includes a latency associated peptide (LAP) and a latent TGF- β binding protein (LTBP). LTBP localizes latent TGF- β to the ECM. LTBP1 and -3 bind well to all three TGF- β isoforms (109). LTBP1 has specific interactions with fibrillin-1 microfibrils (110). Although direct interactions of LTBP3 with fibrillin-1 have not been shown, LTBP3 protein is reduced in the aorta of fibrillin-1 knockout (*Fbln1*^{-/-}) mice (111). In the early stages of elastic fiber assembly, microfibrils are abundant and there is little elastin. Throughout late embryonic development and early maturation, elastin synthesis increases and eventually obscures the microfibrils (112). It is possible that elastin accumulation indirectly regulates TGF- β availability by modulating LLC binding to the microfibrils. TGF- β 1 immunoreactivity and tropoelastin expression co-localize in developing rat aorta and decrease with age (26). This has been interpreted as evidence of TGF- β 1 regulated expression of tropoelastin *in vivo*, but it could also be interpreted as tropoelastin regulated availability of TGF- β 1 as elastin accumulates on the microfibrils. TGF- β 1 signaling is altered when arterial elastic fibers are not assembled properly and through proteolytic cleavage of elastic fiber associated proteins, indicating bidirectional effects between TGF- β 1 activity and elastic fiber integrity (113). Elastinopathies that alter elastin amounts or elastic fiber integrity may then affect TGF- β activity (114).

2.4 Cardiovascular Disease

Several genetic and acquired cardiovascular diseases are associated with elastin and elastic fiber defects. The defects include altered amounts of elastin, and improper assembly, fragmentation, and modification of elastic fibers. Additional reviews on cardiovascular diseases associated with elastin or elastic fiber defects have been written by Baldwin et al. (115) and Milewicz et al. (116).

2.4.1 Genetic elastinopathies Supravalvular aortic stenosis

Supravalvular aortic stenosis (SVAS, OMIM #185500) is a rare (~1:20,000 births) congenital obstruction of the LV outflow tract. The defining defect is a lesion in the aorta at the sinotubular junction (STJ) as a result of VSMC hypertrophy, increased collagen, and reduced/disorganized elastic fibers in the medial layer (117, 118). Often there are additional morphological defects in other elastic arteries, but the arteries affected and severity of the defects is patient specific. There are three forms of SVAS: autosomal-dominant familial, sporadic, and Williams-Beuren syndrome (WBS, OMIM #194050) associated. The genetic origin defines the form of SVAS. Familial and sporadic SVAS arise from loss-of-function mutations to the elastin gene that are either inherited or *de novo*, respectively. A variety of mutations have been reported, including translocations, partial deletions, and point mutations (Figure 2.1), often resulting in a truncated elastin protein. In WBS associated SVAS the entire elastin gene, along with 25 - 27 other genes, is encompassed in a large deletion on chromosome 7 (119). In all cases, one functional elastin gene remains and sporadic mutations are more common than inherited mutations (120).

SVAS can present as one of two different types. Type I (discrete) is defined by a localized narrowing at the STJ. Type II (diffuse) shows uniform narrowing beginning at the STJ and

extending as far as the aortic arch or even the descending aorta (121). The ratio of Type I:Type II incidence is approximately 7:3 (122). Due to the rarity of SVAS, data correlating Type I or II to specific elastin mutations is not available (123). In addition to the primary STJ lesion, vascular defects occur in other arteries. Often the aortic valve leaflets are hypertrophic, resulting in partial fusion of the leaflets to the STJ (124). 39% of SVAS patients have bicuspid aortic valve (123). Pulmonary artery stenosis is present in 83% of SVAS patients (122, 125). Lesions in the right-ventricular outflow tract are also common (123). Coronary arteries can exhibit fibrodysplasia and may have stenotic lesions (126). Because coronaries are muscular arteries, it is unclear whether the lesions are a direct result of the elastinopathy or are a secondary pathology.

Hypertension is common in WBS patients even at early ages (127) and may be linked to increased arterial structural stiffness due to reduced elastin amounts. Kozel et al. measured PWV in 77 patients with WBS and found an increase versus healthy controls. However, the increased PWV was independent of whether or not the patient was hypertensive (128). While hypertension and increases in arterial structural stiffness generally develop coincidentally in acquired cardiovascular disease, their dissociation in WBS may indicate that reduced elastin amounts are a common causal factor. SVAS patients have an increased risk of sudden cardiac death (SCD), with WBS patients having the highest risk (122). The most common cause of SCD is myocardial ischemia, likely resulting from coronary obstruction and LV hypertrophy (129). Ischemia could also be caused by reduced coronary perfusion during diastole due to a compromised Windkessel effect. Compromised arterial Windkessel function would also increase cardiac afterload and could contribute to LV hypertrophy.

Autosomal dominant cutis laxa-1

Autosomal dominant cutis laxa-1 (ADCL1, OMIM #123700) is a rare connective tissue disorder in which the skin is loose, hyperextensible, and has redundant folds. Patients may have cardiovascular pathologies including bicuspid aortic valve, dilation of the aorta or pulmonary artery, and pulmonary emphysema (130). The majority of reported ADCL1 cases have a frameshift mutation within the last five exons of the *ELN* gene (Figure 2.1). The result of the frameshift is usually an elongation of the tropoelastin protein that is believed to form larger aggregates during coacervation and impair the ability of elastin to bind to the microfibrillar scaffold during elastic fiber assembly. Callewaert et al. demonstrated impaired tropoelastin deposition onto microfibrils, increased TGF- β signaling, and indications of endoplasmic reticulum stress in cultured fibroblasts from ADCL1 patients (131). In nearly 50% of ADCL1 cases, aneurysms are present in the aortic root, aortic arch, or pulmonary artery. Aneurysm development is likely a combined result of reduced elastic fiber synthesis and increased susceptibility to elastic fiber degradation (132).

2.4.2 Mouse models of genetic elastinopathies

Targeted deletion of the elastin gene in mice was first reported by Li et al. in 1998 (133). *Eln*^{-/-} mice represent an extreme elastinopathy and provide insight into the role of elastin in arterial mechanics, VSMC phenotype modulation, and cardiovascular disease. The same year, Li et al. showed that elastin haploinsufficient (*Eln*^{+/-}) mice demonstrate some of the cardiovascular phenotypes observed in SVAS patients, such as increased arterial structural stiffness and an increased number of arterial lamellar units, but do not have the local aortic lesions observed in SVAS (134). A mouse model of WBS with a large deletion that includes the elastin gene (135) has a similar cardiovascular phenotype to *Eln*^{+/-} mice (136). *Eln*^{+/-} mice have been used to study

cardiovascular effects of reduced elastin amounts and the associated increases in arterial structural stiffness.

Due to the insertion of a short exon after exon 4 in the mouse and the loss of two exons (34 and 35) in the human during primate evolution, the mouse *Eln* gene has 37 exons, while the human *ELN* gene has 34 exons (137). The human *ELN* gene also shows unique alternative splicing patterns (138). To create a mouse model to study *ELN* mutations in human disease, Hirano et al. expressed the human elastin gene in a bacterial artificial chromosome (BAC) in *Eln*^{-/-} mice (139). These hBAC-mNull mice only express human elastin and have total elastin amounts at 30 – 40% of normal (139). hBAC-mNull mice also show VSMC hypertrophy and aortic luminal narrowing representative of SVAS lesions (140). Sugitani et al. engineered a single base deletion associated with ADCL1 within the *ELN* gene in a BAC and expressed it in mice (141). The mutant elastin was incorporated into elastic fibers in the mouse skin and lung and compromised tissue function. The mutant elastin was incorporated at low levels into the mouse aorta and did not affect tissue function. The results show tissue specific differences in elastic fiber assembly and highlight the utility of “humanized” mice for studying human disease (141).

2.4.3 Effects of graded elastin amounts in mice

Eln^{-/-}, *Eln*^{+/-}, and hBAC-mNull mice allow investigation of how graded amounts of elastin affect cardiovascular function. They are relevant for determining threshold amounts of elastin necessary for restoring cardiovascular function in genetic and acquired elastinopathies, as well as in tissue-engineered arteries. Each mouse model is discussed in additional detail below.

Comparisons of arterial mechanics, wall structure, and morphology for WT mice with 100% of

normal elastin amounts, *Eln*^{+/-} mice with 50 – 60% of normal elastin amounts, and hBAC-mNull mice with 30 – 40% of normal elastin amounts are shown in Figs. 2.4, 2.5, and 2.6, respectively.

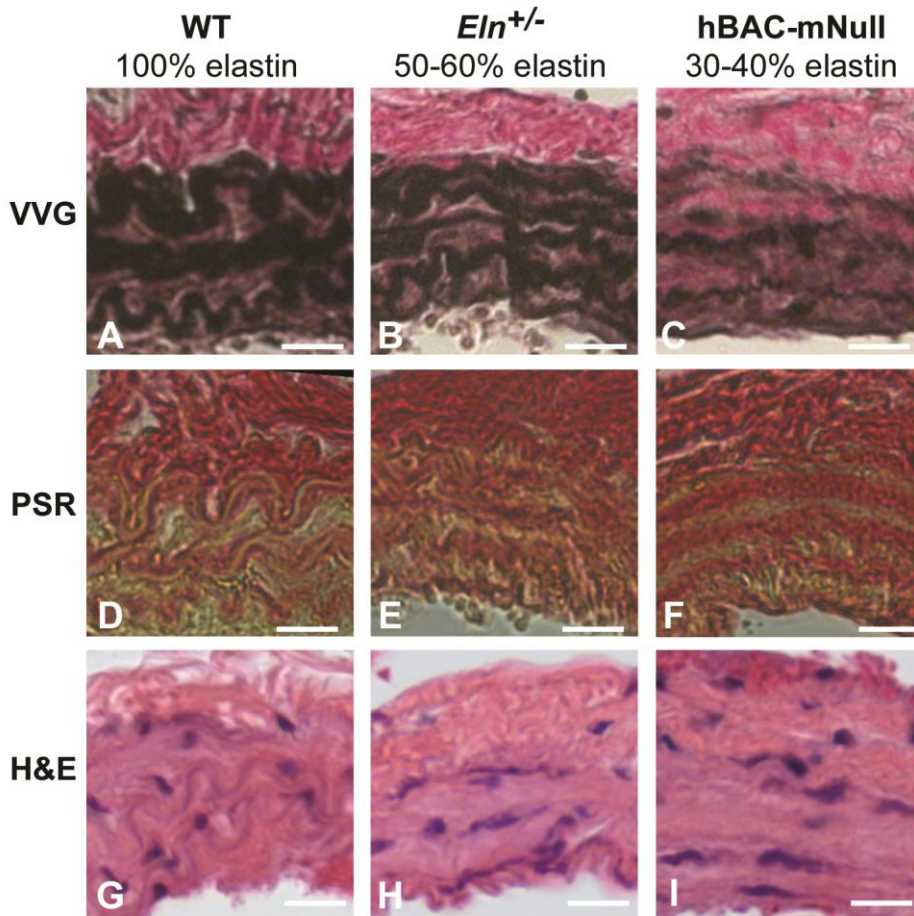


Figure 2.5 - Effects of elastin amounts on arterial wall structure and composition. Histological sections (64) of the left common carotid artery from WT mice with 100% elastin (A, D, G), *Eln*^{+/-} mice with 50-60% elastin (B, E, H), and hBAC-mNull mice with 30-40% elastin (C, F, I). Verhoeff-Van Gieson (VVG) stained sections (A - C) show black elastic laminae, brown muscle tissue, and pink collagen. The elastic laminae are thinner, more numerous, and have more diffuse staining as elastin amounts decrease. Picrosirius red (PSR) stained sections (D - F) show collagen fibers in red and other material in yellow. In WT arteries, red collagen clearly outlines the yellow elastic laminae. In *Eln*^{+/-} and hBAC-mNull arteries, the collagen staining overlaps with the elastic laminae. H&E stained sections (G - I) show cell nuclei in purple and other material in pink. Scale bars = 20 μ m.

0% elastin

Eln^{-/-} mice die within a few days of birth due to VSMC overproliferation in the aortic wall

leading to luminal occlusion that is similar to the aortic root lesion observed in SVAS (133). *Eln*^{-/-}

$^{-/-}$ mice have normal blood pressure and aortic structural stiffness at embryonic day 18 (142), but high blood pressure and increased aortic structural stiffness at birth (143). Aortae from $Eln^{-/-}$ mice have decreased aortic material stiffness compared to WT in the low pressure range, but similar aortic material stiffness to WT in the high pressure range (80). VSMCs from $Eln^{-/-}$ mice have higher proliferation rates (90) and lower material stiffness values (91) and these phenotypes can be partially reversed by the addition of tropoelastin to the cell culture medium. Treatment with mTOR inhibitor rapamycin decreases VSMC overproliferation in $Eln^{-/-}$ mice, but does not extend their lifespan (144). Integrin $\beta 3$ expression is upregulated in $Eln^{-/-}$ aorta and genetically reducing integrin $\beta 3$ dosage extends the lifespan of $Eln^{-/-}$ mice by approximately two days (145). Pharmacologic inhibition of $\beta 3$ with cilengitide reduces VSMC overproliferation in the $Eln^{-/-}$ aorta and may be a novel treatment to prevent SVAS (145).

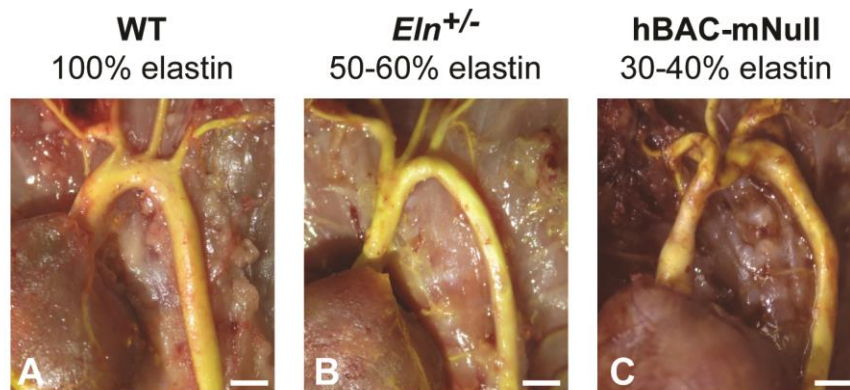


Figure 2.6 - Effects of elastin amounts on arterial morphology. Yellow latex (146) was injected for contrast into the ascending aorta, major branches, and descending thoracic aorta in WT (100% elastin), $Eln^{+/-}$ (50-60% elastin), and hBAC-mNull (30-40% elastin) mice. With decreasing elastin amounts, the aortic diameter decreases and the length increases. There are also changes in branching morphology with reduced elastin amounts. Scale bars = 1 mm.

50 – 60% elastin

Elastin heterozygous ($Eln^{+/-}$) mice live a normal lifespan, but have hypertension, increased arterial structural stiffness (Figure 2.4), and an increased number of lamellar units in the arterial wall (Figure 2.5) (82, 134). Treatment with mTOR inhibitor rapamycin prevents the formation of

increased lamellar units in *Eln*^{+/-} mice (144). *Eln*^{+/-} arteries show reduced *in vivo* axial stretch, residual torsion (81), and increased length (Figure 2.6). Increased arterial structural stiffness precedes increases in blood pressure compared to WT mice during maturation, indicating that it may be a causative factor in the development of hypertension in *Eln*^{+/-} mice (147). *Eln*^{+/-} mice have indications of diastolic dysfunction, which may be linked to compromised arterial Windkessel function and decreased cardiac perfusion during diastole (148). *Eln*^{+/-} mice have impaired glucose metabolism (149) and altered susceptibility to atherosclerotic plaque accumulation (150, 151). Genetic modifiers of the *Eln*^{+/-} cardiovascular phenotype have been identified by outcrossing *Eln*^{+/-} mice. Several genes, including *Ren1*, *Ncf1*, and *Nos1* were identified that may synergize with elastin insufficiency to predispose an individual to hypertension and increased arterial structural stiffness (152). Treatment of *Eln*^{+/-} mice with anti-hypertensive medications improves pulse pressure and subsequently physiologic structural stiffness due to the shift in operating pressures, but does not change material stiffness of the arteries (153). Treatment of *Eln*^{+/-} mice with minoxidil, a K_{ATP} channel opener and vasodilator, also improves physiologic structural stiffness (154). *Eln*^{+/-} mice have reduced susceptibility to vascular calcification (Figure 2.7) (155). Mice with reduced elastin due to a large genetic deletion that mimics the heterozygous deletion observed in WBS (135) have hypertension and increased arterial stiffness, but do not have the increased number of lamellar units observed in *Eln*^{+/-} mice (136).

30 - 40% elastin

Eln^{-/-} mice can be rescued by genetic insertion of a BAC expressing the human elastin gene (139). These hBAC-mNull mice have 35% of normal elastin amounts in the ascending aorta, have extreme hypertension, and increased arterial structural and material stiffness (Figure 2.4)

(139). Increased arterial structural stiffness has been confirmed *in vivo* using ultrasound imaging and may be caused by additional collagen amounts in the aortic media (Figure 2.5) and increased wall thickness (140). While lesion development in SVAS is attributed to VSMC overproliferation in the aortic media, Jiao et al. showed that deficient circumferential growth that limits outward expansion of the aorta, combined with normal VSMC proliferation is a mechanism for luminal narrowing in hBAC-mNull mice (140). Inhibiting mTOR with rapalogs does not prevent luminal narrowing in hBAC-mNull mice, but prevents the observed collagen fibrosis and arterial structural stiffening (156). hBAC-mNull mice have a longer aorta than WT (Figure 2.6) and the axial growth may be a compensation mechanism for the deficient circumferential growth (157).

2.4.4 Acquired cardiovascular diseases

Due to the limited time frame of elastin synthesis, elastic fibers that are damaged or degraded with aging or disease are generally not repaired. Elastic fibers are then replaced by collagens and proteoglycans that stiffen the arterial wall and lead to hypertension and damage to downstream organs. The ratio of elastin:collagen in the human aorta decreases 30 – 40% with age from the 2nd to the 9th decade of life (158). In aging primates, it was recently observed that the elastin:collagen ratio changes with age, but disarray of the remaining elastic and collagen fibers may be an even more important contributor to increased arterial stiffness with aging (159). Many acquired diseases represent accelerated or exacerbated versions of the arterial remodeling observed with aging. The cardiovascular diseases discussed in this review, with a focus on elastic fibers and arterial mechanics, include hypertension and arterial stiffening, diabetes, obesity, atherosclerosis, calcification, and aneurysms and dissections.

Hypertension and arterial stiffening

Hypertension is frequently observed in conjunction with diseases associated with defects in elastin or elastic fibers (160). While hypertension is typically associated with aging, the coincidental occurrence of hypertension in infants with SVAS indicates that age related factors are not required for SVAS associated hypertension (127, 128) and that elastin insufficiency likely plays a key role. Modulation of TGF- β availability by Emilin-1, an elastic fiber associated protein, determines systolic blood pressure in mice, supporting a role for elastic fiber integrity and TGF- β signaling in hypertension (161). TGF- β is an important regulator of ECM remodeling in the arterial wall (162). Inflammatory signaling stimulated by EDPs from elastic fiber degradation may also play a role in hypertension. Reduced amounts of elastin or compromised elastic fiber integrity and the subsequent alterations in ECM composition and arterial geometry lead to increased material and/or structural arterial stiffness. While hypertension has long been associated with changes in resistance of the small, muscular arteries, it is now appreciated that increased stiffness of the large arteries can contribute to hypertension. The role of large artery stiffness in hypertension has been reviewed by Greenwald (70), Wagenseil and Mecham (85), and Mitchell (163), among others. Targeting ECM remodeling and the resulting changes in arterial stiffness represent a challenging, but potentially effective treatment for hypertension (164).

Spontaneous hypertensive rats (SHR) are an animal model for essential hypertension developed through selective breeding (165). In young and adult SHR, systolic blood pressure is increased over Wistar-Kyoto rats (WKY), but material stiffness of the thoracic aorta is not different (166), indicating that increased stiffness of the large arteries does not precede hypertension in SHR. SHR have reduced elastin amounts, smaller arterial diameter, and increased structural stiffness of

the mesenteric resistance arteries compared to WKY, suggesting that increased resistance of the distal arteries contributes to hypertension development in SHR (167). With aging, aortic material stiffness dramatically increases in SHR compared to WKY (166). The increased stiffness has been attributed to endothelial dysfunction (168), increases in advanced glycation end products (169), and decreases in the elastin:collagen ratio (170) in aged SHR aorta compared to WKY. These results imply that SHR is not an appropriate model to investigate large artery stiffness in the development of hypertension, but is an appropriate model to investigate mechanisms of ECM remodeling and increased arterial stiffness in aging coupled with hypertension.

Genetic factors associated with selective breeding of inbred rat strains are linked to changes in amount and organization of the aortic ECM. Behmoaras et al. found that aortic, blood pressure, elastin, collagen and cytokine amounts, and elastic laminae structure are different among seven inbred rat strains (171). Of the seven strains, the Brown-Norway rat (BNR) has the lowest aortic elastin amount and the lowest elastin:collagen ratio, leading to increased structural stiffness of the aorta compared to young LOU control rats (172). BNR are normotensive, suggesting that they are a good model for investigating interactions between elastin and arterial stiffness that are independent of changes in blood pressure. Treatment of cultured BNR VSMCs with potassium channel openers (minoxidil or diazoxide) increases tropoelastin transcription and mRNA stability. Treatment of BNR rats with minoxidil or diazoxide increases aortic elastic fiber content (173). In contrast, treatment of *Eln*^{+/-} mice with minoxidil increases arterial size and stimulates differential expression of 127 matrix or matrix-associated genes, but does not show an elastin specific effect (154). Therapeutic options for increasing elastic fiber content may depend on the primary cause of the elastinopathy.

Diabetes

In diabetes, the body does not produce or respond to insulin appropriately, leading to increased blood glucose levels. *In vitro* studies have examined the effects of increased glucose on VSMCs, isolated arterial elastin, and arterial mechanical behavior. High glucose media, with the addition of EDPs and TGF- β 1, increases expression of osteogenic genes in cultured VSMCs and may lead to arterial calcification associated with diabetes (174). Incubation of isolated arterial elastin in high glucose solution increases the storage and loss modulus, indicating an increase in material stiffness and viscous energy loss (175). After 48 hours of incubation in a high glucose solution, Zou and Zhang found an increase in the material stiffness of isolated arterial elastin in the longitudinal direction, but not in the circumferential direction (176). With incubation times up to 28 days, Wang et al. found an increased material stiffness in both longitudinal and circumferential directions, as well as increased hysteresis (or energy loss) (177). The mechanical changes in isolated arterial elastin have been attributed to the dehydrating effects of glycation (175), but it is unclear how these results translate *in vivo* for an intact arterial wall with ECs acting as an impermeable barrier. Assuming that the glucose can reach the medial layers, increased glucose may lead to glycation of elastic fibers that alters stiffness and protease susceptibility.

In a rat diabetic model, glycation increases over time in arterial samples as diabetes develops, but is unchanged in control rats (178). Diabetic rats also have reduced elastin protein levels in aortic extracts, as well as an increase in elastolytic activity (179). Decreased elastin:collagen mRNA ratio and increased structural stiffness of the aorta are observed in the leptin-receptor deficient mouse model for type 2 diabetes (*db/db*). Interestingly, the same study found opposite trends in

the elastin:collagen mRNA ratio and structural stiffness for the *db/db* coronary artery (180). Human diabetic patients similarly show a decrease in elastin:collagen protein ratios in aortic tissues (181) and an increase in circulating CatS levels (182). There are increased EDP levels in diabetic children (183), indicating that degradation of elastic fibers may occur in diabetes that contributes to arterial stiffening and inflammatory signaling. EDPs may also contribute to insulin-resistance and the onset of diabetes with aging (184). These results suggest that high glucose associated with diabetes may physically stiffen elastic fibers, as well as make them more susceptible to degradation, altering passive arterial mechanics and initiating a chemical signaling cascade through EDPs.

Obesity

Obesity is a risk factor for increased cardiovascular related mortality, but it is typically associated with additional cardiovascular risk factors including hypertension and diabetes. Rider et al. observed an increase in aortic PWV in obese patients absent other cardiovascular risk factors, providing evidence for a direct correlation between obesity and aortic structural stiffness (185). Elastin is decreased in adipose tissue of obese patients (186); however investigations on elastin and elastic fiber changes in large arteries from obese patients have yet to be performed. TGF- β 1 levels positively correlate with body mass index (BMI) in humans (187) and are upregulated in adipose tissue from obese humans (188) and mice (189). Cathepsin elastases, CatK, -L, and -S, have increased activity with increased BMI in humans and in the leptin-deficient (*ob/ob*) mouse model of obesity (190). In *ob/ob* mice, aortic stiffening was observed by an increase in PWV, an increase in abdominal aorta structural stiffness *in vitro*, and an increase in thoracic aorta material stiffness as measured by AFM. Elastic fiber remodeling in the *ob/ob* aorta was evidenced by a decrease in LOX protein levels and activity, a decrease in desmosine

crosslinks, an increase in elastase activity, and higher degree of fragmentation in the elastic lamellae (191). The observed increase in aortic stiffness with obesity may arise from elastic fiber remodeling through LOX downregulation and an upregulation of elastolytic activity.

Atherosclerosis

Both the synthesis of tropoelastin and degradation of elastic fibers are increased in human atherosclerotic lesions (192). This may be due to the production of tropoelastin (193), metalloproteinases (194), and cathepsins (190) by macrophages involved in atherosclerosis. Elastic fiber degradation allows infiltration of lipids and immune cells into the aortic wall for plaque formation and rupture in mice (195). EDPs resulting from elastic fiber fragmentation further enhance atherogenesis (100). TGF- β 1 activity, which may be modulated by elastic fiber degradation, has a wide range of effects in atherosclerosis (196). Elastin insufficiency and the associated increase in arterial structural stiffness do not increase atherosclerotic plaque deposition in mice (150, 151). Together, these results suggest that elastic fiber degradation and the resulting circulating peptides are key mechanisms linking elastin to atherosclerosis progression.

Calcification

Elastic fiber degradation has been linked to ectopic calcium phosphate mineral deposition (calcification) in the arterial walls, particularly in the medial layer. As demonstrated by Basalyga et al., periadventitial treatment of surgically exposed rat aortas with calcium chloride leads to ectopic mineral deposition along the elastic laminae (197). Calcified aortas of the treated rats show the presence of degraded ECM proteins, including elastin. Later, Khavandgar et al. showed that medial calcification in mice lacking matrix Gla protein (MGP), a potent inhibitor of soft

tissue calcification, is elastin-dependent (155). The amount of deposited minerals in $Mgp^{-/-}$ arteries scales with elastin amounts in the cardiovascular tree, with mineral deposition and elastin amounts decreasing from the thoracic to the abdominal aorta. Khavandgar et al. further showed that $Mgp^{-/-}Eln^{+/-}$ mice have markedly reduced arterial mineral deposition compared to $Mgp^{-/-}$ mice (155) (Figure 2.7). This genetic experiment provides evidence that elastin content, and not just elastic fiber degradation, is a critical determinant of arterial medial calcification.

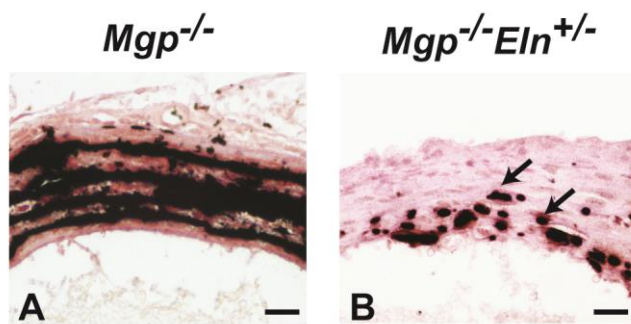


Figure 2.7 - Effects of elastin amounts on medial calcification caused by MGP-deficiency. $Mgp^{-/-}$ mouse arteries show extensive mineral deposition (black) along the elastic laminae (A), which is markedly reduced (arrows) in $Mgp^{-/-}Eln^{+/-}$ mice (B). Thin plastic sections of the thoracic aortae from two week-old mice were stained with von Kossa and van Gieson (155). Scale bars = 20 μ m.

Currently, the mechanism of mineral accumulation by elastin and how this process is inhibited by MGP is not well understood. Also, the role of elastin in intimal calcification associated with atherosclerotic plaques is still unknown. Future mechanistic work focusing on these aspects of elastin biology may lead to new therapeutic approaches to treat vascular calcification, for which no treatment is currently available

Aneurysms and dissections

Degraded and fragmented elastic fibers in the arterial wall are a common histopathology in thoracic and abdominal aortic aneurysms (198, 199). It appears that fragmented elastic fibers or improper elastic fiber deposition is critical to aneurysm formation, rather than reduced elastin amounts. ADCL1, characterized by improper elastic fiber deposition, is generally associated with aneurysms, while SVAS, characterized by elastin insufficiency, is generally not associated with

aneurysms. Additionally, genetic mutations that affect proteins necessary for elastic fiber assembly, such as fibulin-4 (200) and lysyl oxidase (201), cause aneurysms. Loss of function mutations in genes that affect TGF- β 1 sequestration in the ECM, such as fibrillin-1, are associated with aberrant TGF- β 1 activity and aortic aneurysms (202). Fragmented, degraded, or improperly assembled elastic fibers may be more susceptible to protease digestion, allowing aneurysmal dilation over time and stimulating cytokine and inflammatory signaling. Homogenates of abdominal aortic aneurysms show high elastolytic activity (198). Degraded or improperly assembled elastic fibers allow inflammatory cell infiltration, affect TGF- β 1 sequestration, and the released EDPs can enhance macrophage activation (203) and TGF- β 1 activity (104).

Researchers have capitalized on the relationship between elastic fiber degradation, inflammatory cell activation, and chemokine signaling to generate a variety of chemically-stimulated models of abdominal aortic aneurysms and dissections in animals (204-206). The models include intraluminal or periadventitial application of elastase, periadventitial incubation with calcium chloride, and subcutaneous infusion of angiotensin II. Several of the models have been extended to create thoracic aortic aneurysms and dissections (207, 208). It is important to note that many of the chemically-induced animal models demonstrate aortic dilation and aneurysm formation, but do not progress to aortic rupture or dissection (209). Models that progress to rupture and dissection will be critical for translating the results of animal studies to treatment of human disease.

2.5 Tissue Engineering

Increasing elastin amounts in genetic elastinopathies or repairing fragmented elastic fibers in acquired cardiovascular diseases are challenging problems. Tissue engineering, however, encounters the most challenging problem - recreating functional elastic fibers *de novo*.

Elastogenesis has been called the “holy grail” of arterial tissue engineering, as the lack of mature elastic fibers in tissue-engineered constructs results in inferior mechanical properties compared to native arteries (210). Long and Tranquillo showed that the type of scaffold and cells chosen affects elastogenesis in tissue-engineered arteries, with increased elastin amounts secreted from neonatal compared to adult cells and on fibrin compared to collagen scaffolds (211). They also used chemokines known to increase steady state elastin mRNA expression, but the resulting elastic fiber structure in their constructs does not resemble arterial elastic laminae. Trying to replicate *in vivo* loading conditions, Kim et al. showed that long term application of circumferential cyclic strain increases tropoelastin mRNA and protein expression, along with increasing the material stiffness and ultimate tensile strength of tissue-engineered arteries, although the mechanical properties are still inferior to native aorta (212). Huang et al. recently showed that application of biaxial cyclic strain, more representative of the *in vivo* loading environment, produces tissue-engineered arteries with evidence of mature elastic fibers and improved mechanical properties compared to circumferentially strained constructs or constructs grown without cyclic strain (213). A tissue-engineered graft implanted as a pulmonary artery replacement in 8 week old lambs, exposed to cytokines and mechanical loading present in early maturation and growth, showed abundant elastic fiber deposition and about 50% of the insoluble elastin levels of the native pulmonary artery when evaluated 42 weeks after implantation (214). Overall, these results demonstrate the importance of reproducing the biochemical and

biomechanical environment of developing arteries to encourage elastogenesis in tissue engineering.

2.6 Summary and Future Directions

We have summarized genetic and acquired cardiovascular diseases linked to elastin and elastic fiber defects with a focus on large artery mechanics. Elastin and elastic fibers play a critical mechanical role at multiple length scales from pulse wave reflections in the cardiovascular system, to local material properties of the arterial wall, to interactions of tropoelastin with VSMCs. Elastin is a unique protein due to its limited time period of synthesis, long half-life, multi-step assembly process, and high degree of crosslinking that provides mechanical elasticity to the large arteries. Acquired damage to the elastic fibers is especially problematic due to the inability of the organism to generate *de novo* elastic fibers post-adolescence. Despite the increasing therapeutic options for controlling diseases such as hypertension, obesity, and diabetes, elastic fiber damage is currently irreparable meaning that the cardiovascular risks associated with arterial stiffness may persist even when other disease aspects are controlled. The process of elastic fiber assembly, especially inducing assembly *in vitro* or *in vivo*, is an active and important area of investigation for treating elastinopathies and the associated changes in cardiovascular mechanics, as well as advancing tissue engineering.

We would like to highlight the differential effects of reduced elastin amounts compared to improper assembly or degradation of elastic fibers. Reduced elastin amounts lead to altered arterial wall structure, narrowed arterial lumen, increased arterial structural stiffness, and hypertension in humans and mice. In mice, the structural, mechanical, and functional phenotypes scale with elastin amounts. For the most part, mice appear to adapt reasonably well to 50-60%

elastin, with more severe phenotypes appearing when elastin amounts drop to 30-40% of normal. The mouse studies suggest that a threshold amount of elastin may provide near normal cardiovascular function in genetic diseases associated with elastin insufficiency. Hence, therapies that moderately increase elastin amounts, rather than completely restoring them to normal levels, may be sufficient for improved cardiovascular outcomes.

Improperly assembled or degraded elastic fibers alter the passive mechanical properties of the arterial wall. The consequences extend far beyond physical changes to the elastic fibers to the initiation of several arterial remodeling events including VSMC phenotype modulation, ECM deposition, inflammatory cell infiltration, and the release of EDPs. EDPs stimulate cytokine signaling and activate inflammatory cells. The inflammatory cells secrete proteases that contribute to additional elastic fiber degradation in a positive feedback cycle. It is unclear whether the arterial remodeling signaling cascade is similar for genetic diseases with improperly assembled elastic fibers, such as ADCL1, and acquired diseases with elastic fiber degradation such as diabetes or abdominal aortic aneurysms. However, elastic fiber fragmentation, inflammatory signaling, and arterial stiffening are common factors in many of the cardiovascular diseases discussed in this review. Better understanding of the biochemical and biomechanical signaling associated with improperly assembled or degraded elastic fibers may allow therapeutic interventions that halt or slow down the arterial remodeling cascade and prevent disease progression.

2.7 Acknowledgements

Data presented in this study was partially funded by NIH grants HL115560 and HL105314.

2.8 References

1. Vrhovski B, Weiss AS. Biochemistry of tropoelastin. *Eur J Biochem.* 1998;258(1):1-18.
2. Kozel BA, Mecham RP, Rosenbloom J. Elastin. In: Mecham RP, editor. *The Extracellular Matrix: an Overview.* Berlin: Springer-Verlag; 2011. p. 267-301.
3. Sandberg LB, Weissman N, Gray WR. Structural features of tropoelastin related to the sites of cross-links in aortic elastin. *Biochemistry.* 1971;10:52-8.
4. Gray WR, Sandberg LB, Foster JA. Molecular model for elastin structure and function. *Nature.* 1973;246(5434):461-6.
5. Olliver L, Luvalle PA, Davidson JM, Rosenbloom J, Mathew CG, Bester AJ, et al. The gene coding for tropoelastin is represented as a single copy sequence in the haploid sheep genome. *Coll Relat Res.* 1987;7(1):77-89.
6. Tassabehji M, Metcalfe K, Donnai D, Hurst J, Reardon W, Burch M, et al. Elastin: genomic structure and point mutations in patients with supraaortic stenosis. *Human molecular genetics.* 1997;6(7):1029-36.
7. Bashir MM, Indik Z, Yeh H, Ornstein-Goldstein N, Rosenbloom JC, Abrams W, et al. Characterization of the complete human elastin gene. Delineation of unusual features in the 5'-flanking region. *J Biol Chem.* 1989;264(15):8887-91.
8. Yeh H, Anderson N, Ornstein-Goldstein N, Bashir MM, Rosenbloom JC, Abrams W, et al. Structure of the bovine elastin gene and S1 nuclease analysis of alternative splicing of elastin mRNA in the bovine nuchal ligament. *Biochemistry.* 1989;28(6):2365-70.
9. Pierce RA, Deak SB, Stolle CA, Boyd CD. Heterogeneity of rat tropoelastin mRNA revealed by cDNA cloning. *Biochemistry.* 1990;29(41):9677-83.
10. Burnett W, Finnigan-Bunick A, Yoon K, Rosenbloom J. Analysis of elastin gene expression in the developing chick aorta using cloned elastin cDNA. *J Biol Chem.* 1982;257(4):1569-72.
11. Parks WC, Secrist H, Wu LC, Mecham RP. Developmental regulation of tropoelastin isoforms. *J Biol Chem.* 1988;263(9):4416-23.
12. Pollock J, Baule VJ, Rich CB, Ginsburg CD, Curtiss SW, Foster JA. Chick tropoelastin isoforms. From the gene to the extracellular matrix. *J Biol Chem.* 1990;265(7):3697-702.
13. Sephel GC, Buckley A, Davidson JM. Developmental initiation of elastin gene expression by human fetal skin fibroblasts. *J Invest Dermatol.* 1987;88(6):732-5.
14. Davidson JM, Smith K, Shibahara S, Tolstoshev P, Crystal RG. Regulation of elastin synthesis in developing sheep nuchal ligament by elastin mRNA levels. *J Biol Chem.* 1982;257(2):747-54.
15. Dubick MA, Rucker RB, Cross CE, Last JA. Elastin metabolism in rodent lung. *Biochimica et biophysica acta.* 1981;672(3):303-6.
16. Myers B, Dubick M, Last JA, Rucker RB. Elastin synthesis during perinatal lung development in the rat. *Biochimica et biophysica acta.* 1983;761(1):17-22.
17. Ritz-Timme S, Laumeier I, Collins MJ. Aspartic acid racemization: evidence for marked longevity of elastin in human skin. *Br J Dermatol.* 2003;149(5):951-9.
18. Rucker RB, Tinker D. Structure and metabolism of arterial elastin. *Int Rev Exp Pathol.* 1977;17:1-47.
19. Shapiro SD, Endicott SK, Province MA, Pierce JA, Campbell EJ. Marked longevity of human lung parenchymal elastic fibers deduced from prevalence of D-aspartate and nuclear weapons-related radiocarbon. *J Clin Invest.* 1991;87(5):1828-34.

20. James MF, Rich CB, Trinkaus-Randall V, Rosenbloom J, Foster JA. Elastogenesis in the developing chick lung is transcriptionally regulated. *Developmental dynamics : an official publication of the American Association of Anatomists*. 1998;213(2):170-81.
21. Hungerford JE, Owens GK, Argraves WS, Little CD. Development of the aortic vessel wall as defined by vascular smooth muscle and extracellular matrix markers. *Dev Biol*. 1996;178(2):375-92.
22. Swee MH, Parks WC, Pierce RA. Developmental regulation of elastin production. Expression of tropoelastin pre-mRNA persists after down-regulation of steady-state mRNA levels. *J Biol Chem*. 1995;270(25):14899-906.
23. Zhang M, Pierce RA, Wachi H, Mecham RP, Parks WC. An open reading frame element mediates posttranscriptional regulation of tropoelastin and responsiveness to transforming growth factor beta1. *Molecular and cellular biology*. 1999;19(11):7314-26.
24. Kucich U, Rosenbloom JC, Abrams WR, Bashir MM, Rosenbloom J. Stabilization of elastin mRNA by TGF-beta: initial characterization of signaling pathway. *Am J Respir Cell Mol Biol*. 1997;17(1):10-6.
25. Kucich U, Rosenbloom JC, Abrams WR, Rosenbloom J. Transforming growth factor-beta stabilizes elastin mRNA by a pathway requiring active Smads, protein kinase C-delta, and p38. *American journal of respiratory cell and molecular biology*. 2002;26(2):183-8.
26. Sauvage M, Hinglais N, Mandet C, Badier C, Deslandes F, Michel JB, et al. Localization of elastin mRNA and TGF-beta1 in rat aorta and caudal artery as a function of age. *Cell and tissue research*. 1998;291(2):305-14.
27. Marigo V, Volpin D, Bressan GM. Regulation of the human elastin promoter in chick embryo cells. Tissue-specific effect of TGF-beta. *Biochimica et biophysica acta*. 1993;1172(1-2):31-6.
28. Sproul EP, Argraves WS. A cytokine axis regulates elastin formation and degradation. *Matrix Biol*. 2013;32(2):86-94.
29. Gadson PF, Jr., Rossignol C, McCoy J, Rosenquist TH. Expression of elastin, smooth muscle alpha-actin, and c-jun as a function of the embryonic lineage of vascular smooth muscle cells. *In vitro cellular & developmental biology Animal*. 1993;29A(10):773-81.
30. Mecham RP, Madaras J, McDonald JA, Ryan U. Elastin production by cultured calf pulmonary artery endothelial cells. *J Cell Physiol*. 1983;116(3):282-8.
31. Cantor JO, Keller S, Parshley MS, Darnule TV, Darnule AT, Cerreta JM, et al. Synthesis of crosslinked elastin by an endothelial cell culture. *Biochemical and biophysical research communications*. 1980;95(4):1381-6.
32. Ushiki T, Murakumo M. Scanning electron microscopic studies of tissue elastin components exposed by a KOH-collagenase or simple KOH digestion method. *Arch Histol Cytol*. 1991;54(4):427-36.
33. Ruckman JL, Luvalle PA, Hill KE, Giro MG, Davidson JM. Phenotypic stability and variation in cells of the porcine aorta: collagen and elastin production. *Matrix Biol*. 1994;14(2):135-45.
34. Lucero HA, Kagan HM. Lysyl oxidase: an oxidative enzyme and effector of cell function. *Cell Mol Life Sci*. 2006;63(19-20):2304-16.
35. Urry DW. Entropic elastic processes in protein mechanisms. I. Elastic structure due to an inverse temperature transition and elasticity due to internal chain dynamics. *J Protein Chem*. 1988;7(1):1-34.

36. Cox BA, Starcher BC, Urry DW. Communication: Coacervation of tropoelastin results in fiber formation. *J Biol Chem.* 1974;249(3):997-8.
37. Volpin D, Urry DW, Cox BA, Gotte L. Optical diffraction of tropoelastin and alpha-elastin coacervates. *Biochimica et biophysica acta.* 1976;439(1):253-8.
38. Clarke AW, Arnspang EC, Mithieux SM, Korkmaz E, Braet F, Weiss AS. Tropoelastin massively associates during coacervation to form quantized protein spheres. *Biochemistry.* 2006;45(33):9989-96.
39. Toonkool P, Jensen SA, Maxwell AL, Weiss AS. Hydrophobic domains of human tropoelastin interact in a context-dependent manner. *The Journal of biological chemistry.* 2001;276(48):44575-80.
40. Pasquali-Ronchetti I, Baccarani-Contri M. Elastic fiber during development and aging. *Microsc Res Tech.* 1997;38(4):428-35.
41. Kagan HM, Vaccaro CA, Bronson RE, Tang SS, Brody JS. Ultrastructural immunolocalization of lysyl oxidase in vascular connective tissue. *J Cell Biol.* 1986;103(3):1121-8.
42. Narayanan AS, Page RC, Kuzan F, Cooper CG. Elastin cross-linking in vitro. Studies on factors influencing the formation of desmosines by lysyl oxidase action on tropoelastin. *Biochem J.* 1978;173(3):857-62.
43. Kielty CM, Sherratt MJ, Shuttleworth CA. Elastic fibres. *J Cell Sci.* 2002;115(Pt 14):2817-28.
44. Reiser K, McCormick RJ, Rucker RB. Enzymatic and nonenzymatic cross-linking of collagen and elastin. *FASEB J.* 1992;6(7):2439-49.
45. Foster JA, Rubin L, Kagan HM, Franzblau C, Bruenger E, Sandberg LB. Isolation and characterization of cross-linked peptides from elastin. *J Biol Chem.* 1974;249(19):6191-6.
46. Stoilov I, Starcher BC, Mecham RP, Broekelmann TJ. Measurement of elastin, collagen, and total protein levels in tissues. *Methods Cell Biol.* 2018;143:133-46.
47. Sakai LY, Keene DR, Engvall E. Fibrillin, a new 350-kD glycoprotein, is a component of extracellular microfibrils. *J Cell Biol.* 1986;103(6 Pt 1):2499-509.
48. Zhang H, Apfelroth SD, Hu W, Davis EC, Sanguineti C, Bonadio J, et al. Structure and expression of fibrillin-2, a novel microfibrillar component preferentially located in elastic matrices. *J Cell Biol.* 1994;124(5):855-63.
49. Wagenseil JE, Mecham RP. New insights into elastic fiber assembly. *Birth Defects Res C Embryo Today.* 2007;81(4):229-40.
50. Yanagisawa H, Davis EC. Unraveling the mechanism of elastic fiber assembly: The roles of short fibulins. *Int J Biochem Cell Biol.* 2010;42(7):1084-93.
51. Papke CL, Yanagisawa H. Fibulin-4 and fibulin-5 in elastogenesis and beyond: Insights from mouse and human studies. *Matrix Biol.* 2014;37:142-9.
52. Maurice P, Blaise S, Gayral S, Debelle L, Laffargue M, Hornebeck W, et al. Elastin fragmentation and atherosclerosis progression: the elastokine concept. *Trends Cardiovasc Med.* 2013;23(6):211-21.
53. Kim YM, Haghghat L, Spiekerkoetter E, Sawada H, Alvira CM, Wang L, et al. Neutrophil elastase is produced by pulmonary artery smooth muscle cells and is linked to neointimal lesions. *Am J Pathol.* 2011;179(3):1560-72.
54. Yu Q, Stamenkovic I. Cell surface-localized matrix metalloproteinase-9 proteolytically activates TGF-beta and promotes tumor invasion and angiogenesis. *Genes Dev.* 2000;14(2):163-76.

55. Visse R, Nagase H. Matrix metalloproteinases and tissue inhibitors of metalloproteinases: structure, function, and biochemistry. *Circ Res.* 2003;92(8):827-39.
56. Yurchenco PD, O'Rear JJ. Basal lamina assembly. *Curr Opin Cell Biol.* 1994;6(5):674-81.
57. Davis EC. Smooth muscle cell to elastic lamina connections in developing mouse aorta. Role in aortic medial organization. *Lab Invest.* 1993;68(1):89-99.
58. O'Connell MK, Murthy S, Phan S, Xu C, Buchanan J, Spilker R, et al. The three-dimensional micro- and nanostructure of the aortic medial lamellar unit measured using 3D confocal and electron microscopy imaging. *Matrix Biol.* 2008;27(3):171-81.
59. Dingemans KP, Teeling P, Lagendijk JH, Becker AE. Extracellular matrix of the human aortic media: an ultrastructural histochemical and immunohistochemical study of the adult aortic media. *Anat Rec.* 2000;258(1):1-14.
60. Howard PS, Macarak EJ. Localization of collagen types in regional segments of the fetal bovine aorta. *Lab Invest.* 1989;61(5):548-55.
61. Wolinsky H. Comparison of medial growth of human thoracic and abdominal aortas. *Circ Res.* 1970;27(4):531-8.
62. Wolinsky H, Glagov S. A lamellar unit of aortic medial structure and function in mammals. *Circ Res.* 1967;20(1):99-111.
63. Shih CC, Oakley DM, Joens MS, Roth RA, Fitzpatrick JAJ. Nonlinear optical imaging of extracellular matrix proteins. *Methods Cell Biol.* 2018;143:57-78.
64. Le VP, Cheng JK, Kim J, Staiculescu MC, Ficker SW, Sheth SC, et al. Mechanical factors direct mouse aortic remodelling during early maturation. *J R Soc Interface.* 2015;12(104):20141350.
65. Sage H, Gray WR. Studies on the evolution of elastin--I. Phylogenetic distribution. *Comparative biochemistry and physiology B, Comparative biochemistry.* 1979;64(4):313-27.
66. Burton AC. Relation of Structure to Function of the Tissues of the Wall of Blood Vessels 1954 1954-10-01 00:00:00. 619-42 p.
67. Parker KH. A brief history of arterial wave mechanics. *Med Biol Eng Comput.* 2009;47(2):111-8.
68. O'Rourke MF, Safar ME. Relationship between aortic stiffening and microvascular disease in brain and kidney: cause and logic of therapy. *Hypertension.* 2005;46(1):200-4.
69. Ohtsuka S, Kakihana M, Watanabe H, Sugishita Y. Chronically decreased aortic distensibility causes deterioration of coronary perfusion during increased left ventricular contraction. *J Am Coll Cardiol.* 1994;24(5):1406-14.
70. Greenwald SE. Ageing of the conduit arteries. *The Journal of pathology.* 2007;211(2):157-72.
71. Gosling RG, Budge MM. Terminology for describing the elastic behavior of arteries. *Hypertension.* 2003;41(6):1180-2.
72. O'Rourke MF, Hashimoto J. Mechanical factors in arterial aging: a clinical perspective. *J Am Coll Cardiol.* 2007;50(1):1-13.
73. Ferruzzi J, Bersi MR, Humphrey JD. Biomechanical phenotyping of central arteries in health and disease: advantages of and methods for murine models. *Ann Biomed Eng.* 2013;41(7):1311-30.
74. Faury G, Maher GM, Li DY, Keating MT, Mecham RP, Boyle WA. Relation between outer and luminal diameter in cannulated arteries. *The American journal of physiology.* 1999;277(5 Pt 2):H1745-53.

75. Roy CS. Elastic properties of the arterial wall. *J Physiol (Lond)*. 1880;3:125-59.
76. Roach MR, Burton AC. The reason for the shape of the distensibility curves of arteries. *Can J Med Sci*. 1957;35(8):681-90.
77. Dobrin PB, Canfield TR. Elastase, collagenase, and the biaxial elastic properties of dog carotid artery. *American Journal of Physiology*. 1984;247(1 Pt 2):H124-31.
78. Fonck E, Prod'hom G, Roy S, Augsburg L, Rufenacht DA, Stergiopoulos N. Effect of elastin degradation on carotid wall mechanics as assessed by a constituent-based biomechanical model. *American journal of physiology Heart and circulatory physiology*. 2007;292(6):H2754-63.
79. Shadwick RE. Mechanical design in arteries. *J Exp Biol*. 1999;202(Pt 23):3305-13.
80. Kim J, Staiculescu MC, Cocciolone AJ, Yanagisawa H, Mecham RP, Wagenseil JE. Crosslinked elastic fibers are necessary for low energy loss in the ascending aorta. *Journal of biomechanics*. 2017;61:199-207.
81. Wagenseil JE, Nerurkar NL, Knutsen RH, Okamoto RJ, Li DY, Mecham RP. Effects of elastin haploinsufficiency on the mechanical behavior of mouse arteries. *American journal of physiology Heart and circulatory physiology*. 2005;289(3):H1209-17.
82. Faury G, Pezet M, Knutsen RH, Boyle WA, Heximer SP, McLean SE, et al. Developmental adaptation of the mouse cardiovascular system to elastin haploinsufficiency. *J Clin Invest*. 2003;112(9):1419-28.
83. Wan W, Yanagisawa H, Gleason RL, Jr. Biomechanical and microstructural properties of common carotid arteries from fibulin-5 null mice. *Ann Biomed Eng*. 2010;38(12):3605-17.
84. Jain D, Dietz HC, Oswald GL, Maleszewski JJ, Halushka MK. Causes and histopathology of ascending aortic disease in children and young adults. *Cardiovascular pathology : the official journal of the Society for Cardiovascular Pathology*. 2011;20(1):15-25.
85. Wagenseil JE, Mecham RP. Elastin in large artery stiffness and hypertension. *Journal of cardiovascular translational research*. 2012;5(3):264-73.
86. Roccabianca S, Ateshian GA, Humphrey JD. Biomechanical roles of medial pooling of glycosaminoglycans in thoracic aortic dissection. *Biomech Model Mechanobiol*. 2014;13(1):13-25.
87. Gibbons CA, Shadwick RE. Functional similarities in the mechanical design of the aorta in lower vertebrates and mammals. *Experientia*. 1989;45(11-12):1083-8.
88. Wells SM, Langille BL, Lee JM, Adamson SL. Determinants of mechanical properties in the developing ovine thoracic aorta. *Am J Physiol*. 1999;277(4 Pt 2):H1385-91.
89. Wang Z, Lakes RS, Golob M, Eickhoff JC, Chesler NC. Changes in large pulmonary arterial viscoelasticity in chronic pulmonary hypertension. *PLoS One*. 2013;8(11):e78569.
90. Karnik SK, Brooke BS, Bayes-Genis A, Sorensen L, Wythe JD, Schwartz RS, et al. A critical role for elastin signaling in vascular morphogenesis and disease. *Development*. 2003;130(2):411-23.
91. Espinosa MG, Gardner WS, Bennett L, Sather B, Yanagisawa H, Wagenseil JE. The Effects of Elastic Fiber Protein Insufficiency and Treatment on the Modulus of Arterial Smooth Muscle Cells. *J Biomech Eng*. 2013.
92. Karnik SK, Wythe JD, Sorensen L, Brooke BS, Urness LD, Li DY. Elastin induces myofibrillogenesis via a specific domain, VGVAPG. *Matrix Biol*. 2003;22(5):409-25.
93. Senior RM, Griffin GL, Mecham RP, Wrenn DS, Prasad KU, Urry DW. Val-Gly-Val-Ala-Pro-Gly, a repeating peptide in elastin, is chemotactic for fibroblasts and monocytes. *J Cell Biol*. 1984;99(3):870-4.

94. Rodgers UR, Weiss AS. Integrin alpha v beta 3 binds a unique non-RGD site near the C-terminus of human tropoelastin. *Biochimie*. 2004;86(3):173-8.
95. Lee P, Bax DV, Bilek MM, Weiss AS. A novel cell adhesion region in tropoelastin mediates attachment to integrin alphaVbeta5. *J Biol Chem*. 2014;289(3):1467-77.
96. Broekelmann TJ, Kozel BA, Ishibashi H, Werneck CC, Keeley FW, Zhang L, et al. Tropoelastin interacts with cell-surface glycosaminoglycans via its COOH-terminal domain. *The Journal of biological chemistry*. 2005;280(49):40939-47.
97. Fritze O, Romero B, Schleicher M, Jacob MP, Oh DY, Starcher B, et al. Age-related changes in the elastic tissue of the human aorta. *J Vasc Res*. 2012;49(1):77-86.
98. Duca L, Blaise S, Romier B, Laffargue M, Gayral S, El Btaouri H, et al. Matrix ageing and vascular impacts: focus on elastin fragmentation. *Cardiovasc Res*. 2016;110(3):298-308.
99. Fulop T, Jr., Wei SM, Robert L, Jacob MP. Determination of elastin peptides in normal and arteriosclerotic human sera by ELISA. *Clin Physiol Biochem*. 1990;8(6):273-82.
100. Gayral S, Garnotel R, Castaing-Berthou A, Blaise S, Fougerat A, Berge E, et al. Elastin-derived peptides potentiate atherosclerosis through the immune Neu1-PI3Kgamma pathway. *Cardiovasc Res*. 2014;102(1):118-27.
101. Maeda I, Mizoiri N, Briones MP, Okamoto K. Induction of macrophage migration through lactose-insensitive receptor by elastin-derived nonapeptides and their analog. *J Pept Sci*. 2007;13(4):263-8.
102. Simionescu A, Philips K, Vyavahare N. Elastin-derived peptides and TGF-beta1 induce osteogenic responses in smooth muscle cells. *Biochemical and biophysical research communications*. 2005;334(2):524-32.
103. Houghton AM, Quintero PA, Perkins DL, Kobayashi DK, Kelley DG, Marconcini LA, et al. Elastin fragments drive disease progression in a murine model of emphysema. *J Clin Invest*. 2006;116(3):753-9.
104. Guo G, Munoz-Garcia B, Ott CE, Grunhagen J, Mousa SA, Pletschacher A, et al. Antagonism of GxxPG fragments ameliorates manifestations of aortic disease in Marfan syndrome mice. *Human molecular genetics*. 2013;22(3):433-43.
105. Pocza P, Suli-Vargha H, Darvas Z, Falus A. Locally generated VGVAPG and VAPG elastin-derived peptides amplify melanoma invasion via the galectin-3 receptor. *Int J Cancer*. 2008;122(9):1972-80.
106. Hinek A, Wrenn DS, Mecham RP, Baronides SH. The elastin receptor: a galactoside-binding protein. *Science*. 1988;239(4847):1539-41.
107. Hinek A, Pshezhetsky AV, von Itzstein M, Starcher B. Lysosomal sialidase (neuraminidase-1) is targeted to the cell surface in a multiprotein complex that facilitates elastic fiber assembly. *J Biol Chem*. 2006;281(6):3698-710.
108. Rusциani A, Duca L, Sartelet H, Chatron-Colliet A, Bobichon H, Ploton D, et al. Elastin peptides signaling relies on neuraminidase-1-dependent lactosylceramide generation. *PLoS One*. 2010;5(11):e14010.
109. Robertson IB, Rifkin DB. Regulation of the Bioavailability of TGF-beta and TGF-beta-Related Proteins. *Cold Spring Harb Perspect Biol*. 2016;8(6).
110. Ono RN, Sengle G, Charbonneau NL, Carlberg V, Bachinger HP, Sasaki T, et al. Latent transforming growth factor beta-binding proteins and fibulins compete for fibrillin-1 and exhibit exquisite specificities in binding sites. *J Biol Chem*. 2009;284(25):16872-81.

111. Zilberberg L, Todorovic V, Dabovic B, Horiguchi M, Courousse T, Sakai LY, et al. Specificity of latent TGF-beta binding protein (LTBP) incorporation into matrix: role of fibrillins and fibronectin. *J Cell Physiol.* 2012;227(12):3828-36.
112. Wagenseil JE, Mecham RP. Vascular extracellular matrix and arterial mechanics. *Physiol Rev.* 2009;89(3):957-89.
113. Horiguchi M, Ota M, Rifkin DB. Matrix control of transforming growth factor-beta function. *Journal of biochemistry.* 2012;152(4):321-9.
114. Urban Z, Davis EC. Cutis laxa: Intersection of elastic fiber biogenesis, TGFbeta signaling, the secretory pathway and metabolism. *Matrix Biol.* 2014;33C:16-22.
115. Baldwin AK, Simpson A, Steer R, Cain SA, Kielty CM. Elastic fibres in health and disease. *Expert Rev Mol Med.* 2013;15:e8.
116. Milewicz DM, Urban Z, Boyd C. Genetic disorders of the elastic fiber system. *Matrix Biol.* 2000;19(6):471-80.
117. Denie JJ, Verheugt AP. Supravalvular aortic stenosis. *Circulation.* 1958;18(5):902-8.
118. Perou ML. Congenital supravalvular aortic stenosis. A morphological study with attempt at classification. *Arch Pathol.* 1961;71:453-66.
119. Pober BR. Williams-Beuren syndrome. *N Engl J Med.* 2010;362(3):239-52.
120. Ashkenas J. Williams syndrome starts making sense. *American journal of human genetics.* 1996;59(4):756-61.
121. Lev M. The pathologic anatomy of cardiac complexes associated with transposition of arterial trunks. *Lab Invest.* 1953;2(4):296-311.
122. Wessel A, Pankau R, Kececioglu D, Ruschewski W, Bursch JH. Three decades of follow-up of aortic and pulmonary vascular lesions in the Williams-Beuren syndrome. *Am J Med Genet.* 1994;52(3):297-301.
123. Deo SV, Burkhart HM, Dearani JA, Schaff HV. Supravalvar aortic stenosis: current surgical approaches and outcomes. *Expert Rev Cardiovasc Ther.* 2013;11(7):879-90.
124. Morrow AG, Waldhausen JA, Peters RL, Blood-Well RD, Braunwald E. Supravalvular aortic stenosis: clinical, hemodynamic and pathologic observations. *Circulation.* 1959;20:1003-10.
125. McDonald AH, Gerlis LM, Somerville J. Familial arteriopathy with associated pulmonary and systemic arterial stenoses. *British heart journal.* 1969;31(3):375-85.
126. Schmidt RE, Gilbert EF, Amend TC, Chamberlain CR, Jr., Lucas RV, Jr. Generalized arterial fibromuscular dysplasia and myocardial infarction in familial supravalvular aortic stenosis syndrome. *J Pediatr.* 1969;74(4):576-84.
127. Pober B, Johnson M, Urban Z. Mechanisms and treatment of cardiovascular disease in Williams-Beuren syndrome. *J Clin Invest.* 2008;118(5):1606-15.
128. Kozel BA, Danback JR, Waxler JL, Knutsen RH, de Las Fuentes L, Reusz GS, et al. Williams syndrome predisposes to vascular stiffness modified by antihypertensive use and copy number changes in NCF1. *Hypertension.* 2014;63(1):74-9.
129. Bird LM, Billman GF, Lacro RV, Spicer RL, Jariwala LK, Hoyme HE, et al. Sudden death in Williams syndrome: report of ten cases. *J Pediatr.* 1996;129(6):926-31.
130. Hadj-Rabia S, Callewaert BL, Bourrat E, Kempers M, Plomp AS, Layet V, et al. Twenty patients including 7 probands with autosomal dominant cutis laxa confirm clinical and molecular homogeneity. *Orphanet J Rare Dis.* 2013;8:36.

131. Callewaert B, Renard M, Huchtagowder V, Albrecht B, Hausser I, Blair E, et al. New insights into the pathogenesis of autosomal-dominant cutis laxa with report of five ELN mutations. *Hum Mutat.* 2011;32(4):445-55.
132. Duz MB, Kirat E, Coucke PJ, Koparir E, Gezdirici A, Paepe A, et al. A novel case of autosomal dominant cutis laxa in a consanguineous family: report and literature review. *Clin Dysmorphol.* 2017;26(3):142-7.
133. Li DY, Brooke B, Davis EC, Mecham RP, Sorensen LK, Boak BB, et al. Elastin is an essential determinant of arterial morphogenesis. *Nature.* 1998;393(6682):276-80.
134. Li DY, Faury G, Taylor DG, Davis EC, Boyle WA, Mecham RP, et al. Novel arterial pathology in mice and humans hemizygous for elastin. *J Clin Invest.* 1998;102(10):1783-7.
135. Li HH, Roy M, Kuscuoglu U, Spencer CM, Halm B, Harrison KC, et al. Induced chromosome deletions cause hypersociability and other features of Williams-Beuren syndrome in mice. *EMBO Mol Med.* 2009;1(1):50-65.
136. Goergen C, Li H, Francke U, Taylor C. Induced chromosome deletion in a Williams-Beuren syndrome mouse model causes cardiovascular abnormalities. *J Vasc Res.* 2011;48(2):119-29.
137. Szabo Z, Levi-Minzi SA, Christiano AM, Struminger C, Stoneking M, Batzer MA, et al. Sequential loss of two neighboring exons of the tropoelastin gene during primate evolution. *J Mol Evol.* 1999;49(5):664-71.
138. Fazio MJ, Olsen DR, Kauh EA, Baldwin CT, Indik Z, Ornstein-Goldstein N, et al. Cloning of full-length elastin cDNAs from a human skin fibroblast recombinant cDNA library: further elucidation of alternative splicing utilizing exon-specific oligonucleotides. *J Invest Dermatol.* 1988;91(5):458-64.
139. Hirano E, Knutsen RH, Sugitani H, Ciliberto CH, Mecham RP. Functional rescue of elastin insufficiency in mice by the human elastin gene: implications for mouse models of human disease. *Circ Res.* 2007;101(5):523-31.
140. Jiao Y, Li G, Korneva A, Caulk AW, Qin L, Bersi MR, et al. Deficient Circumferential Growth Is the Primary Determinant of Aortic Obstruction Attributable to Partial Elastin Deficiency. *Arterioscler Thromb Vasc Biol.* 2017;37(5):930-41.
141. Sugitani H, Hirano E, Knutsen RH, Shifren A, Wagenseil JE, Ciliberto C, et al. Alternative splicing and tissue-specific elastin misassembly act as biological modifiers of human elastin gene frameshift mutations associated with dominant cutis laxa. *The Journal of biological chemistry.* 2012;287(26):22055-67.
142. Wagenseil JE, Ciliberto CH, Knutsen RH, Levy MA, Kovacs A, Mecham RP. The importance of elastin to aortic development in mice. *American journal of physiology Heart and circulatory physiology.* 2010;299(2):H257-64.
143. Wagenseil JE, Ciliberto CH, Knutsen RH, Levy MA, Kovacs A, Mecham RP. Reduced vessel elasticity alters cardiovascular structure and function in newborn mice. *Circ Res.* 2009;104(10):1217-24.
144. Li W, Li Q, Qin L, Ali R, Qyang Y, Tassabehji M, et al. Rapamycin inhibits smooth muscle cell proliferation and obstructive arteriopathy attributable to elastin deficiency. *Arterioscler Thromb Vasc Biol.* 2013;33(5):1028-35.
145. Misra A, Sheikh AQ, Kumar A, Luo J, Zhang J, Hinton RB, et al. Integrin beta3 inhibition is a therapeutic strategy for supravalvular aortic stenosis. *J Exp Med.* 2016;213(3):451-63.

146. Staiculescu MC, Kim J, Mecham RP, Wagenseil J. Mechanical behavior and matrisome gene expression in aneurysm-prone thoracic aorta of newborn lysyl oxidase knockout mice. *Am J Physiol Heart Circ Physiol*. 2017;ajpheart 00712 2016.
147. Le VP, Knutsen RH, Mecham RP, Wagenseil JE. Decreased aortic diameter and compliance precedes blood pressure increases in postnatal development of elastin-insufficient mice. *American journal of physiology Heart and circulatory physiology*. 2011;301(1):H221-9.
148. Le VP, Wagenseil JE. Echocardiographic Characterization of Postnatal Development in Mice with Reduced Arterial Elasticity. *Cardiovasc Eng Technol*. 2012;3(4):424-38.
149. DeMarsilis AJ, Walji TA, Maedeker JA, Stoka KV, Kozel BA, Mecham RP, et al. Elastin Insufficiency Predisposes Mice to Impaired Glucose Metabolism. *J Mol Genet Med*. 2014;8(3).
150. Maedeker JA, Stoka KV, Bhayani SA, Gardner WS, Bennett L, Procknow JD, et al. Hypertension and decreased aortic compliance due to reduced elastin amounts do not increase atherosclerotic plaque accumulation in Ldlr^{-/-} mice. *Atherosclerosis*. 2016;249:22-9.
151. Stoka K, Maedeker J, Bennett L, Bhayani S, Gardner W, Procknow J, et al. Effects of Increased Arterial Stiffness on Atherosclerotic Plaque Amounts. *J Biomech Eng*. 2018.
152. Kozel BA, Knutsen RH, Ye L, Ciliberto CH, Broekelmann TJ, Mecham RP. Genetic modifiers of cardiovascular phenotype caused by elastin haploinsufficiency act by extrinsic noncomplementation. *J Biol Chem*. 2011;286(52):44926-36.
153. Halabi CM, Broekelmann TJ, Knutsen RH, Ye L, Mecham RP, Kozel BA. Chronic antihypertensive treatment improves pulse pressure but not large artery mechanics in a mouse model of congenital vascular stiffness. *Am J Physiol Heart Circ Physiol*. 2015;309(5):H1008-16.
154. Knutsen R, Beeman SC, Broekelmann TJ, Liu D, Tsang KM, Kovacs A, et al. Minoxidil improves vascular compliance, restores cerebral blood flow and alters extracellular matrix gene expression in a model of chronic vascular stiffness. *Am J Physiol Heart Circ Physiol*. 2018.
155. Khavandgar Z, Roman H, Li J, Lee S, Vali H, Brinckmann J, et al. Elastin haploinsufficiency impedes the progression of arterial calcification in MGP-deficient mice. *Journal of bone and mineral research : the official journal of the American Society for Bone and Mineral Research*. 2014;29(2):327-37.
156. Jiao Y, Li G, Li Q, Ali R, Qin L, Li W, et al. mTOR (Mechanistic Target of Rapamycin) Inhibition Decreases Mechanosignaling, Collagen Accumulation, and Stiffening of the Thoracic Aorta in Elastin-Deficient Mice. *Arterioscler Thromb Vasc Biol*. 2017;37(9):1657-66.
157. Humphrey JD, Eberth JF, Dye WW, Gleason RL. Fundamental role of axial stress in compensatory adaptations by arteries. *J Biomech*. 2009;42(1):1-8.
158. Hosoda Y, Kawano K, Yamasawa F, Ishii T, Shibata T, Inayama S. Age-dependent changes of collagen and elastin content in human aorta and pulmonary artery. *Angiology*. 1984;35(10):615-21.
159. Zhang J, Zhao X, Vatner DE, McNulty T, Bishop S, Sun Z, et al. Extracellular Matrix Disarray as a Mechanism for Greater Abdominal Versus Thoracic Aortic Stiffness With Aging in Primates. *Arterioscler Thromb Vasc Biol*. 2016;36(4):700-6.
160. Arribas SM, Hinek A, Gonzalez MC. Elastic fibres and vascular structure in hypertension. *Pharmacol Ther*. 2006;111(3):771-91.
161. Zacchigna L, Vecchione C, Notte A, Cordenonsi M, Dupont S, Maretto S, et al. Emilin1 links TGF-beta maturation to blood pressure homeostasis. *Cell*. 2006;124(5):929-42.
162. Harvey A, Montezano AC, Lopes RA, Rios F, Touyz RM. Vascular Fibrosis in Aging and Hypertension: Molecular Mechanisms and Clinical Implications. *Can J Cardiol*. 2016;32(5):659-68.

163. Mitchell GF. Arterial stiffness and hypertension: chicken or egg? *Hypertension*. 2014;64(2):210-4.
164. Pierce GL. Mechanisms and Subclinical Consequences of Aortic Stiffness. *Hypertension*. 2017;70(5):848-53.
165. Okamoto K. Spontaneous hypertension in rats. *Int Rev Exp Pathol*. 1969;7:227-70.
166. Marque V, Kieffer P, Atkinson J, Lartaud-Idjouadiene I. Elastic properties and composition of the aortic wall in old spontaneously hypertensive rats. *Hypertension*. 1999;34(3):415-22.
167. Briones AM, Gonzalez JM, Somoza B, Giraldo J, Daly CJ, Vila E, et al. Role of elastin in spontaneously hypertensive rat small mesenteric artery remodelling. *J Physiol*. 2003;552(Pt 1):185-95.
168. Safar M, Chamiot-Clerc P, Dagher G, Renaud JF. Pulse pressure, endothelium function, and arterial stiffness in spontaneously hypertensive rats. *Hypertension*. 2001;38(6):1416-21.
169. Atanasova M, Dimitrova A, Ruseva B, Stoyanova A, Georgieva M, Konova E. Quantification of elastin, collagen, and advanced glycation end products as a function of age and hypertension. In: Nagata T, editor. *Senescence*. Rijeka, Croatia: In Tech; 2012. p. 519 - 30.
170. Chamiot-Clerc P, Renaud JF, Safar ME. Pulse pressure, aortic reactivity, and endothelium dysfunction in old hypertensive rats. *Hypertension*. 2001;37(2):313-21.
171. Behmoaras J, Osborne-Pellegrin M, Gauguier D, Jacob MP. Characteristics Of The Aortic Elastic Network And Related Phenotypes In Seven Inbred Rat Strains. *American journal of physiology Heart and circulatory physiology*. 2004.
172. Osborne-Pellegrin M, Labat C, Mercier N, Challande P, Lacolley P. Changes in aortic stiffness related to elastic fiber network anomalies in the Brown Norway rat during maturation and aging. *Am J Physiol Heart Circ Physiol*. 2010;299(1):H144-52.
173. Slove S, Lannoy M, Behmoaras J, Pezet M, Sloboda N, Lacolley P, et al. Potassium channel openers increase aortic elastic fiber formation and reverse the genetically determined elastin deficit in the BN rat. *Hypertension*. 2013;62(4):794-801.
174. Sinha A, Vyavahare NR. High-glucose levels and elastin degradation products accelerate osteogenesis in vascular smooth muscle cells. *Diab Vasc Dis Res*. 2013;10(5):410-9.
175. Lillie MA, Gosline JM. Swelling and viscoelastic properties of osmotically stressed elastin. *Biopolymers*. 1996;39(5):641-52.
176. Zou Y, Zhang Y. The orthotropic viscoelastic behavior of aortic elastin. *Biomech Model Mechanobiol*. 2011;10(5):613-25.
177. Wang Y, Zeinali-Davarani S, Davis EC, Zhang Y. Effect of glucose on the biomechanical function of arterial elastin. *J Mech Behav Biomed Mater*. 2015;49:244-54.
178. Tomizawa H, Yamazaki M, Kunika K, Itakura M, Yamashita K. Association of elastin glycation and calcium deposit in diabetic rat aorta. *Diabetes Res Clin Pract*. 1993;19(1):1-8.
179. Kwan CY, Wang RR, Beazley JS, Lee RM. Alterations of elastin and elastase-like activities in aortae of diabetic rats. *Biochimica et biophysica acta*. 1988;967(2):322-5.
180. Katz PS, Trask AJ, Souza-Smith FM, Hutchinson KR, Galantowicz ML, Lord KC, et al. Coronary arterioles in type 2 diabetic (db/db) mice undergo a distinct pattern of remodeling associated with decreased vessel stiffness. *Basic Res Cardiol*. 2011;106(6):1123-34.
181. Tanno T, Yoshinaga K, Sato T. Alteration of elastin in aorta from diabetics. *Atherosclerosis*. 1993;101(2):129-34.
182. Liu J, Ma L, Yang J, Ren A, Sun Z, Yan G, et al. Increased serum cathepsin S in patients with atherosclerosis and diabetes. *Atherosclerosis*. 2006;186(2):411-9.

183. Nicoloff G, Petrova C, Christova P, Nikolov A. Detection of free elastin-derived peptides among diabetic children. *Atherosclerosis*. 2007;192(2):342-7.
184. Blaise S, Romier B, Kawecki C, Ghirardi M, Rabenoelina F, Baud S, et al. Elastin-derived peptides are new regulators of insulin resistance development in mice. *Diabetes*. 2013;62(11):3807-16.
185. Rider OJ, Tayal U, Francis JM, Ali MK, Robinson MR, Byrne JP, et al. The effect of obesity and weight loss on aortic pulse wave velocity as assessed by magnetic resonance imaging. *Obesity (Silver Spring)*. 2010;18(12):2311-6.
186. Spencer M, Unal R, Zhu B, Rasouli N, McGehee RE, Jr., Peterson CA, et al. Adipose tissue extracellular matrix and vascular abnormalities in obesity and insulin resistance. *J Clin Endocrinol Metab*. 2011;96(12):E1990-8.
187. Torun D, Ozelsancak R, Turan I, Micozkadioglu H, Sezer S, Ozdemir FN. The relationship between obesity and transforming growth factor beta on renal damage in essential hypertension. *Int Heart J*. 2007;48(6):733-41.
188. Alessi MC, Bastelica D, Morange P, Berthet B, Leduc I, Verdier M, et al. Plasminogen activator inhibitor 1, transforming growth factor-beta1, and BMI are closely associated in human adipose tissue during morbid obesity. *Diabetes*. 2000;49(8):1374-80.
189. Samad F, Yamamoto K, Pandey M, Loskutoff DJ. Elevated expression of transforming growth factor-beta in adipose tissue from obese mice. *Mol Med*. 1997;3(1):37-48.
190. Lafarge JC, Naour N, Clement K, Guerre-Millo M. Cathepsins and cystatin C in atherosclerosis and obesity. *Biochimie*. 2010;92(11):1580-6.
191. Chen JY, Tsai PJ, Tai HC, Tsai RL, Chang YT, Wang MC, et al. Increased aortic stiffness and attenuated lysyl oxidase activity in obesity. *Arterioscler Thromb Vasc Biol*. 2013;33(4):839-46.
192. Akima T, Nakanishi K, Suzuki K, Katayama M, Ohsuzu F, Kawai T. Soluble elastin decreases in the progress of atheroma formation in human aorta. *Circ J*. 2009;73(11):2154-62.
193. Krettek A, Sukhova GK, Libby P. Elastogenesis in human arterial disease: a role for macrophages in disordered elastin synthesis. *Arterioscler Thromb Vasc Biol*. 2003;23(4):582-7.
194. Newby AC. Metalloproteinase production from macrophages - a perfect storm leading to atherosclerotic plaque rupture and myocardial infarction. *Exp Physiol*. 2016;101(11):1327-37.
195. Van der Donckt C, Van Herck JL, Schrijvers DM, Vanhoutte G, Verhoye M, Blockx I, et al. Elastin fragmentation in atherosclerotic mice leads to intraplaque neovascularization, plaque rupture, myocardial infarction, stroke, and sudden death. *Eur Heart J*. 2015;36(17):1049-58.
196. Toma I, McCaffrey TA. Transforming growth factor-beta and atherosclerosis: interwoven atherogenic and atheroprotective aspects. *Cell and tissue research*. 2012;347(1):155-75.
197. Basalyga DM, Simionescu DT, Xiong W, Baxter BT, Starcher BC, Vyavahare NR. Elastin degradation and calcification in an abdominal aorta injury model: role of matrix metalloproteinases. *Circulation*. 2004;110(22):3480-7.
198. Campa JS, Greenhalgh RM, Powell JT. Elastin degradation in abdominal aortic aneurysms. *Atherosclerosis*. 1987;65(1-2):13-21.
199. Milewicz DM, Guo DC, Van T-F, Lafont AL, Papke CL, Inamoto S, et al. Genetic basis of thoracic aortic aneurysms and dissections: Focus on smooth muscle cell contractile dysfunction. *Annual Review of Genomics and Human Genetics* 2008. p. 283-302.
200. Huchtagowder V, Sausgruber N, Kim K, Angle B, Marmorstein L, Urban Z. Fibulin-4: a novel gene for an autosomal recessive cutis laxa syndrome. *Am J Hum Genet*. 2006;78(6):1075-80.

201. Guo D, Regalado ES, Gong L, Duan X, Santos-Cortez RL, Arnaud P, et al. LOX Mutations Predispose to Thoracic Aortic Aneurysms and Dissections. *Circ Res*. 2016.
202. Dietz HC, Loeys B, Carta L, Ramirez F. Recent progress towards a molecular understanding of Marfan syndrome. *American journal of medical genetics Part C, Seminars in medical genetics*. 2005;139C(1):4-9.
203. Dale MA, Xiong W, Carson JS, Suh MK, Karpisek AD, Meisinger TM, et al. Elastin-Derived Peptides Promote Abdominal Aortic Aneurysm Formation by Modulating M1/M2 Macrophage Polarization. *J Immunol*. 2016;196(11):4536-43.
204. Daugherty A, Cassis LA. Mouse models of abdominal aortic aneurysms. *Arterioscler Thromb Vasc Biol*. 2004;24(3):429-34.
205. Lysgaard Poulsen J, Stubbe J, Lindholt JS. Animal Models Used to Explore Abdominal Aortic Aneurysms: A Systematic Review. *European journal of vascular and endovascular surgery : the official journal of the European Society for Vascular Surgery*. 2016;52(4):487-99.
206. Anidjar S, Salzmann JL, Gentric D, Lagneau P, Camilleri JP, Michel JB. Elastase-induced experimental aneurysms in rats. *Circulation*. 1990;82(3):973-81.
207. Johnston WF, Salmon M, Pope NH, Meher A, Su G, Stone ML, et al. Inhibition of interleukin-1beta decreases aneurysm formation and progression in a novel model of thoracic aortic aneurysms. *Circulation*. 2014;130(11 Suppl 1):S51-9.
208. Ikonomidis JS, Gibson WC, Gardner J, Sweterlitsch S, Thompson RP, Mukherjee R, et al. A murine model of thoracic aortic aneurysms. *J Surg Res*. 2003;115(1):157-63.
209. Senemaud J, Caligiuri G, Etienne H, Delbosc S, Michel JB, Coscas R. Translational Relevance and Recent Advances of Animal Models of Abdominal Aortic Aneurysm. *Arterioscler Thromb Vasc Biol*. 2017;37(3):401-10.
210. Patel A, Fine B, Sandig M, Mequanint K. Elastin biosynthesis: The missing link in tissue-engineered blood vessels. *Cardiovasc Res*. 2006;71(1):40-9.
211. Long JL, Tranquillo RT. Elastic fiber production in cardiovascular tissue-equivalents. *Matrix Biol*. 2003;22(4):339-50.
212. Kim BS, Nikolovski J, Bonadio J, Mooney DJ. Cyclic mechanical strain regulates the development of engineered smooth muscle tissue. *Nat Biotechnol*. 1999;17(10):979-83.
213. Huang AH, Balestrini JL, Udelsman BV, Zhou KC, Zhao L, Ferruzzi J, et al. Biaxial Stretch Improves Elastic Fiber Maturation, Collagen Arrangement, and Mechanical Properties in Engineered Arteries. *Tissue Eng Part C Methods*. 2016;22(6):524-33.
214. Syedain Z, Reimer J, Lahti M, Berry J, Johnson S, Tranquillo RT. Tissue engineering of acellular vascular grafts capable of somatic growth in young lambs. *Nat Commun*. 2016;7:12951.

Chapter 3

In vitro screening for Enhanced Elastic Fiber Crosslinking by Drugs and Small Molecules

3.1 Introduction

Elastin has a myriad of physiological functions. As a major component of the arterial wall extracellular matrix (ECM), elastic fibers influence the mechanical behavior of arteries. Specifically, elastin provides elasticity to the large arteries, such that the wall can reversibly deform in response to the pulsatile cardiac loading cycle. Mature elastin, soluble tropoelastin, as well as elastin-derived peptide degeneration products have numerous signaling interactions that affect biological development, vascular smooth muscle cell (VSMC) phenotype, and progression of cardiovascular diseases including hypertension, atherosclerosis, and aneurysms. Loss of elastin function in genetic or acquired elastinopathies is associated with an increased risk of cardiac related death. For a more in-depth review on the role of elastin in physiology and disease, refer to Chapter 2 of this dissertation.

Genetic or acquired elastinopathies are associated with structural damage and compromised mechanical behavior in large arteries and small blood vessels. Tissue engineered blood vessels (TEBVs) are being developed as suitable replacements. Unfortunately, many TEBVs lack burst strength and elastic recoil that are essential to operate under the cyclic load of the cardiac cycle (1-6). Nearly 50% of an artery's dry weight is elastin, yet TEBVs have reduced elastic fiber content and lack functional elastic lamellae (3, 5, 7). Despite the importance of elastic fibers to

the structural and mechanical integrity of the arterial wall, elastic fiber production in TEBVs has been a challenge, severely restricting progress of the field (5). The ability to induce elastic fiber assembly and develop functional elastic lamellae *in vitro* is considered a necessity for the advancement of arterial tissue engineering.

The challenges associated with *in vitro* elastogenesis are likely a result of the complex temporal, mechanical, and molecular interactions that regulate elastic fiber production and maturation during *in vivo* development (8-10). Elastic fibers cannot be solubilized and then spontaneously reassembled *in vitro* like many other ECM component fibers, such as type I collagen. Various methods have been attempted in tissue engineering to induce elastic fiber assembly *in vitro*. Berglund et al. generated TEBVs by seeding cells onto an elastic fiber scaffold isolated from porcine carotids. While these TEBVs demonstrated improved mechanical properties over TEBVs generated from a collagen scaffold, they were not comparable to native arteries. Additionally, the matrix in the TEBVs did not demonstrate the capacity to restructure itself and, most importantly, no *de novo* elastic fiber synthesis was observed (6). The addition of recombinant tropoelastin (rTE) to non-elastin producing cells that maintain the expression of LOX results in the formation of mature elastic fibers. However, adding rTE to elastin producing cells did not improve the efficacy of elastic fiber synthesis (11). This result suggests that increasing the amount of available tropoelastin is not sufficient to induce additional elastic fiber synthesis. Several studies have demonstrated elastic fiber synthesis or elastin mRNA upregulation in response to mechanical stimulation *in vitro*. However, this response appears to be dependent upon the composition of the scaffold and the reported levels of mature elastic fibers are still low compared

to native arteries (12-14). Also, at least one other study had conflicting results by demonstrating attenuated elastic fiber production in response to mechanical stimulation (15).

Over 23 chemical and biological molecules have been shown to increase elastin expression, however, the majority of these studies did not quantify mature elastic fibers (16). This is in large part due to the lack of a ready method for quantifying mature elastic fibers, which is much more challenging than quantifying soluble tropoelastin or expression of elastin mRNA (17).

Additionally, few studies have focused specifically on finding factors that induce mature elastic fiber synthesis. Our study aims to develop a method for identifying factors that induce mature elastic fiber synthesis through high-throughput screening of molecules.

There is an increasing interest in the discovery of small molecules that interact with proteins and other biomolecules. Small molecule screening efforts have the potential to identify small molecules with applications that extend beyond pharmacological use including the development of investigative bioassays. Bioactive small molecules offer a complementary strategy to genetic modification strategies for discerning biological interactions, but offer advantages in that their interactions with biomolecules are usually reversible and can modulate protein-protein interactions that are difficult to investigate with genetic knockouts (18). A small molecule screening platform could identify molecules with pharmaceutical potential in the treatment of elastin deficient diseases. A small molecule inducer of elastic fiber synthesis could be used in arterial tissue engineering efforts to develop TEBVs that better mimic the structure, strength, and elasticity of native arteries. A screening technique will also be useful as an investigative tool for

identifying factors that interact with elastic fiber synthesis to improve our understanding of the elastic fiber synthesis pathway.

Generally, a high-throughput screening process occurs in three major steps; development of an assay for a targeted biological activity, a primary screen of a high number of molecules, and a secondary screen of positive hits from the primary screen to demonstrate a reproducible effect of the molecule on the targeted activity. Initially, a target biological response must be identified, and an assay must be designed to quantify the target activity in a manner that is specific and robust. In the case of our screening efforts, the target biological activity is the formation of mature elastic fibers in cell culture. The assay used to quantify elastic fiber maturation is a competitive ELISA for desmosine, an amino acid that is unique to mature, crosslinked elastic fibers, developed in Dr. Mecham's lab. We performed several validation experiments to demonstrate the ability of the desmosine ELISA to measure varying amounts of mature elastic fibers. This included measuring temporal elastic fiber production in culture across a span of 2-14 days in culture and measuring a lack of elastic fibers in cultures treated with beta-aminopropionitrile (β APN), an inhibitor of LOX which is the primary crosslinker of elastin (17).

Following target and assay selection, a primary screen is performed. Typical primary screens may involve compound libraries containing over 100,000 molecules. The size of the library is resource limited by factors including the per sample cost of the assay, the amount of time it takes to perform the screen, and the degree to which automation can be incorporated. The screen we performed may be more aptly described as a semi high-throughput screen because the compound

library contains around 1600 molecules and the complexity of the cell culture conditions and the desmosine ELISA are not readily adaptable to automation.

Primary screens prioritize high volume output and often the molecules are tested without replication. It is necessary to check assay quality in high-throughput screens since generally more robust and accurate assays have reduced risk of calling false-positives or false-negatives. A parameter called the z-factor is a specialized statistical method to score the suitability of an assay for high-throughput screening and is calculated by the following formula (19),

$$Z = 1 - \frac{(3\sigma_s + 3\sigma_{c+})}{|\mu_s - \mu_{c+}|} \quad (3.1)$$

where σ and μ are the standard deviation and mean, respectively, of the biological activity measured for the samples (s) and positive controls (c+). The z-factor can be calculated to score either the results of the entire screen, or the results from a single plate in the screen since plate-to-plate variability can be large in many assays. An assay scoring a z-factor above zero is suitable for high-throughput screening and assays approaching a z-factor of one have a greater dynamic range for detection and/or decreased variability. If more than one assay for the target biological activity is available, the z-factor can be used to determine which is better suited for high-throughput screening.

The z-factor is a useful parameter; however it requires a positive control, which may not be available. As part of this study, it was necessary to identify a positive control that could be used in the screen. Several studies have reported increased elastic fiber maturation *in vitro* when

certain growth factors were added to the culture media. Insulin promoted elastic fiber synthesis in a concentration dependent manner in primary human aortic smooth muscle cells (20), increased elastic fiber deposition was observed in human skin fibroblasts with the addition of TGF- β 1 (21), and the combination of insulin and TGF- β 1 resulted in increased elastic fibers in cardiovascular tissue-equivalents developed from primary neonatal rat smooth muscle cells (22). As part of this investigation, we tested the effect of insulin and TGF- β 1 on elastic fiber production on a rat lung fibroblast cell line, RFL6, to determine whether these growth factors would be suitable positive controls in our screening platform.

Other potential positive controls may include pharmaceuticals that have demonstrated activity towards increasing elastin expression and elastic fiber production in animal studies. Slove et al. reported increased expression of the elastin gene and other genes associated with elastic fiber synthesis in primary culture of VSMCs from Brown Norway (BN) rats treated with the antihypertensive drugs diazoxide and minoxidil. The same study also reported increased elastic fiber deposition in BN rats treated with either drug; however their method of quantifying elastin content was not reported. (23) More recently, Knutsen et al. reported increased elastic fiber deposition in elastin haploinsufficient mice treated with minoxidil, but they did not investigate the effect of minoxidil on elastic fiber production in wild-type animals (24). To our knowledge, none of these drugs have been specifically investigated for *in vitro* elastic fiber maturation prior to our study. We performed our assay on RFL6 cells treated with one of each of three antihypertensive drugs; diazoxide, captopril, and minoxidil.

After completing the primary screen assay, hit-selection is performed on the results to identify ‘hits’, or agonists to the targeted biological activity. Several statistical methodologies have been developed for hit-selection from a primary screen (25), and the appropriate method is dependent on the design of the primary screen; number of replicates, availability of positive and negative controls, and whether the results are normally distributed. For our primary screen, a single measurement was collected for each molecule tested and a positive control was unavailable so the appropriate method for hit-selection was to calculate the robust strictly standardized mean difference (SSMD*) (25).

$$SSMD^* = \frac{Y_i - \text{median}(Y_n)}{\sqrt{\frac{2}{K}(N_n - 1) \text{MAD}_n}} \quad (3.2)$$

$$K = 2 \cdot \left(\frac{\Gamma\left(\frac{N_n - 1}{2}\right)}{\Gamma\left(\frac{N_n - 2}{2}\right)} \right)^2 \approx N_n - 2.48 \quad (3.3)$$

$$\text{MAD}_n = 1.4826 \cdot \text{median}\left(\left|Y_i - \text{median}(Y)\right|\right) \quad (3.4)$$

In equations (3.2), (3.3), and (3.4), Y is the measured activity of the i th compound or negative control (n). An assumption in the SSMD* is that the majority of the compounds tested will not demonstrate agonistic activity and are treated as negative controls in the calculation such that N_n is the total number of negative controls. Compounds with a SSMD* higher than 2.12 (SSMD*

equivalent of three standard deviations above the plate mean) are positive hits in the primary screen.

A secondary screen is performed following hit selection since the primary screen is susceptible to variance and error. The secondary screen is a replication of the primary screen on only the discovered hits and with increased experimental and technical replicates. Standard *t* statistics are used to validate the activity of the hits from the primary screen. Any compounds which still demonstrate agonistic activity are potential candidates for hit-to-lead development.

We describe the ELISA assay methods, investigation of positive and negative controls, and screening process in the search for a compound that upregulates crosslinked elastic fiber production in cell culture for future application in tissue engineering and treatment of elastinopathies.

3.2 Methods

3.2.1 Cell culture

RFL6 cells retain the capacity to produce mature elastic fibers in the ECM *in vitro* (26) and were used in this study as a platform for elastic fiber crosslinking. Immortalized RFL6 cells (ATCC, CCL-192) were grown in T75 flasks in DMEM/F-12 culture media (MilliporeSigma, D8900) supplemented with 10% fetal bovine serum (FBS) (Biowest, S1620, Lot# 316C13) until 80% confluency. The cells were then detached with a brief trypsin treatment, cell density was counted, and then 6- or 48-well culture treated plates were uniformly seeded at a cell density of $1.3 \cdot 10^4$ cells/mL. At confluency (~3 days after plating) the FBS concentration in the culture media was reduced to 5%, as FBS inhibits elastic fiber synthesis at higher concentrations (17).

Additionally, at this point the cells were treated with the molecule or protein of interest. The media and molecule/protein were replaced every two days and the cell culture was maintained this way for two weeks post confluency.

Along with the molecule/protein treatments, two additional treatments were used as controls for all screening studies. Beta-aminopropionitrile (β APN) is a known inhibitor of LOX activity and is effective at preventing elastic fiber crosslinking (17). 100 μ g/mL β APN (MilliporeSigma, A3134) was used in this study as an antagonistic control. The majority of molecules used to treat the cells in this study were dissolved in (DMSO). DMSO is cytotoxic, and it was necessary to perform a DMSO concentration dependence experiment to establish a DMSO concentration that can be used without adversely effecting cell activity as measured from total protein content. From the results, 0.1v/v% DMSO was chosen as the maximum allowed volume of DMSO for the molecule library screening study and a vehicle control of DMSO was always included in the screening studies, where appropriate. In the growth factor screen, recombinant human TGF- β 1 (rhTGF- β 1, R&D Systems, 240-B) and human insulin (MilliporeSigma, I0908) were dissolved in 4 and 10mM HCl, respectively, and the appropriate vehicle control was used. The final concentration of TGF- β 1 and insulin in the culture media was $2.00 \cdot 10^{-3}$ and 2.00 μ g/mL, respectively, to replicate the experiments performed by Long and Tranquillo, 2003 (22). In the antihypertensive study, the final concentration of diazoxide (MilliporeSigma, D9035), minoxidil (MilliporeSigma, M4145), and captopril (MilliporeSigma, C4042) were 10, 6.5, and 30 μ g/mL, respectively, as determined by each molecule's maximum solubility in DMSO and a final DMSO concentration in the culture media of 0.1v/v%.

At the end of the treatment schedule for each experiment, the cells were rinsed two times with PBS buffer. The cells were scraped from the culture plates and collected in vials. The cells were immediately pelleted and dried using a SpeedVac concentrator (Savant, SPD131DDA) in preparation for hydrolysis.

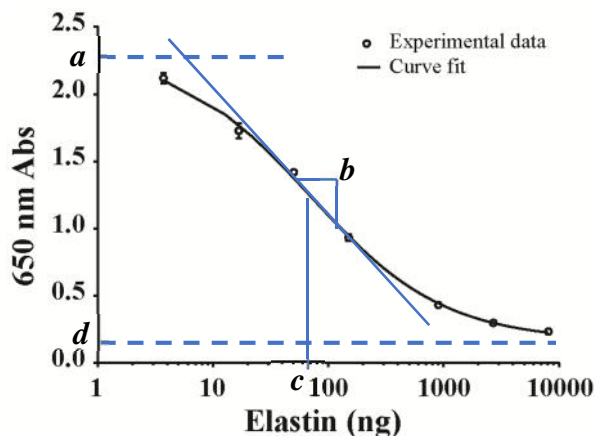
3.2.2 Cell pellet hydrolysis

The vials containing the cell pellets were enclosed in a hydrolysis chamber containing 100 μL of sequencing-grade, 6 N HCl (Thermo Fisher Scientific, 24308) and an additional 10 μL HCl in each sample vial. The hydrolysis chambers were then placed in an oven at 100°C for 48 hours, completely reducing the cellular debris to amino acids. After hydrolysis the samples were dried using a SpeedVac concentrator and then reconstituted in 100 μL of ultrapure water. From this hydrolysate, elastin content is quantified using a competitive ELISA for desmosine and total protein amount is quantified with a ninhydrin-based assay for amino acid content.

3.2.3 Competitive ELISA for desmosine quantitation

Mature elastic fiber content was quantified from the cell-pellet hydrolysates using a competitive ELISA for desmosine that was originally developed in Dr. Robert Mecham's lab (Washington University School of Medicine in St. Louis) (27). All steps of the ELISA were performed at room temperature. High binding 96-well plates (Corning, 9018) were coated with 50 μL coating buffer (50mM carbonate/bicarbonate buffer, 9.6 pH) containing desmosine-ovalbumin protein conjugate (Elastin Products Company, DOC375) for a 30-minute incubation. The coated plates were then blocked with 100 μL of blocking buffer (KPL, 50-61-01) for 15 minutes before being washed thrice with washing buffer (KPL, 50-63-01). A volume of 20 μL or 10 μL of the 100 μL hydrolysate from cells grown on 48- or 6-well plates, respectively, was added to the plate in

triplicate along with enough 0.5 M sodium phosphate buffer (7.8 pH) to bring the final volume to 50 μ L. An elastin standard curve was made from either a serial dilution of hydrolyzed, purified bovine ligament elastin (Elastin Products Company, E60) or a serial dilution of desmosine (Elastin Products Company, D866). Primary antibody binding was initiated by adding 100 μ L of 1:2000 diluted anti-serum raised in rabbits against bovine desmosine (provided by Dr. Barry Starcher's lab, University of Texas Health Science Center). This step introduces competitive binding between the desmosine that is conjugated to the ovalbumin bound to the plate and the desmosine from the sample or standard freely suspended in the well. After a 60-minute incubation period, the plate was washed again and 100 μ L of 1:2000 goat anti-rabbit IgG conjugated horseradish peroxidase (Gar-HRP) (KPL, 074-1506) was added to each well to initiate secondary antibody binding. After another 60-minute incubation period, a final wash was performed and 100 μ L of TMB substrate (KPL, 52-00-00) was promptly added to each well. TMB oxidizes HRP yielding a water-soluble reaction product that is blue in color. Color intensity of each well was measured spectrophotometrically at 650 nm detection with a plate reader (Molecular Devices, SpectraMax M2^e) at 5-minute intervals for 20 minutes. A standard curve was generated by performing a four parameter logistic regression on the absorbance values measured for the standards. An example of the desmosine ELISA standard curve a regression fit is included in Figure 3.1. Raw absorbance of each sample was converted to either elastin or desmosine concentration by comparing against the standard curve and using the 10-minute reading which was consistently below the signal saturation limit.



$$y = d + \frac{a - d}{1 + \left(\frac{x}{c}\right)^b}$$

Figure 3.1 – Example of non-linear regression with the four-parameter logistics model of the elastin standard curve used in the desmosine ELISA.

3.2.4 Ninhydrin assay for total protein quantitation

Total protein content was used to normalize elastin content for the cell-pellets and was measured using a ninhydrin-based assay for amino acid content (28). Briefly, 2 μ L or 1 μ L of the 100 μ L hydrolysate from cells grown on 48- or 6-well plates, respectively, was added to a standard 96-well plate (Thermo Fisher Scientific, 12-565-501) in triplicate. A standard curve was prepared by adding regular increments of amino acid collagen hydrolysate calibrator (Pickering Laboratories, 012506C) from 12 μ L down to 0 μ L in duplicate to the plate. The ninhydrin working reagent was prepared fresh and 100 μ L of the reagent was added to each well of the plate. The plate was covered and placed on an enclosed hotplate for a 10-minute incubation period at 85°C. Absorbance at 575 nm was measured with a plate reader (Molecular Devices, SpectraMax M2^e) and a standard curve was generated by linear regression of the standards. Total protein content of the samples was determined by comparing the raw absorbance of the samples against the standard curve.

3.2.5 Small molecule library NCI Diversity Set V

The Diversity Set V small molecule library was obtained from the Developmental Therapeutics Program (DTP) of the National Cancer Institute (NCI). This library of 1593 compounds was

derived by DTP from their molecule repository of over 140,000 compounds based on pharmacophoric diversity; each compound having at least five unique pharmacophores from the other compounds in the library. All compounds were dissolved in DMSO at 10 mM concentration.

3.2.6 Small molecule library primary screening

A total of 50, 48-well culture treated plates seeded with RFL6 cells were prepared and processed as described in section 3.3.1. Each plate was treated with 100 $\mu\text{g/mL}$ βAPN in three wells, 0.1 v/v% DMSO in three wells, and two wells were untreated. The remaining wells were each treated with one of the compounds from the NCI Diversity Set V library such that 40 different compounds were screened on every culture plate. Each compound was dissolved in DMSO and was administered to the cell culture at 0.1 v/v% such that the final molarity was 0.01 mM. As common practice with primary screening of high volume libraries, each compound was tested without replicates to reduce the time and resources necessary to screen the complete library. After the 14-day treatment schedule the cells were collected, hydrolyzed, and the biochemical assays were performed as described in previous sections.

3.2.7 Small molecule library hit selection and primary screen verification

Hit selection from the results of the primary screen was performed by calculating the SSMD* (equations (3.2), (3.3) and (3.4)) of each tested molecule on a per plate basis, assuming all other molecules on the plate were negative controls. Molecules scoring an SSMD* greater than 2.12, which is equivalent to three standard deviations above the plate mean, were denoted as positive hits. To account for variance in the biochemical assays, the remaining sample from the positive hits was used to quantify elastin and total protein again, this time using three technical replicates.

Only samples that held an elastin-to-total protein ratio three standard deviations above their respective DMSO controls were maintained as positive hits.

3.2.8 Small molecule library secondary screening and replication

A secondary screen of the positive hits identified in the primary screen was performed. The remaining molecule solutions were used to repeat the treatment of RFL6 cells as described previously. This time, experimental replicates were used ($n = 4$ for each molecule) and the desmosine ELISA and ninhydrin total protein assay were performed in triplicate for each sample. A student's *t*-test was performed to determine significant increases in elastin-to-total protein ratios of each treatment compared to a DMSO control group. Additional aliquots of each molecule that maintained an increase in mature elastic fiber production was kindly provide by DTP so that additional studies could be performed. Verification experiments of the newly acquired aliquots were performed by repeating the secondary screen but with an increased number of experimental groups ($n = 6$).

3.3 Results

3.3.1 Time course *in vitro* elastic fiber synthesis

Elastic fiber production *in vitro* tends to occur at a slower rate than other ECM proteins, and the rate of production may be cell-type specific (17). To establish a length of time for culture incubation to maximum detection with the desmosine ELISA we performed a time course experiment (Figure 3.2A). We detected a strong linear correlation ($R^2 = 0.85$) of desmosine content with length of post-confluent culture time, and the elastic fiber content increased 3.71-fold from day 2 to day 14. From these results, we decided to use a post-confluent culture time of 14 days. Although longer time periods were not tested, 14 days generated sufficient elastic fibers

to quantify and increasing the culture time period would expend additional resources unnecessarily and would increase the risk of culture contamination.

3.3.2 β APN as an inhibition control

A β APN concentration of 100 $\mu\text{g}/\text{mL}$ is sufficient for severe inhibition of LOX activity to crosslink tropoelastin into mature elastic fibers (17). We compared desmosine content of β APN treated RFL6 cells grown on 6-well culture plates to untreated cells. Using *t*-test statistics, we identified a significant ($p = 0.0003$) 92.4% reduction in desmosine content from β APN treated cells (Figure 3.2B) with a corresponding 91.2% reduction ($p = 0.0011$) in desmosine-to-total protein ratio, while total protein content remained unchanged ($p = 0.424$). Our results provide verification of the inhibitory activity of β APN within our RFL6 cell culture and demonstrate the capability of the desmosine ELISA to detect the presence and absence of mature elastic fibers produced *in vitro*.

3.3.3 DMSO cytotoxicity

At high enough concentrations, DMSO is toxic to cells and we performed a concentration profile experiment to determine what amount of DMSO can be added to RFL6 cells in culture before adverse effects are observed. The ninhydrin total protein assay was used as a proxy to quantifying cellular activity since changes in cellular processes and cell viability would be reflected in the overall protein content of the cell pellet. The results of this toxicity study are presented in Figure 3.2C. A one-way ANOVA was performed, and demonstrated a significant relationship between DMSO concentration and total protein content ($p < 0.0001$, $R^2 = 0.903$). A Bonferroni's multiple comparisons test was performed to determine p-value significance between each DMSO treated group and the untreated control group. The groups exposed to 1.0

and 0.5 v/v% DMSO had a significant 49.5% ($p < 0.0001$) and 18.6% ($p = 0.0094$) reduction, respectively, in total protein content. The group exposed to 0.1 v/v% DMSO was not significantly changed ($p > 0.9999$) from the control group. All proceeding experiments were performed using 0.1 v/v% DMSO.

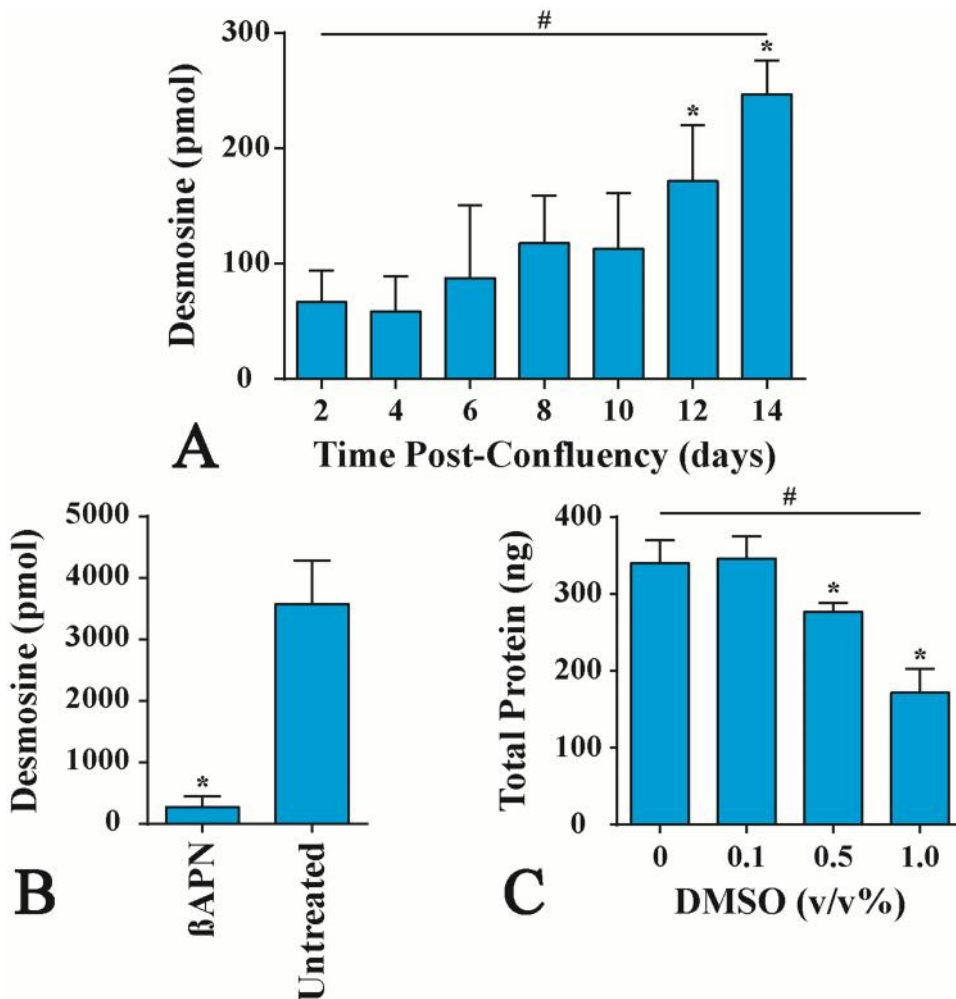


Figure 3.2 - Results from the elastic fiber screening platform development in cultured RFL6 cells. A) Temporal study demonstrating increased elastic fiber assembly over time through the measure of desmosine content. # indicates one-way ANOVA significance ($p < 0.0001$) and * indicates significance from a Bonferroni's multiple comparisons test for the 12 and 14 day samples ($p = 0.0186$ and $p < 0.0001$, respectively) in comparison to 2 days. **B)** Demonstrated elastic fiber assembly knockdown through the inhibition of LOX crosslinking by β APN. * indicates significance ($p = 0.0003$) by student's *t*-test between groups. **C)** Cytotoxicity of DMSO on cultured cells. # indicates significance in total protein content with DMSO volume concentration percentage by one-way ANOVA ($p < 0.0001$). * Higher DMSO concentrations had significantly reduced total protein compared to untreated cells by Bonferroni's multiple comparisons test ($p < 0.01$) whereas the cells treated with 0.1 v/v% DMSO has no significant difference in total protein.

3.3.4 Suitability of insulin and TGF- β 1 as positive controls

Ideally, a positive control for mature elastic fiber production would be used in the small molecule library screen in order to perform a z-factor analysis to gauge the suitability of the desmosine ELISA for high-throughput screening. However, there is a lack of known factors capable of upregulating elastic fiber synthesis *in vitro*. A combination of insulin and TGF- β 1 demonstrated elastic fiber production in cardiovascular equivalents by Long and Tranquillo, 2003 (22). We performed our screening method to determine whether these growth factors could induce elastic fiber formation in our RFL6 cells and be used as a positive control for the small molecule library screen. The resulting desmosine-to-total protein ratio is presented in Figure 3.3.

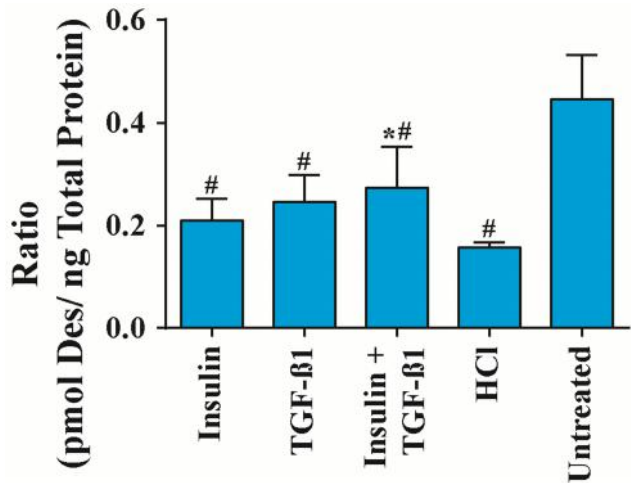


Figure 3.3 - Measured desmosine-to-total protein ratio using our elastic fiber assembly screening platform and a treatment with growth factors insulin and TGF- β 1. Growth factors were solubilized in HCl and an HCl vehicle control was included. # indicates significant ($p < 0.0001$) reduction in the ratio in groups containing HCl compared to the untreated group through Bonferroni's multiple comparisons test. * represents significant increases ($p = 0.0049$) in treatment groups compared to the HCl vehicle control.

All treatment groups used HCl as a solvent for the growth factors and so an HCl vehicle control matching the highest HCl concentration of the treatment groups was used in addition to an untreated group. A one-way ANOVA was performed on the results, and a Bonferroni multiple comparisons test was used to compare individual experiment groups. All groups containing HCl resulted in a significant ($p < 0.0001$) reduction in elastic fiber production compared to the untreated group. In comparison to the HCl vehicle control, the insulin and TGF- β 1 groups were unchanged but the group treated with both growth factors resulted in a 1.75-fold increase ($p = 0.0049$) in elastin-to-total protein ratio. There were no significant changes in the total protein

levels acquired from the ninhydrin assay, indicating the changes observed in the ratio are attributable to changes in elastic fiber production.

The z-factor parameter (equation (3.1)), using the combined insulin and TGF- β 1 treatment as the positive control and the HCl vehicle as the sample, was determined to be -1.18. This z-factor would indicate that our assay is too unreliable to be used in a high-throughput screen, however the result is complicated by the observed reduction in elastic fiber production by the HCl control. This z-factor is not indicative of how the screen would perform because the molecules from the library are dissolved in DMSO rather than HCl. Hence, we decided not to use insulin and TGF- β 1 as a positive control.

3.3.5 Suitability of antihypertensive drugs as positive controls

The result of the antihypertensive drug screen on mature elastic fiber production is presented in Figure 3.4. A one-way ANOVA and Bonferroni's multiple comparisons test was performed on the results. Only the β APN inhibition control demonstrated a significant change compared to either the DMSO ($p = 0.004$) control. None of the antihypertensive drugs tested demonstrated increased elastic fiber production. Hence, the antihypertensive drugs were also not a suitable positive control for the small molecule library screen.

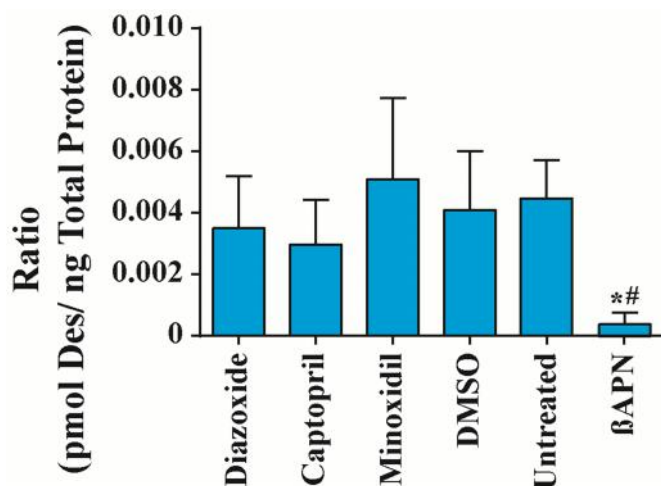


Figure 3.4 - Measured desmosine-to-total protein ratio using our elastic fiber assembly screening platform and treatment of the RFL6 cells with antihypertensive drugs diazoxide, captopril, and minoxidil. Only the APN negative control demonstrated a significant change from either DMSO vehicle control (*, $p = 0.0040$) or untreated control (#, $p = 0.0023$) by Bonferroni's multiple comparisons test.

3.3.6 Primary screening

We proceeded with the small molecule screen with a negative control (β APN), but no positive control. The results of the primary screen of the nearly 1600 molecules from the NCI Diversity Set V small molecule library are presented in Figure 3.5 as a scatterplot of the total protein content on the x-axis and elastin content on the y-axis. Control groups treated with either β APN, 0.1v/v% DMSO, or untreated are also presented on the plot. Without a control for positive upregulation of elastic fiber product a z-factor cannot be determined, however the relative clustering of the control groups on the scatter plot can provide some indication of the reproducibility of the screening process.

The β APN controls from all 25 assay plates appear to cluster low on the elastin content-axis, as expected, but there is a large spread on the total protein content-axis. The ninhydrin total protein assay is very robust, so this spread is likely an indication of variability in the cell culture conditions. The DMSO and untreated controls cluster together on both axes, indicating that DMSO is not having an effect on either the elastin or total protein content. The samples that are treated with one of the molecules from the library have a wide range on both axes. Any sample deviating outside of the range of either the DMSO or untreated control may be an indication that

the molecule has some bioactivity within our cell culture. In the case of total protein content, samples that are lower than any of the control groups could be an indication that the molecule has some level of cytotoxicity. Samples that are below zero on the total protein-axis did not have a cell pellet at the end of the two-week culture. These samples still have a minimal level on the elastin content-axis indicating that this is likely the level of background noise for the desmosine ELISA. This observation is corroborated by the results of the β APN controls which have a similar range on the elastin content-axis.

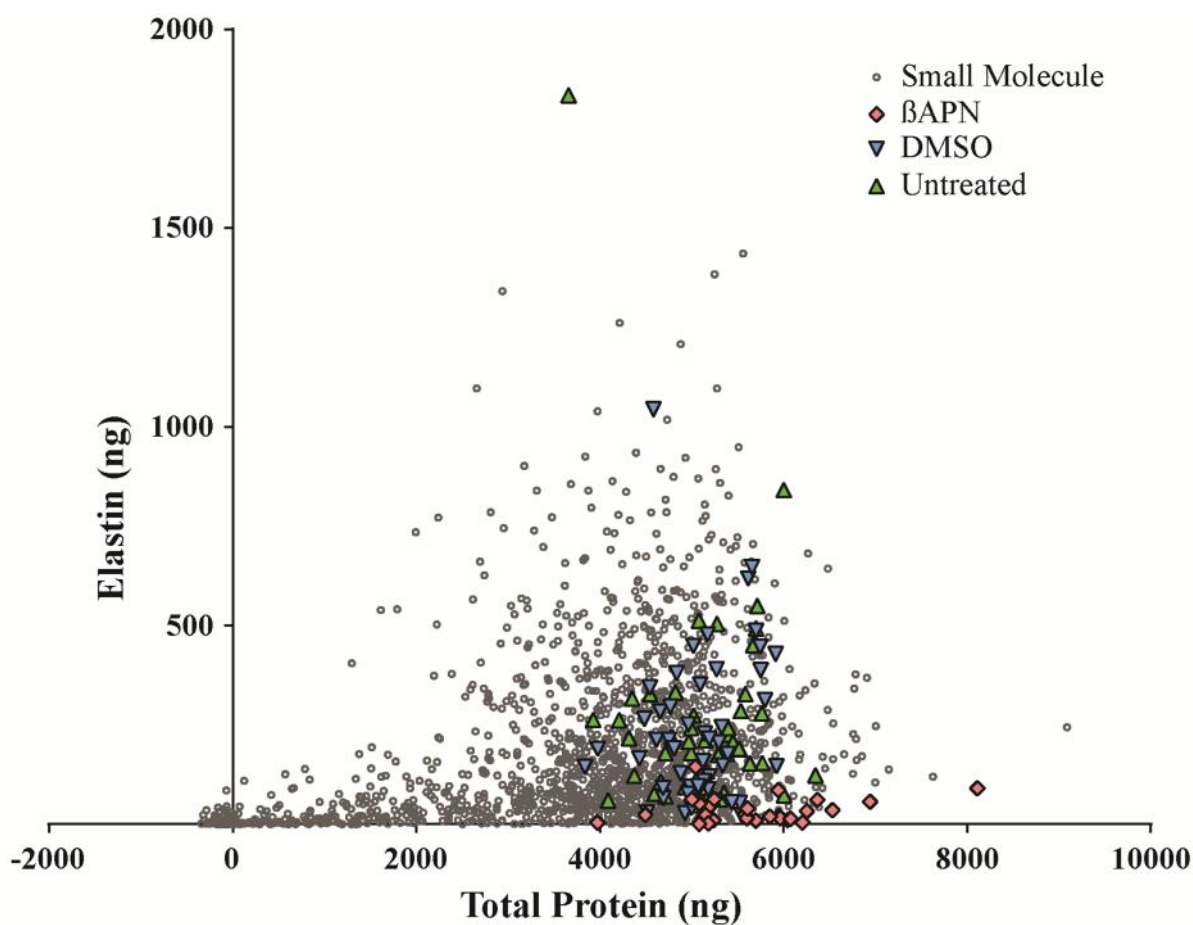


Figure 3.5 - Scatterplot presenting the results of the primary screen of the NCI Diversity Set V small molecule library from DTP. Total protein content is shown on the x-axis and elastin content on the y-axis. The entirety of the screen occurred over 50 48-well plates of cultured RFL6 cells and 25 96-well plates for each of the biochemical assays. APN inhibitory control, DMSO vehicle control and untreated controls from each culture plate are included on the scatterplot. Each small molecule treatment was performed without experimental or technical replicates. Controls had multiple experimental replicates but no technical replicates.

The SSMD* parameter, calculated using equations (3.2), (3.3), and (3.4), for every molecule in the library is present in a histogram in Figure 3.6A. Any sample having an SSMD* greater than 2.12 is scored as a positive hit, of which there were 21 in total. Samples having an SSMD* less than -2.12 may potentially be a negative hit, however all of those samples also lacked a cell pellet or had very low total protein content. Rather than negative hits, these samples either resulted from a cytotoxic effect of the molecule or the cell culture was inviable for other reasons.

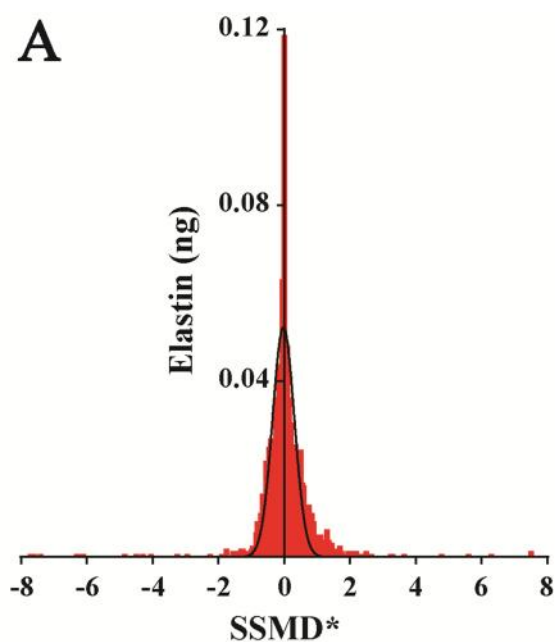
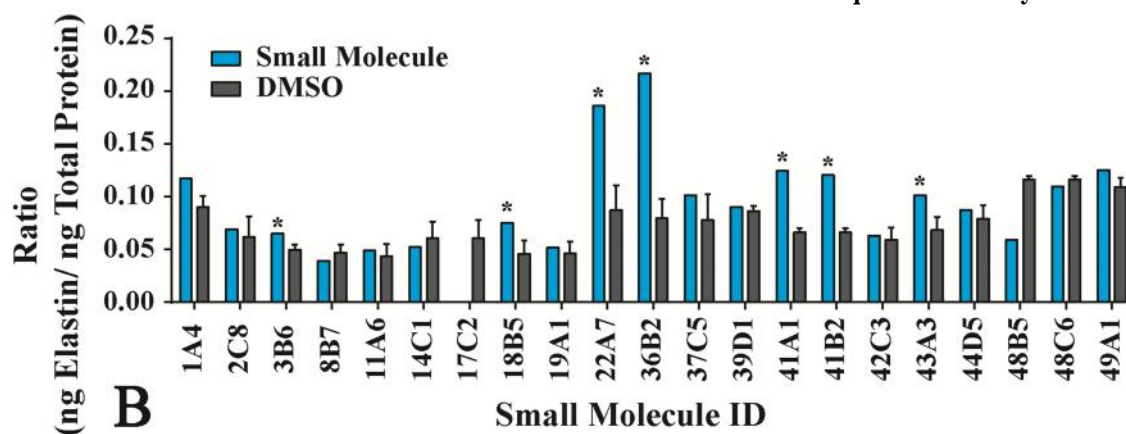


Figure 3.6 - Hit selection of the primary screen and verification of the primary screen positive hits by increased biochemical assay technical replicates of the remaining sample collected in the primary screen. A) Histogram of the SSMD* parameter calculated for each small molecule tested in the screen. Treatments scoring an SSMD* greater than 2.12 are positive hits, of which 21 were tabulated and were used in subsequent screening. B) Elastic fiber content and total protein content measures were repeated with three additional technical replicates along with their respective DMSO controls. * indicates the treatments that maintained an elastin-to-total protein ratio greater than three standard deviations above DMSO control. In total, 7 molecules were maintained as positive hits and we used in the subsequent secondary screen.



Without a z-factor calculation and because of the apparent variability of the desmosine ELISA, the biochemical assays were repeated on the remaining sample for each of the positive hits and

their respective DMSO control, this time in triplicate. The results of this primary screen validation experiment are presented in Figure 3.6B. Of the 21 molecules scored as positive hits in the primary screen, only seven molecules maintained an elastin-to-total protein ratio that was three standard deviations above their respective DMSO control. These seven molecules were used in the secondary screen of this study.

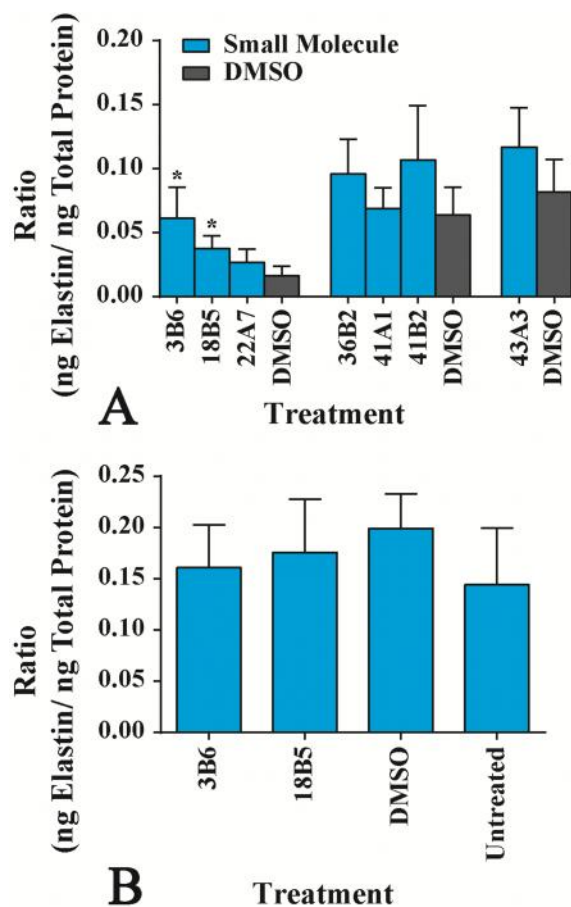


Figure 3.7 - Elastin-to-total protein ratios of the 7 primary screen positive hits in a secondary screen (A) and secondary screen validation (B). A) Treatments in the secondary screen were performed with four experimental replicates and three technical replicates. * indicates significance by student's *t*-test molecules 3B6 ($p = 0.0303$) and 18B5 ($p = 0.0154$) compared to their respective DMSO controls. B) Additional stock of molecules 3B6 and 18B5 was received from DTP and a validation screen was performed with six experimental replicates and three technical replicates. There was no statistical difference between treated and untreated groups.

3.3.7 Secondary screening

The results from the secondary screen are presented in Figure 3.7A as the elastin-to-total protein ratio of each of the seven positive hits and respective DMSO controls from the same cell culture plate.

A student's *t*-test was performed to compare the result of each treatment to the DMSO control. Molecules 3B6 ($p = 0.0303$) and 18B5 ($p = 0.0154$) were significantly increased while these rest of the molecules were statistically

unchanged. Additional stock of molecules 3B6 and 18B5 were requested from, and kindly provided by, DTP for additional experimentation. A secondary screen validation experiment was performed with

these two molecules (Figure 3.7B), however neither of them demonstrated significantly increased elastic fiber production.

3.4 Discussion

High-throughput screening is a high-risk method for identifying bioactive molecules, but the discovery of such molecules could have tremendous positive impact on the area of interest. In our study, the identification of a molecule with elastic fiber synthesis inducing activity could have positive impact on the development of pharmaceutical therapies for diseases related to genetic or acquired elastic fiber deficiency. Additionally, this molecule could move the tissue engineering field forward in the development of TEBVs that better mimic the structural, mechanical, and biochemical properties of native arterials and blood vessels. While an inducer was not uncovered from our screening efforts, we have demonstrated that our platform has the capacity for semi high-throughput screening and serves as a proof of concept. With further improvements on the reliability of the platform it could be used for future screens.

Our platform could also be used to screen factors that have been identified as upregulators of tropoelastin expression for the presence of increased mature elastic fiber production.

Approximately 19 molecular factors have been shown to upregulate elastin gene expression, however it has been shown that increased levels of tropoelastin (elastic fiber precursor) is not sufficient for *de novo* elastic fiber synthesis (11, 16). The majority of these factors are untested for their effect on elastic fiber synthesis.

One improvement needed for our platform is the identification of suitable positive control, but the lack of rigorously tested factors that induce elastic fiber formation is a limitation. While the

combination treatment of insulin and TGF- β 1 did increase elastic fiber production compared to the HCl control, the overall effect of HCl on reducing elastic fiber production was unexpected. The final HCl concentration experienced by the cells was 52 μ M. This low concentration is not expected to drastically change the pH of the culture media and no change to the color of the phenol red in the media was observed. Within a limited context, our results of the growth factor study confirmed the results observed in Long and Tranquillo, 2003. This demonstrated the utility of our platform outside of high-throughput screening.

We also evaluated three antihypertensive drugs; diazoxide, captopril, and minoxidil to potentially serve as positive controls. Diazoxide and minoxidil have been shown to upregulate tropoelastin expression *in vitro*, (23) however our results indicate that none of these drugs have an effect on crosslinked elastin amounts in our RFL6 cell culture. Recently, minoxidil treatment in *Eln*^{+/-} mice demonstrated increased elastic fiber deposition compared to untreated *Eln*^{+/-} mice, however this study did not report any results on minoxidil treated *Eln*^{+/+} mice (24) The result in our study with minoxidil further establishes that upregulation of tropoelastin expression is not sufficient for increased elastic fiber crosslinking and any elastic fiber maturation inductive activity may be dependent on factors including cell type, *in vitro/in vivo* experimentation, or the genetic predisposition of the organism.

Another potential improvement that could be developed for our screening platform is to limit the scope of the bioactivity that we are interested in from a potential molecule enhancer. Elastic fiber assembly is a complex process that may involve as many as 30 proteins, many of which have an undiscovered role in the process (29). Elastic fiber assembly is also a multi-step process and it is

unclear which steps may be rate-limiting *in vitro*. The desmosine ELISA we used in our screening platform specifically targets elastic fiber crosslinking, thereby quantifying the final product of the elastic fiber synthesis pathway. While an increase in mature elastic fibers is the desired effect, there may not be any one single molecule with the bioactivity to accomplish this. It is possible that multiple components of the elastic fiber synthesis pathway are required to be independently influenced to induce mature elastic fiber production. The requirement of both insulin and TGF- β 1 to produce higher levels of elastic fibers than the HCl control is an example of the requirement of multiple factors. TGF- β 1 is believed to promote elastic fiber synthesis by through the stabilization and subsequent accumulation of elastin mRNA (30-32). Insulin may have a role in triggering transcription of the elastin gene and insulin signaling may promote the transport of tropoelastin to the cell membrane (20). It is possible that the cells need to be made more amenable towards elastic fiber synthesis by the inclusion of these growth factors in order to be able to screen a molecule library for agonistic activity.

3.5 Summary

We developed a platform for screening mature elastic fiber production and used this platform to screen the NCI Diversity Set V library of 1593 small molecules provided from DTP. A competitive ELISA for desmosine was used to determine mature, crosslinked elastic fiber content produced by RFL6 cells in culture. To account for plate-to-plate variance in the cell culture conditions, total protein content determined by a ninhydrin assay was used to normalize the results of the desmosine ELISA. Using β APN, an inhibitor of elastin crosslinking, we demonstrated that the ELISA can detect the presence and absence of elastic fibers in our platform (Figure 3.2B). We performed a time course study to determine that 14-days in culture was sufficient for RFL6 cells to produce high levels of elastic fibers (Figure 3.2A). We

determined that 48-well plates are the smallest surface area from which the ELISA can detect desmosine, but when possible, 6-well plates were used to more reliably generate desmosine amounts within range of the ELISA.

The molecules from the Diversity Set V library were dissolved in DMSO, which is cytotoxic at higher concentrations. We performed a concentration profile experiment to identify the highest liquid volume percentage of DMSO could be exposed to cells without significantly inhibiting cellular activity, as measured by total protein amounts (Figure 3.2C). We decided a maximum of 0.1 v/v% would be used in our studies.

With our platform we performed a primary screen on nearly 1600 small molecules from a library donated by the Developmental Therapeutics Program (DTP) of the National Cancer Institute (NCI). From the primary screen, 21 potential hits were identified and 7 of them were maintained as positive hits after a validation study of the primary screen results. The reduction of positive hits on increasing the technical replicates performed on the same samples from the primary screen indicate that the biochemical assays used in our platform, in particular the desmosine ELISA, may be too variable and have too much background noise to reliably select positive hits from a high-throughput screen.

A secondary screen was performed on the 7 positive hits, this time with increased experimental and technical replicates. As a result, two of these molecules demonstrated potential elastic fiber synthesis enhancement. Additional validation experiments were performed on these two molecules, however the enhanced elastic fiber production activity was not reproducible.

Despite our efforts, a novel elastic fiber promoting molecule was not discovered in our screen. Regardless, the adaptation of the desmosine ELISA from Dr. Mecham's lab has enabled our lab to investigate elastic fiber content in several tissues. I have contributed my acquired biochemical assay expertise to numerous investigations including results presented in two publications and ongoing research in our lab.(33, 34)

3.6 Limitations

SSMD* hit selection is only capable of detecting strong effectors from a primary screen.

Molecules from the library that have a subtle influence on the target process, in this case elastic fiber synthesis, would be hidden as false-negatives. This is a weakness of the statistical method because, although strong effectors are most desired, weaker effectors could theoretically contain a useful pharmacophore whose effect could be strengthened by making adjustments to the molecular structure, such as in the development of lead molecule libraries.

3.7 Acknowledgments

Dr. Robert Mecham's lab at Washington University, especially Thomas Broekelmann, is gratefully acknowledged for their assistance with the desmosine ELISA. Barry Starcher from University of Texas Health Science Center is also acknowledged for providing the original source of the desmosine antibody. Data presented in this study was partially funded by NIH grants R01 HL115560 and R01 HL105314. The content is solely the responsibility of the authors and does not necessarily represent the official views of the NIH.

3.8 References

1. Girton TS, Oegema TR, Grassl ED, Isenberg BC, Tranquillo RT. Mechanisms of stiffening and strengthening in media-equivalents fabricated using glycation. *Journal of biomechanical engineering*. 2000;122(3):216-23.
2. Peck M, Gebhart D, Dusserre N, McAllister TN, L'Heureux N. The evolution of vascular tissue engineering and current state of the art. *Cells Tissues Organs*. 2012;195(1-2):144-58.
3. Swartz DD, Russell JA, Andreadis ST. Engineering of fibrin-based functional and implantable small-diameter blood vessels. *American journal of physiology Heart and circulatory physiology*. 2005;288(3):H1451-60.
4. Yao L, Swartz DD, Gugino SF, Russell JA, Andreadis ST. Fibrin-based tissue-engineered blood vessels: differential effects of biomaterial and culture parameters on mechanical strength and vascular reactivity. *Tissue Eng*. 2005;11(7-8):991-1003.
5. Patel A, Fine B, Sandig M, Mequanint K. Elastin biosynthesis: The missing link in tissue-engineered blood vessels. *Cardiovasc Res*. 2006;71(1):40-9.
6. Berglund JD, Nerem RM, Sambanis A. Incorporation of intact elastin scaffolds in tissue-engineered collagen-based vascular grafts. *Tissue Eng*. 2004;10(9-10):1526-35.
7. Opitz F, Schenke-Layland K, Cohnert TU, Starcher B, Halbhuber KJ, Martin DP, et al. Tissue engineering of aortic tissue: dire consequence of suboptimal elastic fiber synthesis in vivo. *Cardiovasc Res*. 2004;63(4):719-30.
8. Kielty CM, Sherratt MJ, Shuttleworth CA. Elastic fibres. *J Cell Sci*. 2002;115(Pt 14):2817-28.
9. Wagenseil JE, Ciliberto CH, Knutsen RH, Levy MA, Kovacs A, Mecham RP. Reduced vessel elasticity alters cardiovascular structure and function in newborn mice. *Circ Res*. 2009;104(10):1217-24.
10. Wagenseil JE, Ciliberto CH, Knutsen RH, Levy MA, Kovacs A, Mecham RP. The importance of elastin to aortic development in mice. *American journal of physiology Heart and circulatory physiology*. 2010;299(2):H257-64.
11. Stone PJ, Morris SM, Griffin S, Mithieux S, Weiss AS. Building Elastin. Incorporation of recombinant human tropoelastin into extracellular matrices using nonelastogenic rat-1 fibroblasts as a source for lysyl oxidase. *Am J Respir Cell Mol Biol*. 2001;24(6):733-9.
12. Isenberg BC, Tranquillo RT. Long-term cyclic distention enhances the mechanical properties of collagen-based media-equivalents. *Ann Biomed Eng*. 2003;31(8):937-49.
13. Opitz F, Schenke-Layland K, Richter W, Martin DP, Degenkolbe I, Wahlers T, et al. Tissue engineering of ovine aortic blood vessel substitutes using applied shear stress and enzymatically derived vascular smooth muscle cells. *Ann Biomed Eng*. 2004;32(2):212-22.
14. Huang AH, Balestrini JL, Udelsman BV, Zhou KC, Zhao L, Ferruzzi J, et al. Biaxial Stretch Improves Elastic Fiber Maturation, Collagen Arrangement, and Mechanical Properties in Engineered Arteries. *Tissue Eng Part C Methods*. 2016;22(6):524-33.
15. Seliktar D, Nerem RM, Galis ZS. Mechanical strain-stimulated remodeling of tissue-engineered blood vessel constructs. *Tissue Eng*. 2003;9(4):657-66.
16. Sproul EP, Argraves WS. A cytokine axis regulates elastin formation and degradation. *Matrix Biol*. 2013;32(2):86-94.
17. Mecham RP. Methods in elastic tissue biology: elastin isolation and purification. *Methods*. 2008;45(1):32-41.
18. Lazo JS, Brady LS, Dingleline R. Building a pharmacological lexicon: small molecule discovery in academia. *Mol Pharmacol*. 2007;72(1):1-7.

19. Zhang JH, Chung TD, Oldenburg KR. A Simple Statistical Parameter for Use in Evaluation and Validation of High Throughput Screening Assays. *J Biomol Screen*. 1999;4(2):67-73.
20. Shi J, Wang A, Sen S, Wang Y, Kim HJ, Mitts TF, et al. Insulin induces production of new elastin in cultures of human aortic smooth muscle cells. *Am J Pathol*. 2012;180(2):715-26.
21. Katsuta Y, Ogura Y, Iriyama S, Goetinck PF, Klement JF, Uitto J, et al. Fibulin-5 accelerates elastic fibre assembly in human skin fibroblasts. *Exp Dermatol*. 2008;17(10):837-42.
22. Long JL, Tranquillo RT. Elastic fiber production in cardiovascular tissue-equivalents. *Matrix Biol*. 2003;22(4):339-50.
23. Slove S, Lannoy M, Behmoaras J, Pezet M, Sloboda N, Lacolley P, et al. Potassium channel openers increase aortic elastic fiber formation and reverse the genetically determined elastin deficit in the BN rat. *Hypertension*. 2013;62(4):794-801.
24. Knutsen RH, Beeman SC, Broekelmann TJ, Liu D, Tsang KM, Kovacs A, et al. Minoxidil improves vascular compliance, restores cerebral blood flow, and alters extracellular matrix gene expression in a model of chronic vascular stiffness. *American journal of physiology Heart and circulatory physiology*. 2018;315(1):H18-H32.
25. Zhang XD. Illustration of SSMD, z score, SSMD*, z* score, and t statistic for hit selection in RNAi high-throughput screens. *J Biomol Screen*. 2011;16(7):775-85.
26. Kozel BA, Ciliberto CH, Mecham RP. Deposition of tropoelastin into the extracellular matrix requires a competent elastic fiber scaffold but not live cells. *Matrix Biol*. 2004;23(1):23-34.
27. Stoilov I, Starcher BC, Mecham RP, Broekelmann TJ. Measurement of elastin, collagen, and total protein levels in tissues. *Methods Cell Biol*. 2018;143:133-46.
28. Starcher B. A ninhydrin-based assay to quantitate the total protein content of tissue samples. *Anal Biochem*. 2001;292(1):125-9.
29. Baldwin AK, Simpson A, Steer R, Cain SA, Kielty CM. Elastic fibres in health and disease. *Expert Rev Mol Med*. 2013;15:e8.
30. Kahari VM, Olsen DR, Rhudy RW, Carrillo P, Chen YQ, Uitto J. Transforming growth factor-beta up-regulates elastin gene expression in human skin fibroblasts. Evidence for post-transcriptional modulation. *Lab Invest*. 1992;66(5):580-8.
31. Kucich U, Rosenbloom JC, Abrams WR, Bashir MM, Rosenbloom J. Stabilization of elastin mRNA by TGF-beta: initial characterization of signaling pathway. *Am J Respir Cell Mol Biol*. 1997;17(1):10-6.
32. McGowan SE, Jackson SK, Olson PJ, Parekh T, Gold LI. Exogenous and endogenous transforming growth factors-beta influence elastin gene expression in cultured lung fibroblasts. *Am J Respir Cell Mol Biol*. 1997;17(1):25-35.
33. Eekhoff JD, Fang F, Kahan LG, Espinosa G, Cocciolone AJ, Wagenseil JE, et al. Functionally Distinct Tendons From Elastin Haploinsufficient Mice Exhibit Mild Stiffening and Tendon-Specific Structural Alteration. *Journal of biomechanical engineering*. 2017;139(11).
34. Kim J, Staiculescu MC, Cocciolone AJ, Yanagisawa H, Mecham RP, Wagenseil JE. Crosslinked elastic fibers are necessary for low energy loss in the ascending aorta. *Journal of biomechanics*. 2017;61:199-207.

Chapter 4

Mass Transport in Arteries with Compromised Elastic Fibers¹

4.1 Introduction

Targeted pharmacological intervention of vascular disease is an increasing area of research for the treatment of localized defects. The prevention of restenosis following the stenting of occluded arteries in coronary artery disease through the use of drug-eluting stents has proven efficacious (1-3) and similar drug eluting stent strategies are being considered for treating atherosclerotic peripheral arteries. Drug delivery strategies are in development to prevent neointimal hyperplasia following arterial reconstruction, grafting, and endarterectomy of the aorta and common carotids (4, 5). Pharmacological management of aortic aneurysms has shown promise in animal studies (6-9) but has been inconsistent clinically (10, 11) and now targeted delivery of these drugs is being considered (12-16). With this increasing focus on localized drug delivery to arterial tissues, the pharmacokinetics of these tissues is of interest to better understand the physical forces that regulate the delivery and retention of the therapeutic agent within the targeted area (17). In part this includes characterization of the transport properties of arterial tissue and how these properties are affected by structure and composition of the arterial wall.

¹ Reprinted with additional changes from Cocciolone AJ, Johnson E, Shao JY, Wagenseil JE. *Elastic fiber fragmentation increases transmural hydraulic conductance and solute transport in mouse arteries*. J Biomech Eng. 2018 Dec 5 with permission from ASME © 2019.

The wall of large elastic arteries is composed of three layers: intima, media, and adventitia. The intima is a single layer of endothelial cells that is directly adjacent to the lumen. The media is the middle layer and makes up the majority of the tissue in the arterial wall. The media is further sub-layered into concentric layers composed of vascular smooth muscle cells (VSMCs) and an extracellular matrix (ECM) rich in collagen and elastic fibers. These sub-layers are defined by dense sheets of elastic fibers called elastic lamellae that appear as concentric formations in the arterial wall. The outermost layer is the adventitia, composed of fibroblasts and a loose collagen-rich ECM (18-20).

The endothelial cell layer of the intima is regarded as the most important barrier to the transport of biological macromolecules and drugs supplied from blood in the lumen to reaching the innermost layers of the arterial wall (21-25). Less attention has been given to mass transport beyond the intima. Many transport models and experiments tend to assume the media to be homogenous and the VSMCs to be the main obstacle to solute transport (23, 25-28). The large ECM component of the media and its unique layered structure attributed to the elastic lamellae are not appreciably considered by these models. Several numerical investigations account for ECM in arterial wall transport and provide evidence that ECM structure and composition are important contributors toward media layer effective porosity (25, 29). Hwang et al. observed anisotropic mass transport in bovine carotid tissue with diffusion in the circumferential direction being greater than diffusion in the transmural direction (30) and they proposed this may be a result of the non-homogenous arrangement of the elastic fiber network.

These previous studies provide evidence of ECM contribution to transport within the arterial wall but none of them are able to isolate the role of individual ECM constituents. Due to its abundance in the wall and its concentric layering as thick sheets within the arterial media, we suspect that elastic fibers play a crucial role in limiting solute transport across the wall. To evaluate the role of elastic fibers in arterial wall transport, we performed transport studies in fibulin-5 null (*Fbln5*^{-/-}) mice. Fibulin-5 has the critical role in elastic fiber assembly of regulating and directing tropoelastin, the monomeric precursor to mature polymeric elastic fibers. The elastic lamellae of *Fbln5*^{-/-} arteries are fragmented and improperly organized (30, 31) and we hypothesized that *Fbln5*^{-/-} arteries have reduced resistance to transmural transport. We measured fluid and solute transport in *Fbln5*^{+/+} and *Fbln5*^{-/-} carotid arteries and observed an increase in the hydraulic conductance and solute flux in the elastic fiber compromised tissue. Additionally, we supplemented our findings from *Fbln5*^{-/-} tissue by measuring transport across *Fbln5*^{+/+} tissues following exposure to elastase, an enzyme with high affinity for digesting elastic fibers, and found similar results.

4.2 Methods

4.2.1 Transport theory

Here we have approximated the arterial wall tissue to be a porous membrane with a homogenous distribution of uniformly shaped, cylindrical pores. Movement of solute molecules across any porous membrane occurs through a combination of diffusive and advective (bulk flow) transport mechanisms. In a sieving membrane, solvent molecules pass unhindered across the membrane while the solute molecules experience some degree of difficulty in transport. Steric exclusion based on the size of the solute and pore contributes to preventing the solute from entering the

membrane. Additionally, the traveling velocity of the solute within the pore may be reduced by hydrodynamic interaction between the pore wall and the solute.

The differential form of the advection-diffusion equation for one-dimensional, steady-state solute transport is the following;

$$J_s = (1 - \dagger) J_v c - D_s \frac{dc}{dx} \quad (4.1)$$

where J_s is the net solute flux across the membrane, J_v is the volumetric fluid flux, D_s is an effective diffusivity coefficient of the solute within the membrane, c is the solute concentration in the membrane at some distance x , and \dagger is the osmotic reflective coefficient which is used to express the fraction of molecules that are reflected back instead of entering the membrane (32).

Theoretical expressions for \dagger are available that depend on solute radius, a , and effective membrane pore radius, r . For a membrane with uniform, cylindrical pores and a solute approximated as a hard sphere the following expression for \dagger is used (33, 34);

$$\dagger = (1 - K)^2 \quad (4.2)$$

$$K = \text{partition coefficient} = (1 - \})^2 \quad (4.3)$$

$$\} = \frac{a}{r} \quad (4.4)$$

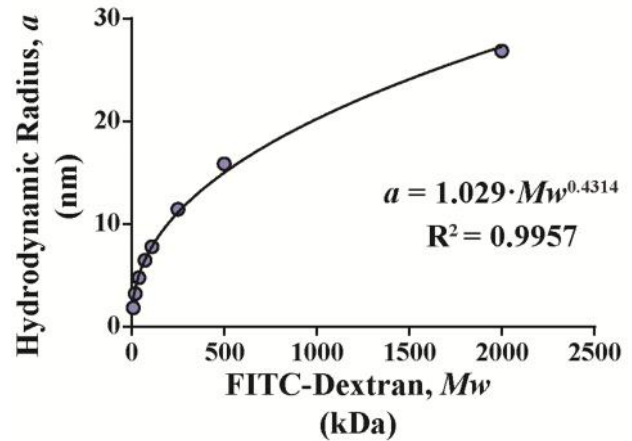


Figure 4.1 - Quasi-elastic light scattering data for FITC-dextran particle radius taken from Armstrong et al. (35) and fit to a power law equation.

Solute hydrodynamic radius can be used as an approximation for a . A power law equation for the dependence of dextran hydrodynamic radius on molecular weight, M_w , was fit ($R^2 = 0.988$) from quasi-elastic light scattering experiment data by Armstrong et al. (Figure 4.1) (35).

$$a = 0.738 \cdot M_w^{0.489} \quad (4.5)$$

An expression for J_v can be derived from D'Arcy's law;

$$J_v = \frac{\dot{Q}_f}{A_m} = \frac{|}{\sim} \left(\frac{dP}{dx} - \dagger RT \frac{dc}{dx} \right) \quad (4.6)$$

where \dot{Q}_f is the volumetric flowrate, A_m is the cross-sectional area of the membrane normal to the flow, $|$ is the intrinsic permeability, \sim is the dynamic fluid viscosity, P is the hydrostatic pressure, R is the gas constant, and T is the temperature.

Equations 4.1 and 4.6 were derived by Kedem and Katchalsky (32) to describe solute transport of a neutral solute across a thin, homogenous porous membrane permeable to both solute and solvent. Integration of equation 4.1 across the thickness of the membrane yields;

$$J_s = (1 - \dagger) J_v \cdot g(c) - \frac{D_s}{\Delta x} \Delta c \quad (4.7)$$

where $g(c)$ is a function of solute concentration across the membrane. Likewise, integration of equation 4.6 yields;

$$J_v = L_p (\Delta P - \dagger RT \Delta c) \quad (4.8)$$

where L_p is the hydraulic conductance, an intrinsic property that describes how easily water can move across the membrane.

$$L_p = \frac{1}{-\Delta x} \quad (4.9)$$

L_p can be determined experimentally by measuring the volumetric fluid flux across a membrane at steady-state, constant pressure, and in absence of a solute concentration gradient. In which case equation 4.8 can be reduced and rearranged to;

$$L_p = \frac{J_v}{\Delta P} \quad (4.10)$$

If advective mediated solute transport is exceedingly larger than diffusive transport, diffusion can be dropped from equation 4.7 yielding the following reduced equation for J_s where $g(c)$ is simply equal to the solute concentration in the lumen, C_L (36).

$$J_s = (1 - \tau) J_v \cdot C_L \quad (4.11)$$

4.2.2 Animal tissue preparation

Intact common carotid arteries were removed from four month old (± 14 days) *Fbln5*^{+/+} and *Fbln5*^{-/-} mice (37) euthanized by carbon dioxide inhalation in compliance with the Institutional Animal Care and Use Committee. The tissue was stored at 4°C in phosphate-buffered saline (PBS) until testing which generally occurred within three days of dissection. Overall 92 mice were used in this study. Structural and mechanical properties of *Fbln5*^{+/+} and *Fbln5*^{-/-} carotids were investigated by Ferruzzi et al. and determined to be gender independent (38). As a result, samples from this study were not separated by gender.

4.2.3 Experimental setup

Mass transport experiments were conducted *ex vivo* using a pressure myograph testing system and the corresponding software (Danish Myotechnology). For each experiment, the ends of the

carotid were cannulated and gently secured in-place using 7-0 suture and placed in a 10 mL PBS bath maintained at 37°C. The carotid was then stretched to a stretch ratio of 1.4, which is the average *in vivo* stretch ratio for a mouse carotid artery (39). Denudation of the endothelium was achieved by bubbling 20 mL of air through the lumen at a constant rate (40). During this step, the integrity of the artery was confirmed by clamping the outlet tubing and pressurizing the carotid with air to 100 mmHg. Air escaping from the lumen to the bath indicated a hole in the tissue and the experiment was not performed. Intact carotids were then pressurized to a hydrostatic pressure of 100 mmHg using a fluid column attached to the myograph inlet and clamping the tubing at the myograph outlet. One of three experimental procedures was performed for the measurement of volumetric fluid flux, net solute flux, or solute uptake into the media. These experiments were performed on carotids from *Fbln5^{+/+}* and *Fbln5^{-/-}* mice as well as carotids from *Fbln5^{+/+}* mice after an elastase treatment.

4.2.4 Elastase treatment

After mounting and stretching the carotid but before inflation with the hydrostatic pressure column, *Fbln5^{+/+}* carotids were subjected to an elastase treatment. 7.5 units/mL elastase (Elastin Products Company, EC134) was introduced into the lumen of the artery by a syringe through the inlet tubing. The outlet tubing was clamped and the artery was pressurized and held at 100 mmHg by further depressing the syringe. After 30 seconds, elastase activity was inhibited by submerging the mounted carotid in a bath containing a stop solution of 100 mM NaCl PBS (41) and the lumen of the carotid was flushed with the same solution. The carotid was pressurized to 100 mmHg and was maintained submerged in stop solution for 30 minutes. The lumen was then flushed with regular PBS and the bath was replaced with 10 mL of fresh PBS and the carotid was ready for experimentation. Effectiveness of the elastase treatment and subsequent inhibition was

verified in a pilot study by tracking post-treatment diameter of the carotid. Uninhibited elastase-treated carotids continued to increase in diameter during the one-hour observation period while the inhibited elastase-treated carotids held a constant diameter (Figure 4.2). An increase of 15.6% ($\pm 5.6\%$) in outer diameter was observed in the elastase-treated carotids used in this study.

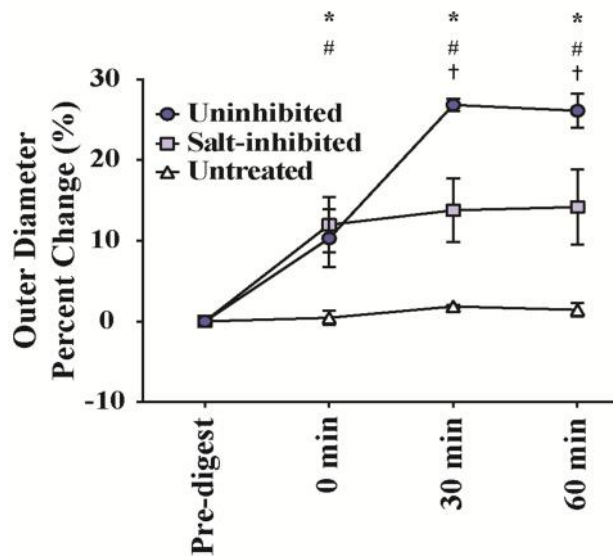


Figure 4.2 - Preliminary investigation in developing and elastase treatment for the arterial tissue. Elastase activity was inhibited through a high salt buffer solution. Two-way ANOVA indicated significance ($p < 0.0001$) between groups in both time and treatment conditions. Bonferroni's multiple comparison test indicated significance ($p < 0.0001$) in the comparisons between uninhibited elastase treated (*) and salt-inhibited elastase treated (#) to the group untreated with elastase. Within the elastase treated groups, significant ($p < 0.0001$) differences were found between uninhibited and salt-inhibited groups (†).

4.2.5 Hydraulic conductance

A modification was made to the experimental setup to include a length of tubing between the myograph inlet and the pressure fluid column. Using a syringe and three-way stopcock, an air bubble was added to this tubing. After preparing the artery for testing, displacement of the bubble was measured by taking an image every two minutes for 60 minutes. By continuity, the volumetric flowrate of the fluid in the tubing is equivalent to the transmural volumetric flowrate across the arterial wall leading to the following relation,

$$Q = A \cdot \bar{V} = A_A \cdot \left. \frac{dx}{dt} \right|_A = A_T \cdot \left. \frac{dx}{dt} \right|_T \quad (4.12)$$

where Q is the fluid volumetric flowrate, A is the cross-sectional area normal to flow and \bar{V} is the mean fluid velocity for the artery (A) and tubing (T). Equation 4.12 can be rearranged to express the transmural fluid flux across the artery (J_v) and expanding the area in terms of

diameter and suture-to-suture length for the artery and inner diameter of the tubing (d_A , $l_{A,S}$ and d_T respectively).

$$J_v = \frac{Q}{A_A} = \frac{d_T^2 \cdot \frac{\Delta x_{bubble}}{\Delta t}}{4 \cdot d_A \cdot l_{A,S}} \quad (4.13)$$

At steady-state the volumetric fluid flux can be determined from the slope of displacement versus time curve for the air bubble and equation 4.13. Further, hydraulic conductance can be calculated using this fluid flux and equation 4.10 in the solute-free case where the reflection coefficient is zero.

4.2.6 Solute flux

Net solute transport was assessed by adding 2.5 mg/mL of 4, 70, or 150 kDa FITC-dextran (Sigma-Aldrich Co.; #46944, #46946, and #46946 respectively) to the fluid column such that the lumen of the carotid contained a molar concentration of 625, 35.7, or 16.7 μ M FITC-dextran, respectively. Transmural solute transport was monitored over 60 minutes by sampling 50 μ l from the fluid bath outside of the artery twice every 10 minutes after mixing. Concentration was determined fluorometrically (480 nm excitation, 525 nm emission) against a serial dilution of the 2.5 mg/mL stock solution using a plate reader (Molecular Devices, SpectraMax M2^e). Net solute flux, J_s , was calculated by the following equation,

$$J_s = \frac{1}{A_A} \cdot \frac{\Delta c_{bath}}{\Delta t} \quad (4.14)$$

where $\frac{\Delta c_{bath}}{\Delta t}$ is the slope of the bath concentration versus time curve at steady-state.

4.2.7 Solute uptake

Similarly to the solute flux experiments, 2.5 mg/mL of 4, 70, or 150 kDa FITC-dextran was added to the fluid column. Transmural advective transport persisted for 30, 60, 120, or 240 minutes in the 4 kDa and 70 kDa experiments but only the 60 minute time point was taken for the 150 kDa experiments. Post experiment, the arterial lumen was flushed with solute-free PBS. The artery was removed from the myograph by cutting each end at the tip of the cannulae. A lateral cut was made the length of the artery to expose the lumen to facilitate the elution of FITC-dextran from the tissue. A series of elutions was performed by placing the artery in a vial containing 120 μ l of PBS and placing the vial on a shaker at 300 rpm and 37°C, transferring the tissue to a fresh vial every 24 hours. In total the artery underwent three elutions and the fluorescence of each elutant was measured and compared to a standard curve generated from a serial dilution of stock 2.5 mg/mL FITC-dextran that had undergone the same conditioning as the samples. Typically 80% of the eluted FITC-dextran appeared in the first elution and the final elution contained less than 5% of the sum between the three elutions providing confidence that the majority of FITC-dextran taken up by the artery during the experiment had been eluted. The values reported are not a true concentration since arterial wall thickness was not measured, however it has been previously determined that wall thickness is similar between *Fbln5*^{+/+} and *Fbln5*^{-/-} arteries (31, 39). Therefore, solute uptake is reported here as the total number of moles of FITC-dextran taken up by the wall normalized to the artery length in the experiment (i.e. μ mol FITC-dextran \cdot mm⁻¹).

4.2.8 Elastin histology by VVG of carotid cross sections

Four each of *Fbln5*^{+/+}, *Fbln5*^{-/-}, and elastase-treated *Fbln5*^{+/+} carotids were fixed in 10% formaldehyde for 24 hours followed by dehydration in ethanol. The samples were paraffin

embedded and sectioned at the Musculoskeletal Histology and Morphometry Core at the Washington University School of Medicine. Verhoeff Van Gieson (VVG) stain was used for visualization of the elastic fiber network structure within the cross section of the carotid wall. Qualitative assessment of the integrity of the elastic lamellae was compared across the three groups.

4.2.9 Two-photon microscopy of elastin auto fluorescence in *en face* carotids

Immediately following dissection and elastase treatment, if required, four each of *Fbln5*^{+/+}, *Fbln5*^{-/-}, and elastase-treated *Fbln5*^{+/+} carotids were fixed for one hour in 4% paraformaldehyde at 4°C. *En face* slides were prepared by performing a lateral cut the length of the artery and mounting the tissue on the slide such that the lumen faced upward and in direct contact with the coverslip. Imaging was performed by the Washington University Center for Cellular Imaging (WUCCI) at the Washington University School of Medicine using a Zeiss LSM 880 Airyscan two-photon microscope and a 40x/1.2 silicon immersion objective. A z-stack of elastin auto fluorescence was captured at 330 nm increments across the thickness of the arterial wall by using a 488 nm laser for excitation and collecting the emission signal between 500 and 550 nm (42, 43). Deconvolution of the z-stacks was performed using the software, Autoquant.

4.2.10 Statistical analysis

Comparisons were made between tissue types at the same FITC-dextran size or time point. All statistics were performed using GraphPad Prism software with significance considered at $P < 0.05$. All comparisons were performed by a one-way ANOVA and Tukey's post hoc. Statistical significance between *Fbln5*^{+/+} and *Fbln5*^{-/-} (*), *Fbln5*^{+/+} and elastase-treated *Fbln5*^{+/+} (†), and *Fbln5*^{+/+} and elastase-treated *Fbln5*^{+/+} (#) samples are indicated on the figures.

4.3 Results

4.3.1 Elastin histology shows compromised elastic fibers

Representative VVG stains of *Fbln5*^{+/+}, *Fbln5*^{-/-}, and elastase-treated *Fbln5*^{+/+} carotid cross-sections are presented in Figure 4.3. The elastic lamellae (stained in black) from the *Fbln5*^{+/+} (1A) appear as smooth, continuous layers within the media. In contrast, the continuity of the elastic lamellae in the *Fbln5*^{-/-} tissue (1B) is disrupted by over-deposition of elastin in some areas and under-deposition in others leading to an overall fragmented appearance. These histological images are in agreement with previously published results (30, 31, 37). The elastase-treated *Fbln5*^{+/+} carotid (1C) retains the continuity of the elastic lamellae and the elastic lamellae appear to be thinner than in untreated *Fbln5*^{+/+}. The elastase treatment used in this study was intended to reduce the transport resistance of the elastic lamellae but to avoid complete removal of the elastic fibers and the histology images indicate that the elastic lamellae are still intact. The surrounding VSMC's appear more loosely arranged than in the *Fbln5*^{+/+} tissue, possibly due to the removal of the thin elastic fibers in the muscle tissue regions between elastic lamellae.

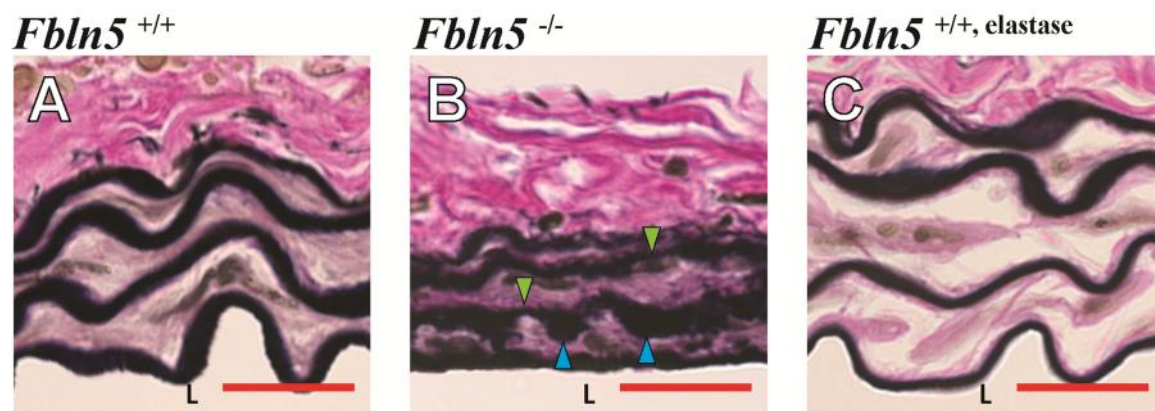


Figure 4.3 - Representative histological cross-sections of *Fbln5*^{+/+} (A), *Fbln5*^{-/-} (B), and elastase-treated *Fbln5*^{+/+} (C) carotid arteries. The elastic lamellae are colored black by the VVG stain. The arterial lumen (L) is towards the bottom of the images. Phenotypic over-deposition and under-deposition of elastin within the elastic lamellae of *Fbln5*^{-/-} are indicated by blue, upward-facing arrows and green, downward-facing arrows respectively. The scale bar indicates 20 μ m.

4.3.2 Elastin auto fluorescence reveals changes in elastic fiber density

Representative *en face* images from the two-photon microscopy of elastin auto fluorescence from *Fbln5^{+/+}*, *Fbln5^{-/-}*, and elastase-treated *Fbln5^{+/+}* carotids are shown in Figure 4.4. A single plane of the *en face* z-stack and the orthogonal views are shown to visualize the elastic fiber network in three-dimensions. The elastic lamellae undulate in-and-out of the *en face* image plane as a result of their characteristic wavy pattern, which is evident from the orthogonal views and the histological cross-sections in Figure 4.3. The over- and under-deposition of elastin within the lamellae of *Fbln5^{-/-}* arteries is evident in the *en face* images and is consistent with the histological images. Changes in the density and arrangement of the elastic fibers may increase the effective porosity of the *Fbln5^{-/-}* elastic lamellae and contribute to the observed increase in solute transport. Fenestrations (holes) in the elastic lamellae are visible in the higher magnification *en face* images and appear similar in all three groups. There is no apparent difference in elastic fiber density or organization due to the elastase treatment, indicating the subtle nature of the treatment protocol. Additional more quantitative investigation is required to identify structural changes in the elastase treated group that may contribute to the observed differences in transport properties.

4.3.3 Hydraulic conductance is influenced by elastic fiber integrity

Steady-state volumetric fluid flux was achieved rapidly after the start of the experiment, evidenced by the linear displacement curves of the tracking bubble (Figure 4.5A, $R^2 > 0.99$ in all experiments). The slope of the displacement curve was used in Eq. (8) to determine volumetric fluid flux, which was then used with Eq. (6) to calculate the intrinsic hydraulic conductance for each group (Figure 4.5B). The elastic fiber compromised tissue of the *Fbln5^{-/-}* and elastase-

treated *Fbln5*^{+/+} carotids resulted in a 6 and 7-fold increase in hydraulic conductance, respectively, compared to *Fbln5*^{+/+} tissue.

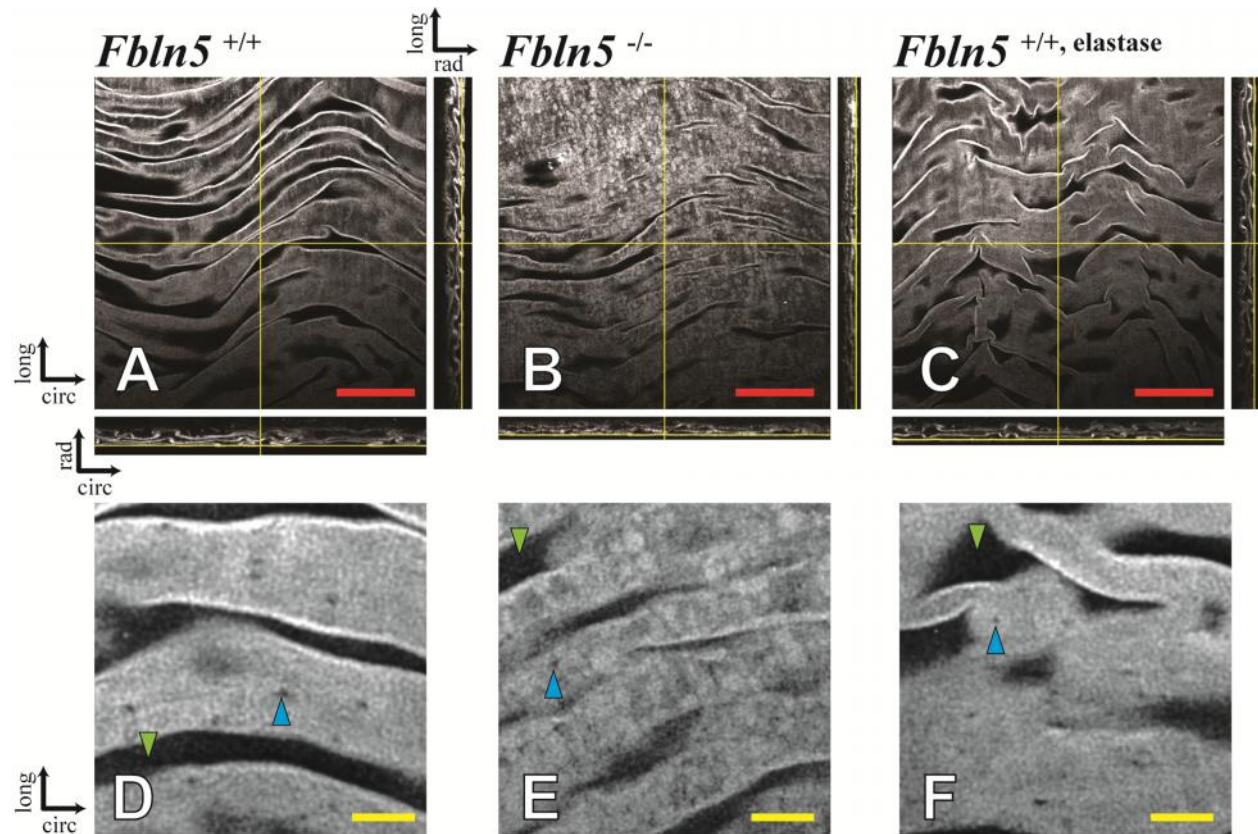


Figure 4.4 - Representative two-photon microscopy images of elastin auto fluorescence from *en face* *Fbln5*^{+/+} (A and D), *Fbln5*^{-/-} (B and E), and elastase-treated *Fbln5*^{+/+} (C and F) carotids. Panels A, B, and C are views of a single plane from the z-stack within the internal elastic lamella. Orthogonal views of the z-stack are shown next to Panels A, B, and C for three-dimensional visualization. The orientation for each image is indicated (circ = circumferential, long = longitudinal, rad = radial). The yellow lines represent the image location within the z-stack. The red scale bar indicates 50 μm . Panels D, E, and F are magnified z-projections of four consecutive planes from the z-stack within the internal elastic lamella. Blue, upward facing arrows indicate a fenestration (hole) within the elastic lamina. Green, downward facing arrows show the elastic lamella undulating out of the z-projection plane. The yellow scale bar indicates 10 μm .

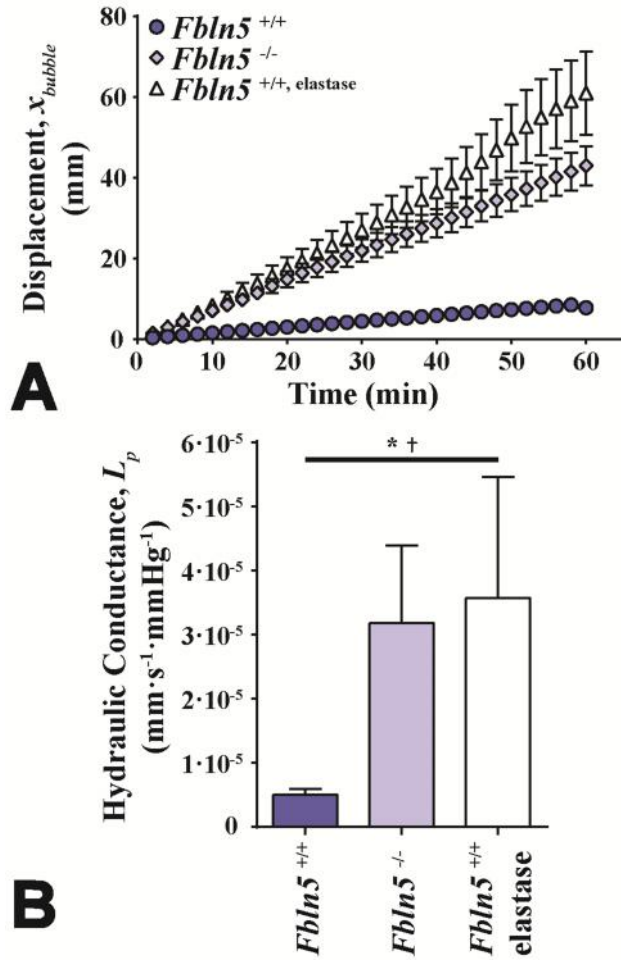


Figure 4.5 - Results from the volumetric fluid flux experiments. Panel A – The displacement of the tracking bubble over time for each of the tissues. Error bars are SEM for clarity. Panel B – Hydraulic conductance of *Fbln5*^{+/+} (n = 7), *Fbln5*^{-/-} (n = 8), and elastase-treated *Fbln5*^{+/+} carotids (n = 8). Error bars are SD. Statistical significance was determined between *Fbln5*^{+/+} and *Fbln5*^{-/-} (* p = 0.0021) and between *Fbln5*^{+/+} and elastase-treated *Fbln5*^{+/+} († p = 0.0004).

4.3.4 Total solute flux reveals size exclusion properties

It is apparent by the constant rate of change in FITC-dextran concentration in the external bath that the solute transport across the arterial wall reached steady-state in less than 10 minutes of experimentation for all tested FITC-dextran sizes (Figures 4.6A-C, $R^2 > 0.98$ in all experiments). The slope of the bath concentration versus time curves and Eq. (9) was used to determine the net solute flux across the wall (Figure 4.6D). *Fbln5*^{-/-} carotids have a 4-fold increase in 4 kDa FITC-dextran solute flux compared to *Fbln5*^{+/+} carotids. The change in solute flux is more drastic in the case of 70 kDa, having a 22-fold increase in *Fbln5*^{-/-} compared to *Fbln5*^{+/+}. However, in the case of 150 kDa the difference drops to a 3-fold increase. Overall, the *Fbln5*^{-/-} tissue exhibits a linear decrease in solute flux with increasing dextran size on the semi-log scale (Figure 4.6D)

while the *Fbln5*^{+/+} tissue experiences a sharper decrease in solute flux from 4 to 70 kDa but a minimal change in solute flux from 70 to 150 kDa. This indicates a shift in the size exclusion limit between the tissues as a result of the elastic fiber fragmentation in the *Fbln5*^{-/-} tissue.

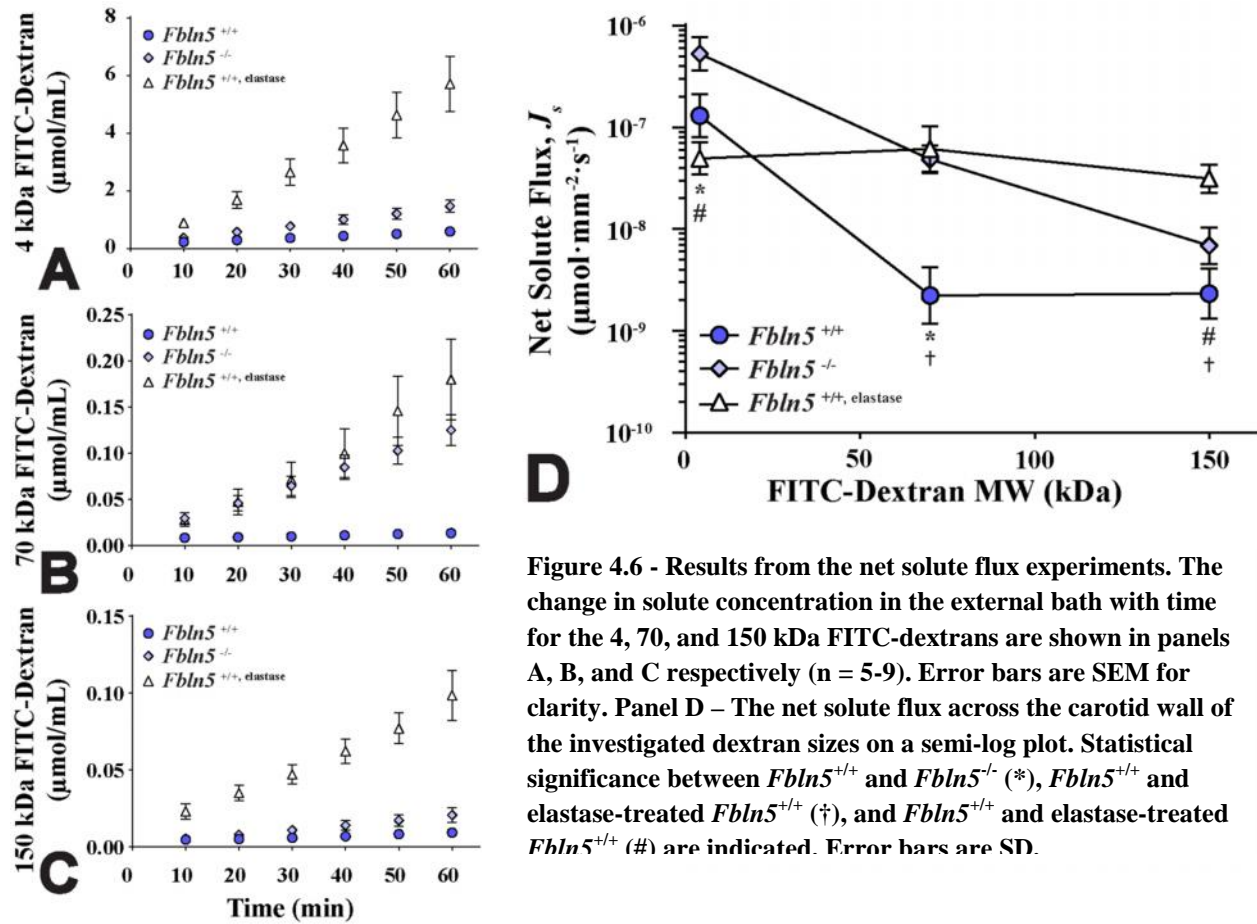


Figure 4.6 - Results from the net solute flux experiments. The change in solute concentration in the external bath with time for the 4, 70, and 150 kDa FITC-dextrans are shown in panels A, B, and C respectively (n = 5-9). Error bars are SEM for clarity. Panel D – The net solute flux across the carotid wall of the investigated dextran sizes on a semi-log plot. Statistical significance between *Fbln5*^{+/+} and *Fbln5*^{-/-} (*), *Fbln5*^{+/+} and elastase-treated *Fbln5*^{+/+} (†), and *Fbln5*^{+/+} and elastase-treated *Fbln5*^{+/+} (#) are indicated. Error bars are SD.

Elastase-treated *Fbln5*^{+/+} carotids have a 4 kDa solute flux that is not significantly different from untreated tissue (Figure 4.6D). There is a significant increase in 70 kDa solute flux and it is comparable in magnitude to the increase demonstrated by *Fbln5*^{-/-} carotids over untreated *Fbln5*^{+/+} carotids at the same dextran size. The 150 kDa solute flux in elastase-treated *Fbln5*^{+/+} carotids is significantly increased 13-fold and 4-fold over *Fbln5*^{+/+} and *Fbln5*^{-/-} carotids, respectively. The net solute flux of FITC-dextran across elastase-treated tissue is independent of dextran size, suggesting that the relative pore size is increased sufficiently that the tissue no

longer has sieving capability at the tested FITC-dextran sizes. The results for the elastase-treated tissue provide additional evidence that changes to the elastic fiber network structure will alter solute transport. Based on the differences in behavior between the groups for different FITC-dextran sizes, it appears that alterations in solute transport depend on the mechanisms leading to elastic fiber defects (i.e. genetic disruptions in elastic fiber assembly versus protease digestion of mature elastic fibers).

4.3.5 Solute uptake is variably affected by elastic fiber disruption treatment

Dextran uptake concentration was decreased in the *Fbln5*^{-/-} tissue compared to *Fbln5*^{+/+} for 4 and 70 kDa FITC-dextran at every time point tested (Figure 4.7A and 4.7B respectively). In these time course experiments there was a steady increase in solute uptake over time. This may be a result of passive diffusion of solute into void spaces within the tissue that are not accessible to the transmural fluid flux.

4 kDa FITC-dextran concentration (Figure 4.7A) was increased in both *Fbln5*^{+/+} and *Fbln5*^{-/-} carotids compared to 70 kDa FITC-dextran (Figure 4.7B) at all time points and is likely a result of a combination of factors including the larger molar concentration and smaller solute size of 4 kDa FITC-dextran.

Solute uptake for 150 kDa FITC-dextran was measured only after 60 minutes. A comparison of solute uptake for each dextran size at 60 minutes is presented in Figure 4.7C. Interestingly, the significant decrease in solute uptake by *Fbln5*^{-/-} carotids in the 4 and 70 kDa studies is lost in the 150 kDa study. This indicates that 150 kDa FITC-dextran is large enough to minimize any impact of the differences in porosity between the *Fbln5*^{+/+} and *Fbln5*^{-/-} tissues

Additionally, solute uptake at each dextran size was measured after 60 minutes for elastase-treated *Fbln5*^{+/+} arteries. The results are included in Figure 4.7C. At the 4kDa FITC-dextran size, there is a decrease in solute uptake for elastase-treated *Fbln5*^{+/+} arteries, comparable to that observed in the *Fbln5*^{-/-} tissues. At 70 kDa the behavior between these groups diverge as the elastase-treated tissue now has increased solute uptake compared to untreated tissue. The same trend is observed at 150kDa FITC-dextran. Overall, the trend of reduced solute uptake observed with dextran size in *Fbln5*^{+/+} and *Fbln5*^{-/-} tissues is diminished in the elastase-treated tissues.

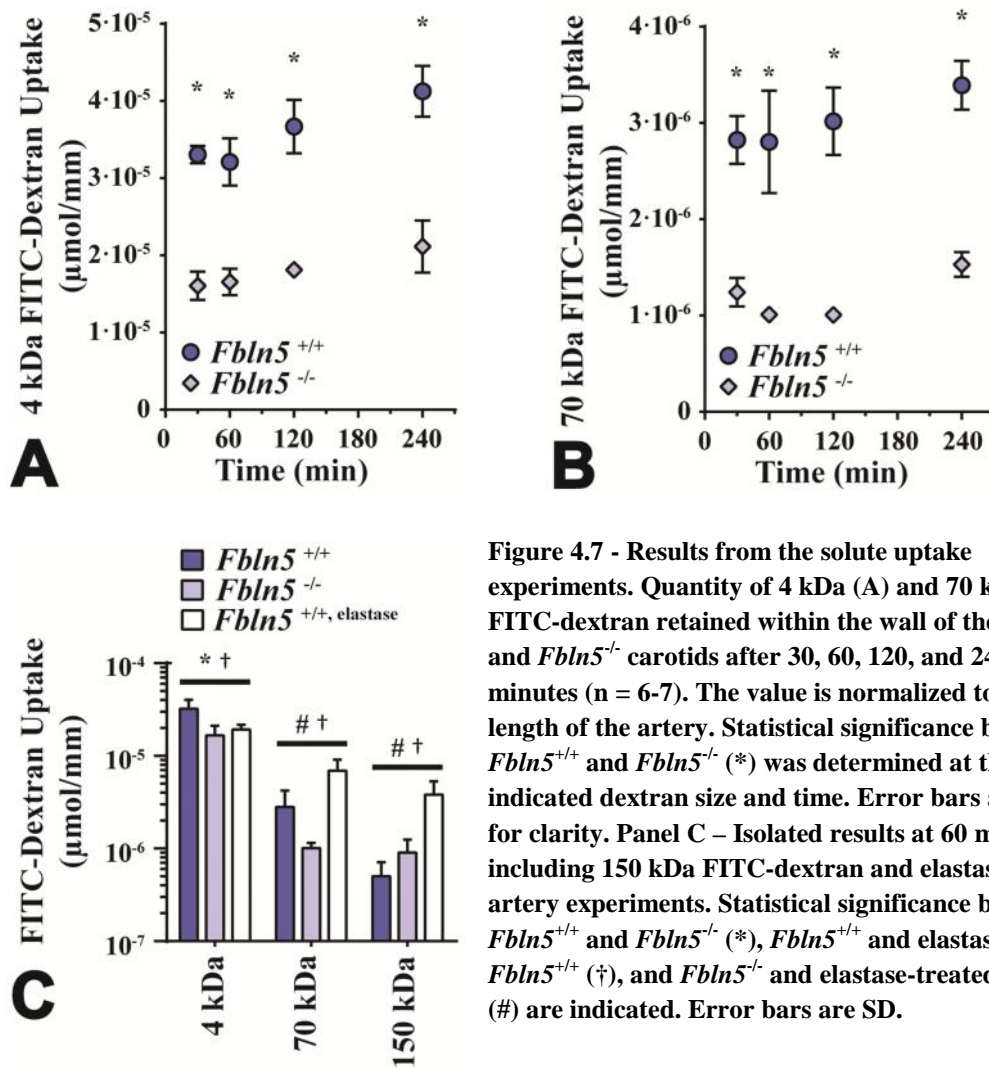


Figure 4.7 - Results from the solute uptake experiments. Quantity of 4 kDa (A) and 70 kDa (B) FITC-dextran retained within the wall of the *Fbln5*^{+/+} and *Fbln5*^{-/-} carotids after 30, 60, 120, and 240 minutes (n = 6-7). The value is normalized to the length of the artery. Statistical significance between *Fbln5*^{+/+} and *Fbln5*^{-/-} (*) was determined at the indicated dextran size and time. Error bars are SEM for clarity. Panel C – Isolated results at 60 minutes including 150 kDa FITC-dextran and elastase-treated artery experiments. Statistical significance between *Fbln5*^{+/+} and *Fbln5*^{-/-} (*), *Fbln5*^{+/+} and elastase-treated *Fbln5*^{-/-} (†), and *Fbln5*^{-/-} and elastase-treated *Fbln5*^{+/+} (#) are indicated. Error bars are SD.

4.3.6 Change to effective pore radius is not adequate to describe results

The mass transport parameters measured in this investigation enable the use of porous membrane mass transport theory to make predictions on the structural changes in the *Fbln5*^{-/-} and elastase treated *Fbln5*^{+/+} arteries that are responsible for the observed results. Darcy's law for fluid transport (equation 4.8) and the expression for advection dominated solute mass transport (equation 4.11) can be used in conjunction to determine the reflection coefficient, \uparrow for each tissue and FITC-dextran size (Figure 4.8A). Subsequently, the expressions in equations 4.2, 4.3, and 4.4 for steric-based determination of \uparrow , along with equation 4.5 for empirical determination of FITC-dextran particle radius can be used to estimate effective pore radius of the tissues (Figure 4.8B). Standard deviation for \uparrow was determined by propagation of standard deviation assuming simple division of the experimentally determined parameters L_p and J_s .

An apparent trend in the results is an increase in effective pore radius with FITC-dextran size in all tissues. Since pore size should remain constant at static mechanical circumferential and axial deformation of the arterial tissue, this result suggests that the assumption of uniform, homogeneous pore network structure is inappropriate, despite its wide use in tissue transport. It is likely that there is a tissue specific distribution of pore size and shape, so that using the current equations will over-estimate the effective pore radius when larger solutes are used since smaller pores are effectively impermissible. The reciprocal is also true. Smaller solute molecules entering a large pore would be indistinguishable from solute entering many smaller pores equaling the pore area of the single larger pore. Additionally, the alterations to fluid and solute transport in elastic fiber compromised tissue that we demonstrate in this investigation inherently violate the assumption of a homogenous porous membrane since the elastic fiber network structure is markedly inhomogeneous. This theoretical investigation of effective pore radius

provides evidence that the currently used transport theory may inadequately describe the mass transport properties across the arterial wall and more comprehensive numerical models must be used.

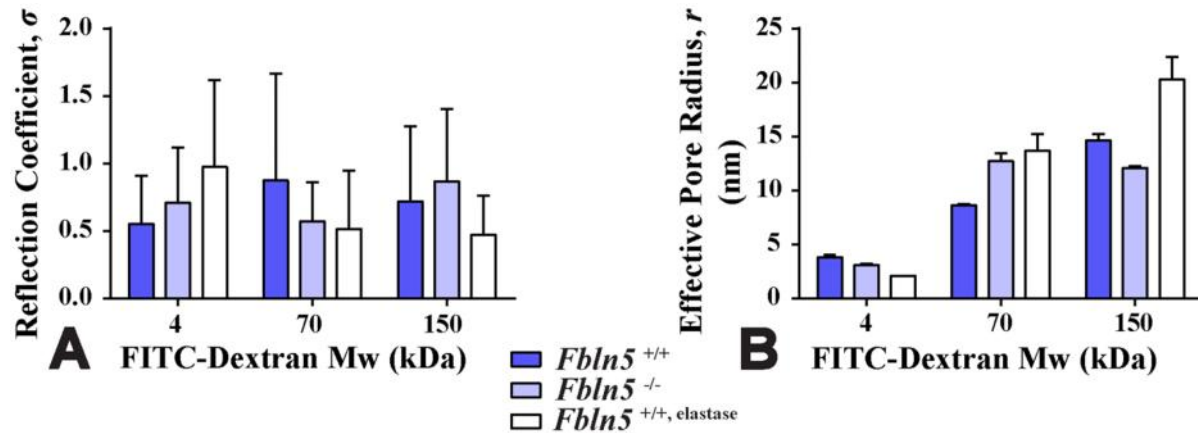


Figure 4.8 – Theoretical reflection coefficient (A) and tissue effective pore radius (B) for the carotid tissues and FITC-dextran molecules utilized in this study.

4.4 Discussion

To the best of our knowledge this is the first empirical investigation of mass transport in the medial layer of arterial tissue in which the elastic fiber network has been specifically compromised. We have continued the assumptions made in other investigations that the media behaves as a homogenous, porous membrane to simplify experimentation and numerical analyses. Our investigation isolates the role of the elastic fiber network on the intrinsic transport properties of the arterial wall by comparing mass transport in wild type mouse common carotids to those with genetically and enzymatically compromised elastic fiber integrity. While our investigation is focused on the elastic fibers, there are additional ECM components in the wall, including collagen fibers and proteoglycans, which may also influence arterial wall transport. Our observations of increased volumetric fluid flux and net solute flux in elastic fiber compromised tissues provide evidence that the ECM should not be overlooked in theoretical or experimental studies of arterial wall mass transport.

The hydrodynamic radius of 4, 70, and 150 kDa FITC-dextran is approximately 1.5, 5.9, and 8.6 nm, respectively (35). These sizes are several orders of magnitude smaller than the radius (0.5 – 5 μm) of the fenestrae that are characteristic of the morphology of elastic lamellae within the arterial wall (44, 45) and can be observed in the two-photon microscopy images presented in Figure 2. The fenestrations implicitly contribute to the transmural hydraulic conductance of the arterial wall. However, their relatively large size suggests they are not a factor towards the resistance of solute transport of the dextran molecules used in this study. Increased size and frequency of fenestrations within the aorta has been observed in a mouse model of Marfan syndrome, an autosomal dominant genetic disorder having numerous connective tissue defects including elastic fiber fragmentation and dilation of the aorta (44). Although the size and density of elastic lamellae fenestrations were not qualitatively different between groups in our study, additional, quantitative analyses may highlight subtle differences that should be considered for transport of targeted pharmacologic therapies in elastic fiber related diseases, such as Marfan Syndrome.

The effective radius of the pores passing between the elastic fibers within the elastic lamellae of wild-type arteries can be approximated to be between the hydrodynamic radii of 4 and 70 kDa FITC-dextran, based on the size exclusion behavior observed in Figure 4D. This size exclusion behavior is diminished in the *Fbln5*^{-/-} artery, indicating a change in the effective pore radius of the genetic mutant and is likely a result of the apparent change in the density and arrangement of the elastic fibers within the elastic lamellae, as indicated in the two-photon microscopy images. The elastase-treated wild-type arteries allowed all sizes of FITC-dextran particles through at

approximately the same rate. The size range at which these solute exclusion behaviors occur, or the absence of size exclusion behaviors, has important physiological implications on which biomolecules can more readily transverse the arterial wall. Cofactors and small molecule pharmaceuticals are generally smaller than 1 kDa and therefore may experience low resistance to transport by the elastic lamellae in wild-type arteries. Biologics and growth factors which can span 10 – 100 kDa in size are likely impacted by the filtration effect of the elastic lamellae in wild-type arteries, but would more easily transverse the wall of arteries with genetic or enzymatic defects in the elastic lamellae. The elastic lamellae in wild-type arteries may be impermeable to much larger macromolecules such as members of the low-density lipoprotein family, which have significant contribution to the onset and progression of atherosclerosis, but may be permeable to these molecules when the elastic lamellae are enzymatically compromised.

Removal of the intimal layer of endothelial cells prior to experimentation allowed more direct measurement of medial layer transport properties, which has a prominent ECM component. The effect of stripping the endothelial layer on the hydraulic conductance of large elastic arteries has been studied previously by other investigators in order to isolate the medial layer contribution to transport. A denuded artery has a hydraulic conductance of nearly twice that of an intact vessel (46-48). Our investigation further advances the knowledge of how arterial wall structural features contribute to advective transport resistance by demonstrating a 6-fold and 7-fold increase in hydraulic conductance in *Fbln5*^{-/-} and elastase-treated *Fbln5*^{+/+} carotids, respectively, compared to untreated *Fbln5*^{+/+}. This increase in hydraulic conductance in the medial layer of elastic fiber compromised artery is strong evidence that the elastic fiber network contributes to the resistance of flow across the arterial wall.

Our investigation appears to be the first to report hydraulic conductance for mouse arterial tissue. Our wild-type arterial hydraulic conductance for the denuded mouse carotid is $49.9 \cdot 10^{-8} \text{ cm} \cdot \text{s}^{-1} \cdot \text{mmHg}^{-1}$ which is 5 to 40 times greater than values reported from studies involving arteries from other organisms. Performing transport experiments on mouse carotids is challenging owing to their small size. As such, the possibility that our results are overestimated due to an unforeseen technical limitation cannot be dismissed. However, there are several physiological differences in the elastic fiber network of mouse carotids compared to the arteries tested by other investigators that could account for this difference. The number of elastic lamellae tends to increase across animal species when ordered by animal size (49). Additionally, the number of elastic lamellae within the media decreases along the arterial tree. We surmise these characteristics of the elastic fiber network structure could account for the differences. Hwang et al. observed differences in transport properties of arteries from different locations in the arterial tree (50). Shou et al. reported a hydraulic conductance of $4.89 \cdot 10^{-8} \text{ cm} \cdot \text{s}^{-1} \cdot \text{mmHg}^{-1}$ at 100 mmHg for denuded rat aorta (8 lamellae) which has several more elastic lamellae than our mouse carotid (4 lamellae) (49), however one caveat is that they did not apply an axial stretch to bring the artery to a physiological conformation for experimentation (48). For the denuded rabbit aorta (~22 elastic lamellae), Tedgui and Lever report a hydraulic conductance at 180 mmHg of $5.27 \cdot 10^{-8} \text{ cm} \cdot \text{s}^{-1} \cdot \text{mmHg}^{-1}$ (46) and Baldwin et al. report a value of $3.5 \cdot 10^{-8} \text{ cm} \cdot \text{s}^{-1} \cdot \text{mmHg}^{-1}$ in one investigation (51) and $10.0 \cdot 10^{-8} \text{ cm} \cdot \text{s}^{-1} \cdot \text{mmHg}^{-1}$ in another investigation at 100 mmHg (47). Tarbell et al. reported a value for the denuded rabbit carotid of $1.25 \cdot 10^{-8} \text{ cm} \cdot \text{s}^{-1} \cdot \text{mmHg}^{-1}$ at 100mmHg which has ~6 more elastic lamellae than the mouse carotid (52-54).

While there is no clear trend in hydraulic conductance with number of elastic lamellae from these literature values, the results from our study suggest the architecture of the elastic fiber network should be a determining factor. We propose that the hydraulic resistance of the arterial media is equivalent to the sum of the hydraulic resistances of each individual lamellae. Our hypothesis is only applicable if the elastic fiber component of the wall has a prominent effect on transport since without elastic fibers the wall would more closely resemble a homogenous tissue of VSMCs and other ECM constituents. Future investigation is needed to determine whether a relationship exists between hydraulic resistance and number of elastic lamellae. If such a relationship exists then it would be beneficial knowledge towards the design of drug delivery strategies. The drug concentration loaded onto the delivery platform may be adjusted according to the elastic fiber network structure of the targeted artery to improve the therapeutic response.

Elastic and collagen fiber arrangement and structure in the arterial wall are affected by physiological mechanical loading. Circumferential strain applied by increases in blood pressure results in the rearrangement and straightening of these ECM components (55, 56). Previous investigations indicate a dependence of arterial hydraulic conductance changes on the pressure gradient across the wall (47, 48, 51). By our findings it is reasonable to suggest that rearrangement of the ECM in response to changes in pressure is one of the mechanisms responsible for this dependence. The large arteries experience dynamic changes in acting forces, implicating that the intrinsic transport properties may be more dynamic than what is typically assumed.

Aortic aneurysms have severe structural defects in the arterial wall ECM microstructure including fragmentation and degradation of the elastic lamellae. The results from our study suggest that aneurysmal tissue could have increased hydraulic conductivity and effective porosity compared to surrounding healthy arterial tissue. One therapeutic strategy may be to design anti-inflammatory drug delivery systems which take advantage of this difference in transport properties. A delivery vehicle small enough to enter into the aneurysmal tissue from the arterial lumen but too large to diffuse to surrounding healthier tissue may effectively concentrate the drug to the diseased area.

Accumulation of defects to the elastic fiber network of arterial tissues is observed in aging and disease progression. Elastic fiber degradation is a factor in numerous cardiovascular diseases including hypertension, aneurysm development, and arterial calcification (57-60). Reduced elastic fiber crosslinking, increased elastolytic activity, and higher elastic fiber fragmentation has been observed in mouse models of obesity (61). Elastic fiber fragmentation may be involved in both the initiation of plaque development in atherosclerosis (62) and exacerbation of the disease (63-65). In aging, elastic fiber composition in the large conduit arteries drops over the human lifespan (60, 66) but this is likely an effect of disproportionate increases of other ECM constituents in the wall while changes to elastic fiber quantity is nominal (67, 68). Elastic fibers do, however, accumulate damage and defects over time resulting in increased fragmentation with aging (69), as *de novo* elastic fiber synthesis or repair is not evident in adult tissues (57). The cause of fragmentation is not well understood but it is likely that the high number of cardiac loading cycles over an organism's lifetime causes mechanical failure in the elastic fiber network (70) for which there is no known repair mechanism. It is also thought that an imbalance in the

elastolytic enzymes contributes to elastic fiber degradation (59, 71). The influence on arterial transport by elastic fiber integrity has important implications on the kinetics of biomolecules involved in aging and cardiovascular disease, warranting future investigation.

Similar to an aged artery, arteries from *Fbln5*^{-/-} mice do not demonstrate appreciable changes in elastic fiber amount although they do not have the same increases in collagen content normally associated with aged arteries (31, 72). Fragmentation in arterial elastic lamellae of *Fbln5*^{-/-} mice is a result of improper elastic fiber assembly in development rather than mechanical fatigue and there is no evidence of heightened elastolytic activity (30, 31, 37). As such, the disruption to the elastic fiber network in *Fbln5*^{-/-} mouse occurs through a different mechanism than the damage that accumulates in the elastic fibers of aged human arteries. Regardless, in the context of transport the result is likely similar such that a similar decrease in resistance to advective mass transport that we report for *Fbln5*^{-/-} carotids may also occur in aged arteries. Additionally, the experiments using an elastase treatment for elastic fiber degradation in most cases demonstrate similar results as the *Fbln5*^{-/-} experiments providing evidence that elastic fiber degradation, regardless of the mechanism responsible, can largely impact transport. The degradation of an individual's arterial elastic fiber network in aging and disease could impact the transport of biomolecules and drugs across the arterial wall and has implications for the progression of vascular disease and efficacy of drug delivery therapies that target the arterial media.

4.5 Conclusions

We have investigated the transport properties of elastic fiber compromised arterial tissue to evaluate whether changes to the elastic fiber network structure have significant impact on the transport properties of the arterial wall. It is apparent from our histological cross-section and *en*

face two-photon microscopy images that *Fbln5*^{-/-} carotids have several phenotypic changes to the structure of the elastic lamellae including a fragmented appearance. We hypothesized that these structural changes would translate to a increase in tissue porosity and tested this hypothesis with measures of fluid and solute transport. We observed an increase in hydraulic conductance, net solute flux, and reduced solute uptake compared to *Fbln5*^{+/+} carotids and conclude this to be strong evidence that the elastic fiber network plays a significant role in determining the transport properties of the arterial wall. Similar changes in most cases were observed when the elastic fiber network was exposed to a brief elastase treatment.

From our results, the native elastic fiber network within the arterial media contributes to the resistance of bulk transport across the arterial media. Elastic fibers predominately form sheet-like layers within the arterial wall and are partly responsible for the non-homogenous structure of the media. Previous transport studies have approximated the media to be homogenous and have largely ignored the elastic fiber component. Our results suggest this may be an oversimplification that should be addressed in future studies to improve the understanding of transport within arterial tissue. Fragmentation, rearrangement, and degradation of the elastic fiber network in disease and aging may have significant impact on the transport of macromolecules within the arterial wall and could impact effectiveness of drug delivery therapies targeting these tissues.

4.6 Limitations

In this study we made the assumption that diffusive solute transport was insignificant compared to advective transport. This is supported by several previous numerical and experimental investigations that have reported high Péclet numbers for small molecules and small proteins in arterial tissue (17, 29, 73, 74). However, we observed a steady increase in solute uptake within

the tissue even after 4 hours despite steady-state, transmural advective transport being achieved in less than 10 minutes. This is possibly a consequence of passive diffusion including diffusion in directions other than across the wall. This observation indicates that arterial wall transport from the lumen and across the wall is not sufficiently described in the one-dimensional scenario, especially since the non-homogenous elastic fiber network has an impact on solute transport. Three-dimensional diffusion is difficult to measure given the small size of the mouse carotid tissue, especially if *in vivo* conformation is to be retained. However, our results provide new evidence for the contribution of the elastic fiber component to arterial wall transport to better inform more complex theoretical transport models.

Another limitation to this study is that concentration polarization may be a contributing factor towards the overall solute transport. Without measurements of changes in FITC-dextran concentration in the lumen throughout the course of the experiment it is difficult to conclude to what degree concentration polarization affects the results of this study. However, the constant rate of solute transport for each FITC-dextran in Figure 4 is evidence against concentration polarization having a significant affect in this study but may be an important in future studies.

4.7 Acknowledgments

Hiromi Yanagisawa at the University of Tsukuba is gratefully acknowledged for providing the *Fbln5*^{-/-} mice. Data presented in this study was partially funded by NIH grants R01 HL115560, R01 HL105314, and T32 EB018266. Histological data was partially provided the Washington University Musculoskeletal Research Center funded by NIH grant P30 AR057235. Confocal data was generated on a Zeiss LSM 880 Airyscan Confocal Microscope which was purchased with support from the Office of Research Infrastructure Programs (ORIP), a part of the NIH Office of the Director under grant OD021629. The content is solely the responsibility of the authors and does not necessarily represent the official views of the NIH.

4.8 References

1. Pellegrini DO, Gomes VO, Lasevitch R, Smidt L, Azeredo MA, Ledur P, et al. Efficacy and safety of drug-eluting stents in the real world: 8-year follow-up. *Arq Bras Cardiol.* 2014;103(3):174-82.
2. Buchanan K, Steinvil A, Waksman R. Does the new generation of drug-eluting stents render bare metal stents obsolete? *Cardiovasc Revasc Med.* 2017;18(6):456-61.
3. Cui K, Lyu S, Song X, Yuan F, Xu F, Zhang M, et al. Drug-eluting balloon versus bare-metal stent and drug-eluting stent for de novo coronary artery disease: A systematic review and meta-analysis of 14 randomized controlled trials. *PLoS One.* 2017;12(4):e0176365.
4. Collins MJ, Li X, Lv W, Yang C, Protack CD, Muto A, et al. Therapeutic strategies to combat neointimal hyperplasia in vascular grafts. *Expert Rev Cardiovasc Ther.* 2012;10(5):635-47.
5. Seedial SM, Ghosh S, Saunders RS, Suwanabol PA, Shi X, Liu B, et al. Local drug delivery to prevent restenosis. *J Vasc Surg.* 2013;57(5):1403-14.
6. Golledge J, Cullen B, Moran C, Rush C. Efficacy of simvastatin in reducing aortic dilatation in mouse models of abdominal aortic aneurysm. *Cardiovasc Drugs Ther.* 2010;24(5-6):373-8.
7. Steinmetz EF, Buckley C, Shames ML, Ennis TL, Vanvickle-Chavez SJ, Mao D, et al. Treatment with simvastatin suppresses the development of experimental abdominal aortic aneurysms in normal and hypercholesterolemic mice. *Ann Surg.* 2005;241(1):92-101.
8. Moore G, Liao S, Curci JA, Starcher BC, Martin RL, Hendricks RT, et al. Suppression of experimental abdominal aortic aneurysms by systemic treatment with a hydroxamate-based matrix metalloproteinase inhibitor (RS 132908). *J Vasc Surg.* 1999;29(3):522-32.
9. Fraga-Silva RA, Trachet B, Stergiopoulos N. Emerging Pharmacological Treatments to Prevent Abdominal Aortic Aneurysm Growth and Rupture. *Curr Pharm Des.* 2015.
10. Kurosawa K, Matsumura JS, Yamanouchi D. Current status of medical treatment for abdominal aortic aneurysm. *Circ J.* 2013;77(12):2860-6.
11. Yoshimura K, Morikage N, Nishino-Fujimoto S, Furutani A, Shirasawa B, Hamano K. Current Status and Perspectives on Pharmacologic Therapy for Abdominal Aortic Aneurysm. *Curr Drug Targets.* 2017.
12. Shirasu T, Koyama H, Miura Y, Hoshina K, Kataoka K, Watanabe T. Nanoparticles Effectively Target Rapamycin Delivery to Sites of Experimental Aortic Aneurysm in Rats. *PLoS One.* 2016;11(6):e0157813.
13. Nosoudi N, Chowdhury A, Siclari S, Parasaram V, Karamched S, Vyavahare N. Systemic Delivery of Nanoparticles Loaded with Pentagalloyl Glucose Protects Elastic Lamina and Prevents Abdominal Aortic Aneurysm in Rats. *Journal of cardiovascular translational research.* 2016;9(5-6):445-55.
14. Wang X, Searle AK, Hohmann JD, Liu AL, Abraham MK, Palasubramaniam J, et al. Dual-Targeted Theranostic Delivery of miRs Arrests Abdominal Aortic Aneurysm Development. *Mol Ther.* 2018;26(4):1056-65.
15. Nosoudi N, Nahar-Gohad P, Sinha A, Chowdhury A, Gerard P, Carsten CG, et al. Prevention of abdominal aortic aneurysm progression by targeted inhibition of matrix metalloproteinase activity with batimastat-loaded nanoparticles. *Circ Res.* 2015;117(11):e80-9.

16. Sivaraman B, Ramamurthi A. Multifunctional nanoparticles for doxycycline delivery towards localized elastic matrix stabilization and regenerative repair. *Acta Biomater.* 2013;9(5):6511-25.
17. Hwang CW, Wu D, Edelman ER. Physiological transport forces govern drug distribution for stent-based delivery. *Circulation.* 2001;104(5):600-5.
18. Davis EC. Stability of elastin in the developing mouse aorta: a quantitative radioautographic study. *Histochemistry.* 1993;100(1):17-26.
19. Dingemans KP, Teeling P, Lagendijk JH, Becker AE. Extracellular matrix of the human aortic media: an ultrastructural histochemical and immunohistochemical study of the adult aortic media. *Anat Rec.* 2000;258(1):1-14.
20. O'Connell MK, Murthy S, Phan S, Xu C, Buchanan J, Spilker R, et al. The three-dimensional micro- and nanostructure of the aortic medial lamellar unit measured using 3D confocal and electron microscopy imaging. *Matrix Biol.* 2008;27(3):171-81.
21. Ramirez CA, Colton CK, Smith KA, Stemerman MB, Lees RS. Transport of 125I-albumin across normal and deendothelialized rabbit thoracic aorta in vivo. *Arteriosclerosis.* 1984;4(3):283-91.
22. Caro CG, Lever MJ, Laver-Rudich Z, Meyer F, Liron N, Ebel W, et al. Net albumin transport across the wall of the rabbit common carotid artery perfused in situ. *Atherosclerosis.* 1980;37(4):497-511.
23. Pfeffer R, Ganatos P, Nir A, Weinbaum S. Diffusion of macromolecules across the arterial wall in the presence of multiple endothelial injuries. *Journal of biomechanical engineering.* 1981;103(3):197-203.
24. Proctor SD, Vine DF, Mamo JC. Arterial permeability and efflux of apolipoprotein B-containing lipoproteins assessed by in situ perfusion and three-dimensional quantitative confocal microscopy. *Arterioscler Thromb Vasc Biol.* 2004;24(11):2162-7.
25. Tada S, Tarbell JM. Internal elastic lamina affects the distribution of macromolecules in the arterial wall: a computational study. *American journal of physiology Heart and circulatory physiology.* 2004;287(2):H905-13.
26. Huang ZJ, Tarbell JM. Numerical simulation of mass transfer in porous media of blood vessel walls. *The American journal of physiology.* 1997;273(1 Pt 2):H464-77.
27. Fry DL. Mathematical models of arterial transmural transport. *The American journal of physiology.* 1985;248(2 Pt 2):H240-63.
28. Caro CG, Lever MJ. Factors influencing arterial wall mass transport. *Biorheology.* 1984;21(1-2):197-205.
29. Kim WS, Tarbell JM. Macromolecular transport through the deformable porous media of an artery wall. *Journal of biomechanical engineering.* 1994;116(2):156-63.
30. Nakamura T, Lozano PR, Ikeda Y, Iwanaga Y, Hinek A, Minamisawa S, et al. Fibulin-5/DANCE is essential for elastogenesis in vivo. *Nature.* 2002;415(6868):171-5.
31. Le VP, Cheng JK, Kim J, Staiculescu MC, Ficker SW, Sheth SC, et al. Mechanical factors direct mouse aortic remodelling during early maturation. *J R Soc Interface.* 2015;12(104):20141350.
32. Kedem O, Katchalsky A. Thermodynamic analysis of the permeability of biological membranes to non-electrolytes. *Biochim Biophys Acta.* 1958;27(2):229-46.
33. Anderson JL, Malone DM. Mechanism of osmotic flow in porous membranes. *Biophys J.* 1974;14(12):957-82.

34. Giddings JC, Kucera E, Russell CP, Myers MN. Statistical theory for the equilibrium distribution of rigid molecules in inert porous networks. Exclusion chromatography. *The Journal of Physical Chemistry*. 1968;72(13):4397-408.
35. Armstrong JK, Wenby RB, Meiselman HJ, Fisher TC. The hydrodynamic radii of macromolecules and their effect on red blood cell aggregation. *Biophys J*. 2004;87(6):4259-70.
36. Brace RA, Granger DN, Taylor AE. Analysis of lymphatic protein flux data. III. Use of the nonlinear flux equation to estimate sigma and PS. *Microvasc Res*. 1978;16(3):297-303.
37. Yanagisawa H, Davis EC, Starcher BC, Ouchi T, Yanagisawa M, Richardson JA, et al. Fibulin-5 is an elastin-binding protein essential for elastic fibre development in vivo. *Nature*. 2002;415(6868):168-71.
38. Ferruzzi J, Bersi MR, Uman S, Yanagisawa H, Humphrey JD. Decreased elastic energy storage, not increased material stiffness, characterizes central artery dysfunction in fibulin-5 deficiency independent of sex. *J Biomech Eng*. 2015;137(3).
39. Luetkemeyer CM, James RH, Devarakonda ST, Le VP, Liu Q, Han HC, et al. Critical buckling pressure in mouse carotid arteries with altered elastic fibers. *J Mech Behav Biomed Mater*. 2015;46:69-82.
40. Ralevic V, Kristek F, Hudlicka O, Burnstock G. A new protocol for removal of the endothelium from the perfused rat hind-limb preparation. *Circ Res*. 1989;64(6):1190-6.
41. Winkler RH. The effect of halides (NaCl and NaI) on in vitro pancreatic elastase activity. *Connect Tissue Res*. 1978;6(2):89-92.
42. Wan W, Yanagisawa H, Gleason RL, Jr. Biomechanical and microstructural properties of common carotid arteries from fibulin-5 null mice. *Ann Biomed Eng*. 2010;38(12):3605-17.
43. Wong LC, Langille BL. Developmental remodeling of the internal elastic lamina of rabbit arteries: effect of blood flow. *Circ Res*. 1996;78(5):799-805.
44. Lopez-Guimet J, Andilla J, Loza-Alvarez P, Egea G. High-Resolution Morphological Approach to Analyse Elastic Laminae Injuries of the Ascending Aorta in a Murine Model of Marfan Syndrome. *Sci Rep*. 2017;7(1):1505.
45. Ushiki T. Collagen fibers, reticular fibers and elastic fibers. A comprehensive understanding from a morphological viewpoint. *Arch Histol Cytol*. 2002;65(2):109-26.
46. Tedgui A, Lever MJ. Filtration through damaged and undamaged rabbit thoracic aorta. *The American journal of physiology*. 1984;247(5 Pt 2):H784-91.
47. Baldwin AL, Wilson LM. Endothelium increases medial hydraulic conductance of aorta, possibly by release of EDRF. *The American journal of physiology*. 1993;264(1 Pt 2):H26-32.
48. Shou Y, Jan KM, Rumschitzki DS. Transport in rat vessel walls. I. Hydraulic conductivities of the aorta, pulmonary artery, and inferior vena cava with intact and denuded endothelia. *American journal of physiology Heart and circulatory physiology*. 2006;291(6):H2758-71.
49. Wolinsky H, Glagov S. A lamellar unit of aortic medial structure and function in mammals. *Circ Res*. 1967;20(1):99-111.
50. Hwang CW, Edelman ER. Arterial ultrastructure influences transport of locally delivered drugs. *Circ Res*. 2002;90(7):826-32.
51. Baldwin AL, Wilson LM, Simon BR. Effect of pressure on aortic hydraulic conductance. *Arterioscler Thromb*. 1992;12(2):163-71.
52. Tarbell JM, Lever MJ, Caro CG. The effect of varying albumin concentration of the hydraulic conductivity of the rabbit common carotid artery. *Microvasc Res*. 1988;35(2):204-20.

53. Williams C, Liao J, Joyce EM, Wang B, Leach JB, Sacks MS, et al. Altered structural and mechanical properties in decellularized rabbit carotid arteries. *Acta Biomater.* 2009;5(4):993-1005.
54. Rees PM. Electron microscopical observations on the architecture of the carotid arterial walls, with special reference to the sinus portion. *J Anat.* 1968;103(Pt 1):35-47.
55. Sugita S, Matsumoto T. Multiphoton microscopy observations of 3D elastin and collagen fiber microstructure changes during pressurization in aortic media. *Biomechanics and modeling in mechanobiology.* 2017;16(3):763-73.
56. Chow MJ, Turcotte R, Lin CP, Zhang Y. Arterial extracellular matrix: a mechanobiological study of the contributions and interactions of elastin and collagen. *Biophys J.* 2014;106(12):2684-92.
57. Cociolone AJ, Hawes JZ, Staiculescu MC, Johnson EO, Murshed M, Wagenseil JE. Elastin, arterial mechanics, and cardiovascular disease. *American journal of physiology Heart and circulatory physiology.* 2018.
58. Baldwin AK, Simpson A, Steer R, Cain SA, Kielty CM. Elastic fibres in health and disease. *Expert Rev Mol Med.* 2013;15:e8.
59. Duca L, Blaise S, Romier B, Laffargue M, Gayral S, El Btaouri H, et al. Matrix ageing and vascular impacts: focus on elastin fragmentation. *Cardiovasc Res.* 2016;110(3):298-308.
60. Tsamis A, Krawiec JT, Vorp DA. Elastin and collagen fibre microstructure of the human aorta in ageing and disease: a review. *J R Soc Interface.* 2013;10(83):20121004.
61. Chen JY, Tsai PJ, Tai HC, Tsai RL, Chang YT, Wang MC, et al. Increased aortic stiffness and attenuated lysyl oxidase activity in obesity. *Arterioscler Thromb Vasc Biol.* 2013;33(4):839-46.
62. Akima T, Nakanishi K, Suzuki K, Katayama M, Ohsuzu F, Kawai T. Soluble elastin decreases in the progress of atheroma formation in human aorta. *Circ J.* 2009;73(11):2154-62.
63. Van der Donckt C, Van Herck JL, Schrijvers DM, Vanhoutte G, Verhoye M, Blockx I, et al. Elastin fragmentation in atherosclerotic mice leads to intraplaque neovascularization, plaque rupture, myocardial infarction, stroke, and sudden death. *Eur Heart J.* 2015;36(17):1049-58.
64. Maedeker JA, Stoka KV, Bhayani SA, Gardner WS, Bennett L, Procknow JD, et al. Hypertension and decreased aortic compliance due to reduced elastin amounts do not increase atherosclerotic plaque accumulation in *Ldlr*^{-/-} mice. *Atherosclerosis.* 2016;249:22-9.
65. Stoka KV, Maedeker JA, Bennett L, Bhayani SA, Gardner WS, Procknow JD, et al. Effects of Increased Arterial Stiffness on Atherosclerotic Plaque Amounts. *J Biomech Eng.* 2018;140(5).
66. Hosoda Y, Kawano K, Yamasawa F, Ishii T, Shibata T, Inayama S. Age-dependent changes of collagen and elastin content in human aorta and pulmonary artery. *Angiology.* 1984;35(10):615-21.
67. Spina M, Garbisa S, Hinnie J, Hunter JC, Serafini-Fracassini A. Age-related changes in composition and mechanical properties of the tunica media of the upper thoracic human aorta. *Arteriosclerosis.* 1983;3(1):64-76.
68. Fritze O, Romero B, Schleicher M, Jacob MP, Oh DY, Starcher B, et al. Age-related changes in the elastic tissue of the human aorta. *J Vasc Res.* 2012;49(1):77-86.
69. Sans M, Moragas A. Mathematical morphologic analysis of the aortic medial structure. Biomechanical implications. *Anal Quant Cytol Histol.* 1993;15(2):93-100.
70. Avolio A, Jones D, Tafazzoli-Shadpour M. Quantification of alterations in structure and function of elastin in the arterial media. *Hypertension.* 1998;32(1):170-5.

71. Wang M, Lakatta EG. Altered regulation of matrix metalloproteinase-2 in aortic remodeling during aging. *Hypertension*. 2002;39(4):865-73.
72. Wan W, Gleason RL, Jr. Dysfunction in elastic fiber formation in fibulin-5 null mice abrogates the evolution in mechanical response of carotid arteries during maturation. *American journal of physiology Heart and circulatory physiology*. 2013;304(5):H674-86.
73. Baldwin AL, Wilson LM, Gradus-Pizlo I, Wilensky R, March K. Effect of atherosclerosis on transmural convection an arterial ultrastructure. Implications for local intravascular drug delivery. *Arterioscler Thromb Vasc Biol*. 1997;17(12):3365-75.
74. Tedgui A, Lever MJ. The interaction of convection and diffusion in the transport of ¹³¹I-albumin within the media of the rabbit thoracic aorta. *Circ Res*. 1985;57(6):856-63.

Chapter 5

Conclusions

The research presented in this thesis has focused on one core motivation – to contribute to an improved understanding of elastic fiber assembly and degeneration such that intervention for genetic and acquired elastinopathies may be better designed. While it is clear from our review of elastic fiber function in physiology and disease in chapter 2 that prior investigations have contributed substantial knowledge, it is also evident that there is a significant amount of the elastic fiber assembly and degradation process that is not yet understood. If we are to advance modern medicine towards the attenuation of elastic fiber degradation in cardiovascular diseases including hypertension, atherosclerosis, diabetes, obesity, and aneurysm progression there is more research to be done. We submit that our research presented here has provided small, but significant advancement to the field.

The first research aim accomplished in this thesis was the development of a platform for screening molecular factors for an elastic fiber assembly agonist. To do this, we selected an immortalized cell line, RFL6, that is known to produce elastic fibers *in vitro* and measured significant increases in elastic fiber production with in-culture time using a competitive ELISA for desmosine. We assessed the effect of DMSO concentration on cell protein production in order to avoid cytotoxic effects from DMSO in future screening endeavors. We demonstrated utility in our screening platform by observing a reduction in elastic fiber production in cell treated with β APN, an inhibitor of elastic fiber cross-linking. The suitability of growth factors,

insulin and TGF- β 1, and of antihypertensive drugs, diazoxide, minoxidil, and captopril, to serve as positive controls of elastic fiber production in our screening platform was investigated but we determined that none of these factors upregulate elastic fiber assembly in our cell culture conditions. Finally, we performed a high-throughput screen of the NCI Diversity Set V library of nearly 1600 small molecules using the platform we developed. While 7 molecules scored as positive hits in the primary screen, none of them were agonistic to elastic fiber assembly in subsequent, more robust secondary investigations. Regardless of the lack of success in identifying a small molecule to upregulate crosslinked elastic fiber production *in vitro*, the biochemical assay platform that we optimized has been useful to our lab and collaborations for determining elastic fiber content in tissues such as the aorta and tendon.

We maintain that our screening platform can be improved with additional development. While RFL6 cells produce elastic fibers *in vitro*, their elastic fiber producing capability may be saturated and they may be unable to be pushed towards increased production. Investigation into alternate elastic fiber producing cell types may identify a more suitable option for the screening platform. The caveat is that many cell types that produce elastic fibers are primary cells from neonatal animal tissues, which may be too variable in viability and phenotype for large screens, but may be suitable for smaller scale investigations. Another possibility is that our cells need to be made more amendable towards elastic fiber production with growth factors like insulin and TGF- β 1, in addition to the compound of interest. Future elucidation of the elastic fiber assembly mechanism may also reveal conditions or factors required to promote elastic fiber assembly *in vitro*. In the more immediate future, factors that have demonstrated regulation of elastin gene expression can be investigated for elastic fiber maturation using our platform. The identification

of elastic fiber agonists would advance the field of tissue-engineered arteries and pharmaceutical development for the treatment of elastin-related diseases.

The second aim of this research was to address the hypothesis that elastic fiber network structure in the extracellular matrix of arterial tissue impedes the transport of fluid and solute across the arterial wall. To perform this investigation, we adapted mass transport experimental techniques normally used in larger, undeformed tissues for mouse carotid arteries mechanically loaded to the physiological axial and circumferential conformation. Using the *Fbln5*^{-/-} mouse with disrupted elastic fiber formation and an elastase treatment we developed, we investigated the effects of compromised elastic fiber integrity on mass transport parameters. From our measures of increased hydraulic conductance and increased advective solute transport, we concluded that the elastic fiber component of the arterial wall has significant impact on mass transport. This discovery is significant because previous investigations have ignored the elastic fiber component and attributed all of the mass transport properties to the distribution and arrangement of the vascular smooth muscle cells. With the increasing attention to the development of targeted pharmaceutical therapies for treating vascular diseases associated with elastinopathies, our conclusions provide an improved understanding of the pharmacokinetics of arterial tissue.

The evidence of elastic fiber contribution to arterial mass transport is only the beginning of this investigative area. Future investigations are needed to better gauge the impact of elastic fiber degradation on therapies. The models used here are more extreme, but viable examples of elastic fiber disruption. Repeated studies in human tissue from individuals having a genetic or acquired elastinopathy would reveal whether the influence elastic fibers have on transport is significant

with a pathophysiological range of elastic fiber perturbation. Additionally, technical limitations have limited our investigation towards advection driven mass transport but diffusive transport would become more relevant in the study of transport of larger macromolecules. To measure diffusive properties, larger scale tissues are required and a testing apparatus is needed that can stretch the tissue to physiological conformation but without a pressure gradient across the tissue. Finally, our results reveal that the heavily simplified mass transport theory most often used for arterial tissue is insufficient. Large arteries from humans experience more dynamic physical forces, have extensive tissue inhomogeneity, and likely have a distribution of effective pore size and shape. Even more sophisticated, computational models tend to underestimate elastic fiber contribution and the results from our empirical investigation may help refine these models in the future.